The Developmental Testbed Center's
Final Report on the NEMS/NMMB Microphysics Sensitivity Testing

29 May 2015

1. Introduction

The NOAA Environmental Modeling System (NEMS) with the Nonhydrostatic Multiscale Model on the B-grid (NMMB) core (Janjic and Gall 2012) is currently utilized in operational forecasting applications at the National Centers for Environmental Prediction (NCEP). Recently, a new microphysics option, the Thompson microphysics scheme (Thompson et al. 2008), was introduced into NEMS/NMMB; this scheme is coupled with the RRTM radiation scheme in order to better represent cloud-radiation interactions. The Developmental Testbed Center (DTC) conducted a test and evaluation activity to assess the forecast performance of two microphysical schemes in NEMS/NMMB. The first configuration was based on the operational physics suite at the NCEP for the North American Mesoscale (NAM) model, while the second configuration substituted the Thompson microphysics for the current operational Ferrier-hires microphysics scheme. For this testing, the two configurations will be referred to as NAMOC and ThompsonMP, with NAMOC used as the baseline. In addition to documenting the performance of the two configurations against each other, both were designated as DTC Reference Configurations (RCs), and the results have been made available to the NWP community.

2. Experiment Design

For this test, the end-to-end forecast system consisted of the NMMB Preprocessing System (NPS), NEMS/NMMB, Unified Postprocessor (UPP) and the NCAR Command Language (NCL) for graphics generation. Post-processed forecasts were verified using the Model Evaluation Tools (MET). In addition, the full data set was archived and is available for dissemination to the user community upon request. The codes utilized were based on the friendly user released versions of NPS (v0.9) and NMMB (v0.9), UPP (v2.2) with modifications for addressing output of reflectivity fields, and the official release of MET (v5.0) with relevant big fixes.

2.1 Forecast Periods

Forecasts were initialized every 36 hours for one month in each season (Table 1), consequently creating initialization times including both 00 and 12 UTC, for a total of 94 possible cases. The forecasts were run out to 48 hours with output files generated every 3 hours.

Table 2 below lists the forecast initializations that failed to complete the end-to-end process; the missing data and reason for failure is described in the table. Table 3 lists cases that ran to completion but were missing observations for verification. A total of 84 cases ran to completion and were used in the verification results.

Table 1. Case list.

Season	00 UTC Initializations	12 UTC Initializations
Fall	Oct 2013: 12, 15, 18, 21, 24, 27, 30	Oct 2013: 13, 16, 19, 22, 25, 28, 31
	Nov 2013: 2, 5, 8, 11, 14	Nov 2013: 3, 6, 9, 12, 15
Winter	Jan 2014: 16, 19, 22, 25, 28, 31	Jan 2014: 17, 20, 23, 26, 29
	Feb 2014: 3, 6, 9, 12, 15, 18	Feb 2014: 1, 4, 7, 10, 13, 16, 19

Spring	Apr 2014: 16, 19, 22, 25, 28 May 2014: 1, 4, 7, 10, 13, 16	Apr 2014: 17, 20, 23, 26, 29 May 2014: 2, 5, 8, 11, 14, 17
Summer	Jul 2014: 6, 9, 12, 15, 18, 21, 24, 27, 30 Aug 2014: 2, 5, 8	Jul 2014: 7, 10, 13, 16, 19, 22, 25, 28, 31 Aug 2014: 3, 6, 9

Table 2. Missing case list.

Affected Case	Missing data	Reason
2013101800	Model output	Missing NAMX input data
2013110500	Model output	Missing NAMX input data
2013110800	Model output	Missing NAMX input data
2014011600	Model output	Missing NAMX input data
2014012312	Model output	Missing NAMX input data
2014020412	Model output	ThompsonMP model crash
2014041712	Model output	Missing NAMX input data
2014072512	Model output	Missing NAMX input data
2014072700	Model output	Missing NAMX input data
2014080612	Model output	Missing NAMX input data

Table 3. Missing verification.

Affected Case	Missing data	Reason
2013110612	Missing reflectivity for 6,9,15,18,21,24,27,30-h	Missing radar observation file
2013111512	Missing reflectivity for 39,42,45-h	Missing radar observation file
2014021312	Missing reflectivity for 18,21,48-h	Missing radar observation file
2014021500	Missing reflectivity for 12-h	Missing radar observation file
2014042012	Missing reflectivity for 48-h	Missing radar observation file
2014042200	Missing reflectivity for 12-h	Missing radar observation file
2014072100	Missing reflectivity for 48-h	Missing radar observation file
2014072212	Missing reflectivity for 12-h	Missing radar observation file
2014073000	Missing reflectivity for 48-h	Missing radar observation file
2014073112	Missing reflectivity for 12-h	Missing radar observation file
2014080500	Missing reflectivity for 24-h	Missing radar observation file

2.2 Initial and Boundary Conditions

Initial conditions (ICs) and lateral boundary conditions (LBCs) were derived from an archive of the parallel version of the NAM (NAMX) on grid 151 with a model top of 10 hPa. While no data assimilation was conducted in the end-to-end workflow of this test, NAMX used the global ensemble Kalman filter (EnKF) in the regional North American Data Assimilation System (NDAS). The time-invariant component of the lower boundary conditions (topography, soil and vegetation type, etc.), using the International Geosphere-Biosphere Programme (IGBP) input data, were generated through the *geogrid* program of NPS.

2.3 Model Configuration Specifics

2.3.1 Domain Configuration

A 12-km North American parent domain with a 3-km one-way CONUS and Alaska nest (*nest_mode=1-way*) was used in this test (Fig. 1). While the parent domain was slightly smaller than the operational NAM

parent domain, the 3-km CONUS nest matched the 3-km NAM Rapid Refresh (RR) domain, and the 3-km Alaska nest replicated the coverage area of the operational 6-km Alaska nest. The outer domain was 875 x 815 grid points, while the inner CONUS domain was 1371 x 1100, and the inner-Alaskan domain was 595 x 625. The rotated latitude-longitude map projection was used, and the configurations had 60 vertical levels, with a pressure top of 10 hPa.

2.3.2 Model Configuration

The physics suite configurations for the NAMOC baseline configuration and the ThompsonMP replacement configuration are described in Table 4 below.

Table 4. Physics suite combination for the NAMOC and ThompsonMP configuration.

Parameterization	NAMOC	ThompsonMP Configuration
Microphysics	Ferrier-hires	Thompson
Radiation SW and LW	RRTM	RRTM
Surface Layer	MYJ	MYJ
Land-Surface Model	Noah	Noah
Planetary Boundary Layer	MYJ	MYJ
Convection	BMJ (parent only)	BMJ (parent only)

Select configuration options by domain are provided in Table 5 below.

Table 5. Select model configuration file settings

Option	d01	d02	d03	Description
dt_int	26 2/3	6 2/3	6 2/3	Integer seconds
secadv	True	True	True	2nd order advection
smag2	0.4	0.3	0.3	Smagorinsky constant for 2nd order diffusion
codamp	9.0	12.0	12.0	Divergence damping constant
wcor	0.18	0.18	0.18	Divergence correction factor
gwdflg	True	False	False	
spec_adv	False (True for Thompson)	True	True	
fres	0.75	0.25	0.25	Resolution factor for dsp's
fsl	0.85	0.75		Reduction factor for "slow" dsp's over land
fss	0.85	0.75		Reduction factor for "slow" dsp's over

				water
nphs	2	2	2	Number of dynamics timesteps between calls to landsurface and turbulence
nprecip	2	2	2	Number of dynamics timesteps between calls to convection and microphysics
nrads	45	180	180	Number of dynamics timesteps between calls to shortwave
nradl	45	180	180	Number of dynamics timesteps between calls to longwave

Appendix A provides relevant portions of the *model_configure* file.

2.4 Post-processing

The *unipost* program within UPP was used to destagger the forecasts, interpolate them to three separate grids depending on the domain (the 12-km parent was interpolated to G218, the 3-km CONUS nest to G187, and the 3-km Alaska nest to G91), generate derived meteorological variables, and vertically interpolate fields to isobaric levels. The post-processed files included two- and three-dimensional fields on constant pressure levels, both of which were required by the plotting and verification programs. Three-dimensional post-processed fields on model native vertical coordinates were also output and used to generate graphical forecast sounding plots.

3. Computational Efficiency

For the 84 initializations that ran to completion, the central processing unit (CPU) time required to run NEMS/NMMB for the two configurations was calculated to assess the increase in computational demands when running the two differing configurations (Fig. 2). This testing effort was conducted on an IBM system, and each model initialization was run on 1680 processors. Overall, a relatively consistent difference in computational run time between the NAMOC and the ThompsonMP configurations was noted, indicating the ThompsonMP configuration, on average, takes about 54% longer to run to completion. Due to ThompsonMP being more sophisticated, this increase in computational resources was expected.

4. Model Verification

The MET package was used to generate objective model verification. MET is comprised of grid-to-point verification, which was utilized to compare gridded surface and upper-air model data to point observations, as well as grid-to-grid verification, which was utilized to verify Quantitative Precipitation Forecast (QPF) and composite reflectivity. An additional type of grid-to-grid verification was also performed for this test using the series-analysis tool in MET which accumulates a metric of choice on a

cell-by-cell basis over a specified time period and can be used to quantify how model performance varies over the domain. This tool can be used to identify regional differences within a single configuration as well as to highlight differences between the two configurations. While traditional line series plots provide an overall statistic for a region, investigating metrics on a grid-by-grid basis can offer additional insight on the spatial distribution of errors. Verification statistics generated by MET for each retrospective case were loaded into a MySQL database. Data was then retrieved from this database to compute and plot specified aggregated statistics using routines developed by the DTC in the statistical programming language, R.

Several domains were verified for the surface and upper air, as well as precipitation variables. Area-averaged results were computed for the CONUS domain, East and West regions, 14 CONUS sub-regions, the full Alaska domain, and 2 Alaska sub-regions (Fig. 3). While only a portion of the full results will be discussed in detail for this report, all results are available on the DTC webpage established for this particular testing and evaluation activity (http://www.dtcenter.org/eval/meso_mod/nmmb_test/nems_v0.9/). In addition to the regional stratification, the verification statistics were also stratified by vertical level and lead time for the 00 UTC and 12 UTC initialization hours combined, and by forecast lead time and precipitation threshold for 00 UTC and 12 UTC initialized forecasts individually for surface fields in order to preserve the diurnal signal.

Each type of verification metric is accompanied by confidence intervals (CIs), at the 99% level, computed using the appropriate statistical method. Both configurations were run for the same cases allowing for a pair-wise difference methodology to be applied, as appropriate. The CIs on the pair-wise differences between statistics for the two configurations objectively determine whether the differences are statistically significant (SS); if the CIs on the pair-wise difference statistics include zero, the differences are not SS. Due to the nonlinear attributes of frequency bias, it is not amenable to a pair-wise difference comparison. Therefore, the more powerful method to establish SS could not be used and, thus, a more conservative estimate of SS was employed based solely on whether the aggregate statistics, with the accompanying CIs, overlapped between the two configurations. If no overlap was noted for a particular threshold, the differences between the two configurations were considered SS.

When testing with a robust number of cases, it is possible to get an increased number of SS pair-wise differences; however, the magnitude of the SS pair-wise differences can be quite small and not yield practically meaningful results. Therefore, in addition to determining SS, the concept of establishing practical significance (PS) was also utilized in this test. PS was determined by filtering results to highlight pair-wise differences greater than the operational measurement uncertainty requirements and instrument performance as specified by the World Meteorological Organization (WMO; http://www.wmo.int/pages/prog/gcos/documents/gruanmanuals/CIMO/CIMO_Guide-7th_Edition-2008.pdf). To establish PS between the two configurations, the following criteria were applied: temperature and dew point temperature differences greater than 0.1 K and wind speed differences greater than 0.5 m s^{-1}. PS was not considered for metrics used in precipitation (accumulation and composite reflectivity) verification [i.e., Gilbert Skill Score (GSS) or frequency bias] because those metrics are calculated via a contingency table, which is based on counts of yes and no forecasts.

4.1 Temperature, Dew Point Temperature, and Winds

Forecasts of surface and upper air temperature, dew point temperature, and wind were bilinearly interpolated to the location of the observations (METARs and RAOBS) within the NCEP NDAS prepbufr files. Objective model verification statistics were then generated for surface (using METARs) and upper air (using RAOBS) temperature, dew point temperature, and wind. Because shelter-level variables are not available in the model at the initial time, surface verification results start at the 3-hour lead time and go out 48 hours by 3-hour increments. For upper air, verification statistics were computed at the mandatory levels using radiosonde observations and computed at 12-hour intervals out to 48 hours. Because of known errors associated with radiosonde moisture measurements at high altitudes, the analysis of the upper air dew point temperature verification focuses on levels at and below 300 hPa. Bias and bias-corrected root-mean-square-error (BCRMSE) were computed separately for surface and upper

air observations. The CIs were computed from the standard error estimates about the median value of the stratified results using a parametric method and a correction for first-order autocorrelation.

4.2 Precipitation

For the QPF and simulated composite reflectivity verification, a grid-to-grid comparison was made. For QPF, the budget method was used to interpolate the precipitation analyses to G218 and G187, which conserves the total area-average precipitation amounts. For composite reflectivity, the nearest neighbor method was used to interpolate the radar mosaic data to G218 and G187. These regridded analyses were then used to evaluate the forecasts. Accumulation periods of 3 and 24 hours were examined. NCEP's Climatology-Calibrated Precipitation Analysis (CCPA) was used as the observational dataset for both the 3- and 24-hour precipitation accumulations, while the radar mosaic product generated at NCEP was used for the composite reflectivity. Traditionally 24-h QPF verification is performed at times valid at 12 UTC; therefore, the 24-hour QPFs were examined for the 24- and 48-hour lead times for the 12 UTC initializations and 36-hour lead time for the 00 UTC initializations. Traditional verification metrics computed, included the GSS and frequency bias. For the precipitation statistics, a bootstrapping CI method was applied.

5. Verification Results

The full suite of verification results produced in the testing and evaluation activity are available on the project webpage: http://www.dtcenter.org/eval/meso_mod/nmmb_test/nems_v0.9/. Due to the considerable amount of data and plots produced in the testing, the report presented here will focus on discussion of results for the CONUS nest (G187) and Alaska nest (G91) domains. This testing effort revealed many differences between the two configurations, with the largest differences typically seen in the mean error (bias) statistics. The first part of the evaluation will dissect configuration performance over the CONUS East and West regions for all temporal aggregations using the standard verification metrics; the second part of the evaluation will focus on the full Alaska domain. In addition to the time series plots provided, further investigation of forecast performance for both configurations over diverse regions of the CONUS is included. The bias at each observation station is presented by surface variable to provide a means to spatially assess the configurations performance respective to the observations. When visualizing the results in this manner, seasonal differences are apparent, both regionally and between configurations. On a similar note, precipitation verification scores will also be visualized by accumulating metrics on a grid-by-grid basis over a specified time period to quantify configuration performance over the domain. For the precipitation analysis, focus in this report will be on the 24-h accumulation period (i.e., at times valid from 12 UTC – 12 UTC).

Differences between the two configurations are computed by subtracting ThompsonMP from NAMOC. Since BCRMSE is always a positive quantity with a perfect score of zero, this results in negative (positive) differences indicating the NAMOC (ThompsonMP) configuration has a lower BCRMSE and is favored. Bias also has a perfect score of zero but can have positive or negative values; therefore, when examining pair-wise differences, it is important to note the magnitude of the bias in relation to the perfect score for each individual configuration to know which has a smaller bias and is, thus, favored. For GSS, the perfect score is one, and the no-skill forecast is zero and below with a lower limit of $-1/3$. Thus, when both configurations have skillful forecasts (i.e., GSS greater than zero), if the pair-wise difference is positive (negative), the NAMOC (Thompson) configuration has a higher GSS and is favored. Frequency bias has a perfect score of one, but as described earlier, SS is determined by the overlap of CIs attached to the aggregate value. A breakdown of the configurations with SS and PS better performance by variable, season, statistic, level, threshold, initialization hour, and forecast lead time aggregated over the CONUS domain is summarized in Tables 6-23 and for the full Alaska domain in Tables 24-29, where the favored configuration is highlighted. While some SS pair-wise differences will be highlighted, focus will be placed on PS pair-wise differences in this report.

5.1 CONUS Nest Upper Air Analysis

5.1.1 Temperature BCRMSE and Bias

In general, for all seasons and both regions, BCRMSE grows with forecast lead time (not shown) and has maximum values at 850 hPa and 200 hPa and above; an exception is noted at the longer lead times in the fall season in the West region, where all levels above 850 hPa have more uniform BCRMSE (Fig. 4). Wide CIs are noted for both configurations as well as the associated difference lines. Overall, minimal differences are seen, with none being PS (Tables 6, 14).

While the shape of the bias distribution is highly dependent on temporal aggregation, vertical level, and forecast lead time, two distinct trends emerge (Fig. 5). First, median values for both configurations at 850 hPa are consistently warmer in the East than the West. Second, ThompsonMP typically has lower median bias values from 850 hPa to between 700 – 400 hPa, depending on the season, which then transitions to NAMOC having lower median bias values up to 200 hPa. This leads to ThompsonMP having a more amplified bias distribution with height. Generally, the West and East regions have relatively similar distributions, with an exception in the fall season. In the West during fall, a cool bias extends to 500 hPa before transitioning to a warm bias at 300 hPa (Fig. 5a). In the East, the bias values for both configurations decreases with height to 700 hPa and from 400 – 150 hPa,both configurations have a neutral or cold bias (Fig. 5b). In the summer season, a large warm bias at 850 hPa exists for both configurations, with ThompsonMP being closer to the observations; with height, the bias decreases in magnitude (Fig. 5g,h). A large number of pair-wise differences are seen in the West, with PS pair-wise differences being dependent on season and vertical level (Table 6). For all seasons, any PS pair-wise differences at and above 300 hPa favor NAMOC, while those that favor ThompsonMP are at and below 400 hPa. In the fall and winter seasons, all PS pair-wise differences show NAMOC as the better performer. In the East, a number of pair-wise differences are seen with the highest concentration of PS pair-wise differences after the 12-h forecast lead time and in the low- to mid-levels (Table 14). At the 850 and 700 hPa levels ThompsonMP is the better performer, with exception to the winter season, where any PS pair-wise differences favor NAMOC. PS pair-wise differences in the middle- to upper-levels typically favor the NAMOC configuration.

5.1.2 Dew Point Temperature BCRMSE and Bias

Upper air dew point temperature BCRMSE indicates that for both configurations and temporal aggregations, a maximum in BCRMSE generally occurs at mid-levels (at and surrounding 500 hPa), with smaller values above and below (Fig. 6; forecast hour 48). BCRMSE ranges from around 4 – 8 ºC at lower and upper levels and approach 10 ºC at mid-levels, with larger values seen over the East. Very few SS or PS pair-wise differences are noted between the two configurations (Tables 7, 15). When they do occur, the favored configuration depends on region, season, level, and forecast hour, with no pair-wise differences for the summer aggregation.

Due to the large CIs about the median values, the dew point temperature bias with height often encompasses zero (Fig. 7). One consistent trend, however, is that near the surface, both configurations indicate a dry bias for the fall, summer and spring aggregations. Overall, while the shape of the distribution is similar between both configurations, ThompsonMP has a tendency to have higher median biases than NAMOC. Each seasonal aggregation has SS and PS pair-wise differences; however, the favored configuration varies by level and forecast lead time (Tables 7, 15). One consistent finding is that NAMOC is favored for both East and West in the spring and West for the summer, when there are SS/PS pair-wise differences.

5.1.3 Wind Speed BCRMSE and Bias

For both configurations, regardless of region, wind speed BCRMSE generally increases from a minimum at the lowest levels to a maximum around 300 – 150 hPa, with decreasing error further aloft (Fig. 8); this distribution is most prevalent in the summer and winter aggregations. As forecast lead time increases, the errors also tend to increase. Overall, very few differences between the two configurations are noted;

only an occasional SS pair-wise difference is noted, with more differences in the West than East, and none of the differences are PS (Tables 8, 16). Most often, when there is a SS pair-wise difference, ThompsonMP is the better performer.

In general, for all seasonal aggregations, a neutral-to-low wind speed bias is frequently observed at 850 hPa, which becomes higher in magnitude as pressure decreases up to 200 hPa (Fig. 9). The shape of the vertical bias distribution is more pronounced in the East compared to the West, where very large CIs frequently encompass zero. While there are no PS pair-wise differences between the two configurations (Tables 8, 16), there are several occasions of SS pair-wise differences. Across the East, NAMOC is most often favored, especially for the fall aggregation in the mid- to upper-levels. For the West, NAMOC continues to be favored more often; however, ThompsonMP is favored at the upper-most levels, especially in the winter, spring, and summer aggregations.

5.2 CONUS Nest Surface Analysis

5.2.1 Temperature BCRMSE and Bias

For both configurations, a diurnal signal in 2 m temperature BCRMSE is present in both regions and all seasons, but strength of the diurnal signal varies (Fig. 10). In the fall and winter, maximum errors are at and near the 12 UTC valid time (Fig. 10a-d); conversely, in the summer, maximum BCRMSE values are at times surrounding the 21 – 00 UTC valid times (Fig. 10g,h). The spring season displays a double peak structure that appears to be a blend of the surrounding winter and summer seasons (Fig. 10e,f). Distributions between the two configurations are very similar which is reflected in the SS/PS pair-wise difference tables (Tables 9, 17). Several SS pair-wise differences are noted in both regions, but none are PS. In general, in the West, most SS pair-wise differences favor ThompsonMP and occur most frequently at times valid around 21 – 00 UTC. NAMOC is typically the better performer in the East region, with an exception to the summer, where ThompsonMP has lower errors.

Both configurations, for both regions and all seasons, have a marked diurnal signal (Fig. 11) in the 2 m temperature bias time series. Overall, NAMOC has higher median bias values than the ThompsonMP configuration; another common finding is that the East region typically has warmer biases than the West. For all seasons, the largest differences between the two configurations are typically seen during the daytime hours, with differences between the configurations growing with forecast lead time. It is also important to note that the confidence intervals are generally wider in the winter and surrounding transition seasons than in the summer. In the fall and winter seasons, the highest biases are at times valid at and around 12 UTC, while the lower biases are at valid times surrounding 21 – 00 UTC (Fig. 11a-d). In the spring and summer seasons, a reversed signal is seen, with lowest bias values around times valid between 09 – 12 UTC, with the highest bias values at times valid from 18 – 21 UTC (Fig. 11e-h). For the summer season, at all forecast lead times, both configurations have a SS high bias; similar behavior is noted for the East region in the spring, where a majority of lead times have a high bias for both configurations. With NAMOC generally having higher median biases than ThompsonMP for all seasons and in both regions, the favored model is dictated by the sign of the bias. When considering bias for the West, most differences are PS, with the favored configuration depending on season and forecast lead time (Table 9). In the summer season, when there is a warm bias, any PS pair-wise differences show ThompsonMP being closer to the observations. In the winter season, when there is a cold bias during the day, PS differences are typically seen at valid times of 18 – 00 UTC and show NAMOC as the better performer. In the fall, several times at and around 00 UTC favor NAMOC with most other times favoring ThompsonMP. Spring is dependent on initialization hour, but overall ThompsonMP is favored more often. In the East, a majority of the pair-wise differences are PS, with ThompsonMP overwhelmingly the better configuration (Table 17). The only notable exception is in the winter season when NAMOC is the better performer at times valid around 15 – 03 UTC.

A number of regional trends for temperature bias distribution are seen across all seasons and for both configurations (Fig. 12). The 42-h forecast was chosen to highlight areas where some of the largest differences were seen. In general, for all seasons, the NAMOC has higher mean biases across the CONUS with the East region typically having higher mean biases than the West region; this relates well to

the time series verification (recall Fig. 11). In the transition seasons (Fig. 12a-b,e-f), a gradient going from cool to warm biases progressing south in the East is present. In the winter season, there is predominantly a cold bias covering most of the CONUS, with a concentration of cold bias values in the lower Midwest, eastward through the Appalachian Mountains; in these areas ThompsonMP has larger cold biases than NAMOC. In the summer season, a prominent warm bias is noted, with the largest warm biases (most points exceeding 4ºC) in the East region. In the West region, the largest warm bias values are seen in the Great Plains and the Rocky Mountain region for both configurations.

5.2.2 Dew Point Temperature BCRMSE and Bias

The time series plots for 2 m dew point temperature (Fig. 13) show a gradual increase in BCRMSE through the 48-hr forecast window for both regions and each seasonal aggregation, with spring and summer indicating a stronger diurnal cycle than the other two seasons. When looking at pair-wise differences, NAMOC is occasionally favored in the early portion of the forecast period, especially for 00 UTC initializations (Tables 10, 18); ThompsonMP is favored more often later in the forecast period, especially for the spring and summer aggregations. The smallest number of pair-wise differences occurs during the winter aggregation. When pair-wise differences are noted, they are SS with exception to one instance, which is PS.

With the exception of winter, the 2 m dew point temperature bias values are wet to neutral during the first 12 hours, and then transition to a strong dry bias later in the forecast period, especially across the East (Fig. 14). Bias changes with time also reflect a strong diurnal cycle, which limits the dry bias during the night, and then increases the dry bias during the day; this is especially true for the summer aggregation. The winter aggregation dew point temperature bias shows a moist bias over both the East and West for all forecast hours. A diurnal cycle is still present in these plots, with an increasing moist bias during the day to decreasing bias overnight. SS pair-wise differences occur more frequently in bias compared to BCRMSE and several of the differences in the summer aggregation are PS in the East (Table 18). For the 00 UTC initializations across all seasonal aggregations over the East in the first 12 hours (except spring where there are no SS pair-wise differences during this time), the NAMOC is often favored with SS. For later forecast hours and all seasons (except winter where there are fewer pair-wise differences), ThompsonMP is favored. A similar trend is seen in the West (Table 10), except there are even fewer pair-wise differences in the winter and only one instance is PS. Regardless of region, if PS pair-wise differences are noted, they all favor ThompsonMP.

Spatial plots provide a valuable way to visualize the 2 m dew point temperature bias and these can be found for all four seasonal aggregations for the 42-hr forecast in figure 15. A strong eastern dry bias is clearly evident for both NAMOC and ThompsonMP schemes for fall, spring, and summer; the dry bias is concentrated in the southeast for the fall and spring, but expands northward and into a large portion of the western US for the summer aggregation. There is also a marked dry bias in the western coastal valleys for these seasons as well. The winter aggregation indicates a moist bias for both schemes, especially within the intermountain west and away from the coasts, with a dry bias evident in the coastal valleys of the West and extreme southeastern United States.

5.2.3 Wind BCRMSE and Bias

For 10 m wind speed BCRMSE, median values range from about 1.3 to 2.4 m s^{-1}; the lowest errors are seen for the East region during the summer while the highest errors are across the West region during the spring (Fig. 16). A small diurnal signal is noted during the summer and spring aggregations for both regions with a small increase in error with lead time. The errors are largest for valid times between 21 – 03 UTC, while the smallest errors are around 12 UTC. In contrast, there is very little diurnal signal during the winter aggregation, and the values are nearly constant with forecast lead time. No PS pair-wise differences are seen (Tables 11, 19); however, occasional SS pair-wise differences are noted. A majority of the SS pair-wise differences favor the ThompsonMP configuration; the most frequent exception is during the winter aggregation for the 12 UTC initializations where NAMOC is favored. The fewest number of SS pair-wise differences occur during the winter and spring aggregations, with the most found in the summer aggregation.

A prominent diurnal signal in bias is seen for all temporal and regional aggregations for 10 m wind speed bias, with the largest values typically seen at times valid around 06 – 09 UTC and the lowest values near 18 – 21 UTC (Fig. 17). With only a couple of exceptions during the late afternoon hours for the winter aggregation, a high bias is noted at most forecast lead times across the East region. In general, the NAMOC has higher wind speed bias across this region, so when there are SS pair-wise differences, ThompsonMP is often favored (Table 19). The main exception is during the winter aggregation where NAMOC is frequently favored. Across the West region, the overnight bias values during the summer and fall are generally high but are neutral-to-low for the winter and spring aggregations (Fig. 17). During the daytime, the wind speed bias is often negative, with exception to summer where the CIs on the NAMOC frequently encompass zero. Similar to the East, it is noted that the NAMOC tends to have higher wind speed values for the West region. This leads to the NAMOC typically being favored when SS pair-wise differences are noted between the two configurations (Table 11). The most frequent exception is during the summer aggregation, where ThompsonMP is favored occasionally. For both regions, there are no PS pair-wise differences, and most SS pair-wise differences occur during the daytime hours.

While there are several statistically significant differences between the two configurations, the spatial differences of wind speed bias are small across the CONUS. Figure 18 illustrates the 42-hour forecast lead time mean wind speed bias by observation station for each season. For the spring, summer, and fall aggregations, a clear signal of a high bias across the East is noted; there is an obvious increase in low bias values over the East region during the winter aggregation. Across the West, a low bias is generally seen in the Northern Plains and Rocky Mountain regions especially during the fall, winter, and spring, while a high bias persists for most seasons along the West Coast. In general, a slight shift towards higher bias values is noted CONUS-wide for NAMOC compared to ThompsonMP.

5.2.4 Daily Precipitation GSS and Bias

In general, GSS for 24-h accumulated precipitation (accumulation from 12 – 12 UTC) decreases with increasing threshold for both initializations, configurations and regions for all lead times (Fig. 19). The base rate also decreases significantly from the lowest threshold of >0.01" to the >0.25" threshold and then gradually decreases to near zero by the highest threshold of >3". The CIs that encompass the aggregated values for both configurations as well as those associated with the difference curve are large, with ThompsonMP CIs generally larger than those for NAMOC. While the aggregated GSS values are generally higher for ThompsonMP at the lowest threshold (>0.01"), the only SS pair-wise difference observed is in the West during the summer (Table 12). When comparing the higher thresholds, the only SS pair-wise difference between the two configuration is at the >2" threshold in the East during the fall (Table 20).

When considering frequency bias for the two configurations (Fig. 20), high aggregated bias values are frequently observed regardless of initialization, forecast hour, region, or seasonal aggregation. Two notable exceptions include aggregated values for both configurations across the East for most thresholds in the fall and for the lowest thresholds in the summer. A general trend of increasing bias with increasing threshold is noted for a majority of the forecast hours, for both configurations and initializations. As was seen for GSS, CIs are often larger for ThompsonMP compared to NAMOC, with width of the CIs growing with increasing threshold. In most cases, the NAMOC has a higher aggregated bias value than ThompsonMP; however, the only SS pair-wise differences are for the lowest threshold during summer in the West and the highest threshold during the winter in the East , both favoring ThompsonMP (Tables 12, 20).

The series-analysis tool available in MET was run to calculate base rate, GSS and frequency bias on a grid-by-grid basis with the goal of identifying regional differences for a single configuration as well as differences between the two configurations. The lowest threshold of 0.01" was chosen due to the high frequency of events across much of the CONUS. The series-analysis discussion will focus on the summer aggregation for the 12 UTC initializations, 48-h forecasts due to the fact that there were SS pair-wise differences noted for the >.01" threshold in both GSS and frequency bias for that particular aggregation (Table 12).

The base rate at 0.01" in the summer of the 48-hour forecast for the 12 UTC initialization (Fig. 21) is characteristic of typical summer time convection, with higher base rates observed over areas of higher terrain where it is common to see daily orographic convection due to differential heating. Large base rates are also observed over the Florida peninsula where daily sea breezes initiate convection, as well as in the Gulf of Mexico Coast and eastern Midwest and Lower Mississippi Valley regions. Low base rates in California and parts of Texas and Oklahoma correlate with regions of extreme drought conditions (per the U.S. Drought Monitor) during 2014. A low frequency of events was also observed in a region over Minnesota and North and South Dakota. In regions where base rate is zero, GSS and frequency bias statistics cannot be computed, since there are no events.

A comparison of GSS spatially for each configuration during the summer shows that ThompsonMP exhibits higher GSS values than NAMOC nearly CONUS-wide (Fig. 22, left column). When examining the difference plot, high spatial variability in noted, with ThompsonMP having higher GSS more frequently. This further reinforces what was observed in the threshold plots where ThompsonMP was consistently higher at the lowest threshold. As noted before, even though differences are observed across much of the CONUS, only the western region was SS at the 48-hour forecast time (Table 12) and favored ThompsonMP.

Frequency bias is generally low across all sub-regions during the summer for the 48-hour forecast for both configurations (Fig. 22, right column). Regions with higher frequency bias tend to be co-located with areas of low base rate, such as the Northwest, portions of Texas and Oklahoma, and the border of Minnesota, North Dakota, and South Dakota. When considering differences between the two configurations, ThompsonMP exhibits higher frequency bias values across much of the CONUS, with noted exceptions along the eastern coast south to southern Texas, and parts of Kansas and Minnesota where NAMOC is higher. While differences are seen across the CONUS, the only SS is over the western region, favoring ThompsonMP, similar to GSS (Table 12).

5.2.5 Composite Reflectivity GSS and Bias

When looking at time series plots of aggregated GSS for composite reflectivity, values are generally between 0.1 and 0.4 with higher values seen over the East, which also exhibits a higher base rate, compared with the West (Fig. 23). During the winter aggregation for both initializations, ThompsonMP has consistently higher aggregated GSS values than NAMOC for all forecast lead hours at the ≥ 10 dBZ (Fig. 23c,d) and ≥ 20 dBZ thresholds (not shown); however, no SS pair-wise differences are noted (Tables 13, 21). During the spring and fall aggregations for both initializations, ThompsonMP continues to have higher median GSS values for a majority of forecast lead times at the ≥ 10 dBZ threshold; however, again, no SS pair-wise differences are noted for either threshold. For the summer aggregation, ThompsonMP is more frequently higher than NAMOC, with differences between the aggregated GSS values smaller. The only SS pair-wise difference for the summer is observed at the 48-h forecast lead time in the East 00 UTC initialization at both thresholds, where NAMOC is the better performer. For higher thresholds (≥30, ≥40, and ≥50), where the base rate is near-zero with minimal events, SS is not evaluated.

With very few exceptions when examining frequency bias by forecast lead time for season, region, or threshold, while both configurations show a general high bias, the aggregated values for NAMOC are larger than ThompsonMP (Fig. 24). A diurnal signal is noted in the time series, mainly in the West for fall, spring and summer, with higher frequency bias values between 06 – 18 UTC and lower values between 21 – 03 UTC. A diurnal signal of opposite sign is noted in base rate, as well. Overall, the frequency bias values tend to be highest for the West region, with the highest during the winter aggregation, while the smallest values are noted in the East, with the lowest during the summer aggregation. All SS pair-wise differences found at the ≥ 10 and ≥ 20 dBZ threshold favor ThompsonMP (Tables 13, 21). For the ≥ 10 dBZ threshold, there are SS pair-wise differences at most all forecast lead times in the winter across the East and in the spring across the West for both initializations, with a similar trend but fewer SS pair-wise differences at the ≥ 20 dBZ threshold. The fewest pair-wise differences occur in summer for both regions and thresholds.

5.3 Alaska Nest Upper Air Analysis

5.3.1 Temperature BCRMSE and Bias

For BCRMSE over the full Alaska domain (Fig. 25), the largest errors are at 850 and 200 hPa, with the lowest errors typically at levels in between. In general, for both configurations and the difference between the two, the confidence intervals are wide, with the narrowest CIs in the summer. The high variability is reflected in the significance testing, where there are very few SS and no PS pair-wise differences (Table 22). When there are pair-wise differences, ThompsonMP is most often favored; no pair-wise differences are present in the winter season.

For all seasons, ThompsonMP has lower median temperature bias values from 850 hPa up to and around 500 hPa, where ThomsponMP transitions to having higher median bias values than NAMOC up to and around 300 hPa (Fig. 26). From 200 hPa and above, both configurations have a neutral-to-cold bias by the 48-h forecast lead times; these general trends are similar to what was observed in the CONUS East and West regions. In all but the summer season, there is generally a warming trend with height for both configurations until 300 hPa, where temperatures then have a cooling trend up to 150 hPa, above which there is a sharp reversal. At the 48-h forecast lead time, both configurations during the summer season have a warm bias at 850 hPa that gradually decreases with height until 500 hPa; above 500 hPa, the distribution is similar to all other seasons. A large number of SS and PS pair-wise differences are seen in the full Alaska domain, with all PS differences occurring at and below 300 hPa. For PS pair-wise differences, with exception to the summer, where ThompsonMP is the better configuration at low- to middle-levels, NAMOC is the better performer in all other seasons (Table 22).

5.3.2 Dew Point Temperature BCRMSE and bias

The Alaska upper air dew point BCRMSE profiles (Fig. 27) show a similar maximum in error in the mid-levels (500 – 700 hPa) as was seen for the CONUS. In general, the pair-wise differences that occur in the summer and spring at the lower levels favor ThompsonMP, while for the fall, winter and spring the SS/PS differences in the upper levels favor NAMOC (Table 23).

Generally, dew point biases with height tend to be smallest at lower (~850 hPa) and upper levels (~300 hPa) and positive (i.e., wet) in mid-levels for both schemes (Fig. 28). For the summer aggregation, pair-wise differences favor NAMOC in all cases and the differences are PS at 300 hPa (Table 23). For fall, winter, and spring, ThompsonMP is favored with PS for nearly all lead times at 300 hPa. At lower levels, the favored configuration depends on season, level, and lead time.

5.3.3 Wind Speed BCRMSE and bias

Similar to the CONUS discussion, both configurations, regardless of season, indicate a general increase in BCRMSE from the lowest levels to around 300 hPa, with decreasing error further aloft (Fig. 29) for the AK nest. The errors tend to be larger for the fall and winter aggregations compared to the spring and summer aggregations and generally increase with lead time. Again, very few differences between the two configurations are noted with none in the spring aggregation (Table 24). None of the pair-wise differences are PS.

For bias (Fig. 30), the median values for many levels, especially between 700 – 200 hPa, are typically negative; however, the CIs are often very large and encompass zero. The vertical distribution is generally the same regardless of season and the values do not change much with forecast lead time. While there are no PS pair-wise differences between the two configurations (Table 24), there are several occasions of SS pair-wise differences. The NAMOC is favored at levels 300 hPa and below, while the ThompsonMP is most often favored at 200 hPa and above. The fewest pair-wise differences are noted in the winter and the most in the spring and summer.

5.4 Alaska Nest Surface Analysis

5.4.1 Temperature BCRMSE and Bias

For 2 m temperature BCRMSE, all configurations show a general increase in error throughout the forecast period (Fig. 31). In the fall and winter seasons, there is a prominent diurnal signal, with the highest errors at times valid from 06 – 15 UTC and the lowest BCRMSE values at times valid from 18 – 03 UTC. Minimal to no diurnal signal is seen in the spring and summer seasons, with spring having a slightly stronger signal than summer with peak biases at times valid at 12 UTC. This result may be a product of the high variability in latitude within the domain as well as time of year; during the spring and summer seasons, the sun angle allows for differing periods of light, twilight and darkness and may result in a complicated diurnal signal when considering the full domain. In general, distributions of the BCRMSE values are similar between the two configurations, and this is reflected in the statistical significance (Table 25). The largest differences occur in the winter season for the 00 UTC initializations, where NAMOC is PS better than ThompsonMP for the 30 – 42 hour forecast lead times. While only SS, it is worth noting that ThompsonMP has lower errors at a number of lead times during the summer for both 00 and 12 UTC initializations.

Both configurations for all seasons had an amplified diurnal signal when considering 2 m temperature bias (Fig. 32). Typically, for all seasons, the highest bias values are generally between valid times of 09 – 12 UTC, with lowest values around times valid from 21 – 00 UTC. When differences between the configurations exist, ThompsonMP typically has lower bias values than NAMOC. This translates into the better performing configuration depending on the sign of the bias, which often changes by season and forecast lead time. Most PS pair-wise differences are in the summer and spring, and no PS differences occur in the winter (Table 25). In the summer, all PS pair-wise differences favor the ThompsonMP configuration, where both configurations have median biases above 0 (i.e., warm bias). In the spring and fall, time-of-day dictates which configuration is the better performer. In the spring, NAMOC is favored at times valid from 18 – 03 UTC, while ThompsonMP is closer to the observations at and around times valid at 12 UTC; trends in the fall are similar but have less PS pair-wise differences.

For the point verification, trends are similar to what is seen over the CONUS. Generally, spatial distributions are consistent between the two configurations, but NAMOC has larger bias values compared to ThompsonMP (Fig. 33). In the fall, both configurations have neutral-to-cool biases along the western portion of Alaska as well as most coastal areas (Fig. 33a,b). Warm biases are seen along the interior East part of the state and into Canada. Similar patterns are seen in the winter; however, the cold bias strengthens in the western part of Alaska, and the warm bias is enhanced in Eastern Alaska (Fig. 33c,d). In spring, there is an overall shift toward cooler biases across the south and Eastern portions of the domain (Fig. 33e,f). Warmer biases are seen in the summer throughout most areas of Alaska, with NAMOC having higher overall biases (Fig. 33g,h). The warmest biases are seen in the interior part of Alaska, with cooler biases along the coastal regions.

5.4.2 Dew Point Temperature BCRMSE and Bias

The spatially aggregated time series analyses for the full Alaska domain are shown in figure 34 for the 00 UTC initializations and all four seasons for 2 m dew point BCRMSE. Lower BCRMSE values are noted for the transition seasons of fall and spring, while winter and summer have larger values and a more prominent diurnal signal with the variation. BCRMSE shows a general increase with increasing forecast lead time, similar in magnitude to that seen for CONUS. The fewest pair-wise differences between the two configurations occur during the fall and spring aggregations (Table 26). For the summer aggregation, when there are pair-wise differences, ThompsonMP is favored with SS. The opposite is true for winter, where there are several PS pair-wise differences favoring NAMOC.

A diurnal signal in 2 m dew point temperature bias is evident in all temporal aggregations except winter (Fig. 35). A moist bias is generally noted for every temporal aggregation except summer, which has a dry bias that increases in severity with forecast lead time. When looking at pair-wise differences (Table 26), with a few exceptions during the 12 UTC initializations, the NAMOC configuration is favored with SS for

the fall and winter aggregations, a few of which are PS in the winter. For the summer and spring aggregations, ThompsonMP is favored with SS for all but one of the times when pair-wise differences are noted.

The spatial bias plots for forecast hour 42 (Fig. 36) indicate that, for fall, there is no clear pattern to bias distribution for either configuration, but it has an overall moist bias. The winter aggregation shows a dry to moist transition in bias from southwest to northeast, while a gradually increasing moist bias from south to north is apparent for spring. Finally, a very clear dry bias increasing from west to east is seen for summer. In general, the two configurations have similar spatial distributions of dew point temperature bias with the only differences coming in the magnitude of the values.

5.4.3 Wind BCRMSE and Bias

For 10 m wind speed BCRMSE, a weak diurnal signal is noted during the summer aggregation, with a peak in error around 00 UTC and a minimum near 12 UTC, while all other seasons show consistent BCRMSE values across the forecast lead times (Fig. 37). While none of the pair-wise differences are PS, there are a number of differences that are SS (Table 27). All pair-wise differences favor the ThompsonMP configuration for the 00 UTC initializations. The same is true for the summer and fall aggregations from the 12 UTC aggregations; however, during the winter and spring the NAMOC is favored when there are pair-wise differences.

The bias distribution for 10 m wind speed aggregated over the Alaska domain varies by seasonal aggregation (Fig. 38). For the fall aggregation, a fairly consistent high bias is noted for most forecast lead times, and the diurnal signal is weak. While the diurnal signal becomes a little more pronounced for the winter aggregation, the large CIs about the median frequently encompass zero. A distinct diurnal signal is present in the spring aggregation with neutral-to-high wind speed biases seen overnight and low wind speed biases noted during the day. Finally, the summer aggregation trends back toward a high bias for many forecast lead times with the exception of a few during the day that have CIs encompassing zero. Again, while there are no PS pair-wise differences, there are several SS pair-wise differences; the favored configuration depends on season and valid time (Table 27). In generally, the NAMOC is favored during the spring, while ThompsonMP is more often favored during the summer. The fewest SS pair-wise differences occur during the fall and winter aggregations.

Spatial distributions of the 10 m wind speed bias aggregated at each observation station illustrate the similarities between the two configurations (Fig. 39). Overall, the bias values are highest for the fall and summer at the 42-hour forecast lead time, and lowest for the spring. Regionally, the southern Alaskan region typically has higher wind speed biases than the northern Alaska region, especially during the fall and winter. Winter (and to a lesser extent, fall) spatial plots clearly illustrate why the CIs are wide in the time series plots; a large variation in high and low bias values are noted across the domain.

6. Configuration Comparisons

Apart from the atmospheric temperature, dew point temperature, and wind fields, additional model variables, which describe the simulated planetary boundary layer (PBL) height, radiation, and heat fluxes, were examined and compared for the two configurations for the CONUS nest domain. Since gridded observations of these variables are not readily available, no verification or evaluation against observations is attempted for these variables. Instead, discussion is included on the differences between the fields due to different microphysics schemes used in NMMB. Differences between the two configurations were calculated by subtracting ThompsonMP from the NAMOC.

6.1 Planetary Boundary Layer (PBL) Height

In all temporal aggregations, both configurations displayed pronounced daily variations in PBL height with shallower PBL heights observed overnight as the surface layer became more stable, and PBL heights

growing to maximum values with peak solar heating in the afternoon hours. Both the 36-h forecast (valid 12 UTC) and the 42-h forecast (valid 18 UTC) are discussed, which is when approximate minimums and maximums of PBL heights are found, respectively, for the fall, winter, spring and summer.

During the fall aggregation at the 36-h forecast lead time (Fig. 40, left column) the shallowest PBL heights are located over the Mountain regions westward and in the Southeast Coast, while higher heights are observed in the Midwest. Differences between the plots show ThompsonMP generally having higher PBLs compared to NAMOC, especially in regions where the PBL is deepest. For the 42-h forecast (Fig. 40, right column), lower PBLs are observed over the same regions as the 36-h time, excluding the Southern Mountain region. An increasing depth in PBL height from the northwest to the southeast is seen, with heights along the Southeast Coast over 1500 m. Unlike the 36-h forecast, the configuration with the deepest heights, seen over much of the east CONUS, is NAMOC with differences often exceeding 200 m.

For the winter aggregation at the 36-h forecast lead time (Fig. 41, left column), PBL height is again distributed similarly across the CONUS, with notable differences between the two configurations mainly observed within the Northern Plains, Midwest and eastern Lower Mississippi Valley where ThompsonMP is higher. The lowest heights are observed over the southwest, which also exhibit the lowest magnitude configuration differences, while the highest heights are found just east of the Rocky Mountains, across the southern Midwest, and up to the western edge of the Appalachians. Similar to the 36-h forecast, the 42-h forecast (Fig. 41, right column) has a narrow strip of elevated PBL heights east of the Rocky Mountain slopes; elevated heights are also seen along sections of the East Coast. Spatial differences between the two configurations at this forecast hour show NAMOC exhibiting a deeper PBL across much of the southern CONUS, while the only notable region where ThompsonMP is deeper is a swath extending from the northwest Northern Plains, eastward into the Midwest. The areas of the Gulf of Mexico Coast and the Southeastern Coast, where NAMOC shows a deeper boundary layer, correlate with 2 m temperature bias, which revealed that ThompsonMP exhibited larger cold biases over this region (Fig. 12). Conversely, a correlation between the swath of higher ThompsonMP heights through the Northern Rocky Mountain region and the Midwest and 2 m temperature bias is not evident.

PBL depths seen during the spring at the 36-h forecast (Fig. 42, left column) are similar in magnitude to those observed during the winter, with notable differences in spatial distribution. The shallowest heights are found over the Mountain regions westward while deeper PBL heights extend from the Plains regions eastward, with the deepest PBLs located over the coast of North and South Carolina, Virginia and Oklahoma. When comparing the two configurations, differences show ThompsonMP having a deeper PBL more often; however, there is high variability spatially. At the 42-h forecast lead time (Fig. 42, right column) the deepest PBLs are found in the southeast CONUS and the Southern Plains; heights are shallower over the north CONUS compared to the south CONUS, with the shallowest still observed along the West Coast. At this forecast hour, NAMOC has larger PBL depths across much of the CONUS.

During the summer, at the 36-h forecast lead time (Fig. 43, left column), the PBL height distribution across the CONUS is quite similar for both configurations. Since this forecast is in the early morning hours, PBL differences from disparities between radiation handling within the different microphysics schemes would be minimal. The shallowest heights, around 150 m, are observed over the West, from the Rocky Mountains across to the West Coast, while the deepest heights can be seen mainly within the eastern coastal regions of GMC, SEC and NEC. Larger differences between the two configurations are observed within the central CONUS regions including MDW, LMV, GMC and the plains; however, they are highly variable spatially. At forecast hour 42 (Fig. 43, right column), for both configurations throughout much of the East, PBL heights have grown to values exceeding 2500 m, while heights decrease westward to around 700 m along the West Coast. Similar to the 36-h forecast lead time, smaller differences are generally observed from the Rocky Mountains westward. On the other hand, a majority of the other regions show NAMOC having higher heights, with only small pockets where ThompsonMP heights are higher, mainly in the Central Plains. This relates to the discussion on downward shortwave radiation (DSWRF; 6.3.1) where ThompsonMP shows a reduction in DSWRF over these regions (Fig. 55), which would lead to the decreased PBL height compared to NAMOC. These results also correlate with the distribution results of 2 m temperature bias discussed previously (Fig. 11); higher mean

temperature biases were observed over the East compared to the West, and grew in magnitude from the 36-h to 42-h forecast, with NAMOC having a higher mean bias at the 42-h lead time.

6.2 Surface Heat Fluxes and Energy Budget

6.2.1 Latent Heat Flux (LH)

During the fall for the 00 UTC initializations at the 42-h forecast lead time (Fig. 44), the highest LH is observed over LMV, extending into parts of MDW and Southern Plains regions; the coastline of GMC also sees higher LH. A look at the spatial differences between the two configurations shows that NAMOC has higher LH than ThompsonMP, especially in SPL, MDW, APL, and southern Texas. This however, does not correlate with findings on comparisons of 2 m dew point temperature bias (Fig. 14), where ThompsonMP had less of a dry bias compared to NAMOC (i.e. ThompsonMP had higher dew points), for both the East and West regions.

Lower LH is seen during the winter compared to summer (Fig. 45); a similar LH distribution is observed over the West with low (near-zero) values found along the coast and the highest values over the mountain regions. The East generally has low LH in the northern regions and higher LH in the southern regions, excluding Florida, with a narrow tongue of higher LH extending along the Northeast Coast. Differences between the two configurations are again < 20 Wm^{-2} and show NAMOC having higher LH CONUS-wide, especially in the East over the regions where LH is highest. Recall that at this forecast lead time over the East, the NAMOC had higher moist dew point temperature biases than ThompsonMP, which were SS favored (Fig. 14d).

The spring aggregation for the 42-h forecast lead time (Fig. 46) has the highest LH values, exceeding 150 W m^{-2} extending north-south over the Mississippi Valley. Higher LH is also extends from the upper Mississippi valley, west, into NMT. Differences between the two configurations are generally found over the northern CONUS as well as along the Mississippi Valley, with NAMOC producing higher LH values compared to ThompsonMP. Recall 2 m dew point temperature bias (Fig. 14) showed that, over the East, NAMOC had a SS lower dry bias at forecast hour 42; however, over the West ThompsonMP had a lower dry bias.

The distribution of latent heat flux (LH) averaged for the 42-h forecasts from the 00 UTC initializations during the summer is similar for both configurations (Fig. 47), with values across much of the Eastern CONUS region less than 50 W m^{-2}. High fluxes (with values exceeding 100 W m^{-2}) are observed over parts of the Rocky Mountain and Plains regions as well as small areas in LMV and GMC, while lower (near-zero) LH is observed over the West Coast, MDW, APL and northern NEC. Differences between the configurations are most always < 20 W m^{-2}, with the smallest differences found in regions of lowest LH. In the East, NAMOC has higher latent heat, especially across the GMC and SEC regions, while there is small spatial scale variability across the West. The small values of LH across the East may be related to the overall dry bias seen in the 2-m dew point temperature bias plots (Fig. 15g,h). On the other hand, across the West, the 2-m dew point temperature bias varies more with location; a dry bias is seen along the West Coast, where LH values are smallest, and a wet bias is noted across SWD northeast into NMT, where LH values are larger.

6.2.2 Sensible Heat Flux (HFX)

Sensible heat flux (SHTFL) analysis between NAMOC and ThompsonMP was conducted using the 42-hr forecasts from the 00 UTC initializations, as this forecast time allowed for simultaneous exposure to sunlight for the entire CONUS, and therefore the potential for positive SHTFL across the domain. Figures 48-51 show the mean SHTFL for the all four seasonal aggregations for both the NAMOC and ThompsonMP configurations, as well as the difference between the schemes. With no gridded verification available for SHTFL for this analysis, surface temperature bias (related to sensible heat flux) and the difference field between the configurations were used to assess changes between NAMOC and ThompsonMP configurations.

SHTFL exhibits seasonal differences, with higher values for both NAMOC and ThompsonMP in the spring (Fig. 50) and summer (Fig. 51), with the exception of the desert southwest, the Southeast and Florida, which have higher SHTFL in the fall (Fig. 48) and winter (Fig. 49) for both schemes. Maximum SHTFL can be found in Texas and the Southern Plains during the spring, and over the Southeast and Florida during fall and winter. During the spring, the upper Midwest and Plains into the northern Rocky Mountains have the smallest SHTFL values of the year.

Mean seasonal differences between the schemes generally indicate a lower CONUS-wide SHTFL during the spring and summer for the ThompsonMP configuration, with the strongest differences occurring over the central Plains in the spring and the southeastern United States during the summer. Similar to what is seen with DSWRF, the lower SHTFL values for ThompsonMP are associated with a reduction in surface temperature bias (Fig. 12e-h) when compared to NAMOC surface temperature bias. Fall and winter differences show lower SHTFL overall for ThompsonMP, with the largest differences occurring across the Upper Midwest (fall only), the South and the Gulf Coast. During the winter, northern CONUS SHTFL remains similar to that found when using the NAMOC scheme. For southern regions of the CONUS, these reductions are associated with a stronger cold bias in surface temperature for ThompsonMP compared to NAMOC when compared against surface temperature observations (Fig. 12c,d). While SHTFL differences between schemes in the winter are minimal in more northern regions, such as the Midwest, these regions still exhibit a stronger negative cold bias in surface temperature than for NAMOC. This finding suggests that other sources of cooling may be at work.

6.3 Radiation

6.3.1 Short-wave Radiation (SW)

To analyze the differences in downward shortwave radiation flux (DSWRF) between NAMOC and ThompsonMP, the 42-hr forecast of the 00 UTC initialization was chosen, as all areas over the CONUS experience some amount of solar radiation at this time. Figures 52-55 show the mean DSWRF for all four seasonal aggregations for each configuration as well as the difference between the two schemes. Since there is no gridded verification available for DSWRF, the difference field, along with surface temperature bias (temperature is strongly related to downward SW), is used to assess contrasting forecasts between NAMOC and ThompsonMP.

The mean DSWRF plots highlight seasonal differences, with higher values for both NAMOC and ThompsonMP in the summer (Fig. 55) compared to winter (Fig. 53), but some of the strongest DSWRF occurred for both configurations in the desert southwest during the spring (Fig. 54). The smallest amount of DSWRF was seen in the northern tier states for fall (Fig. 52), winter, and spring, especially the Pacific Northwest, whereas the North Carolina coast had the lowest DSWRF in the summer.

Mean seasonal differences (NAMOC-ThompsonMP) between the schemes indicate a generally lower CONUS DSWRF in the spring and summer for ThompsonMP, with the strongest differences occurring over the Upper Midwest for the spring, and the southeastern United States and the eastern seaboard for summer. These lower DSWRF values for ThompsonMP are associated with a reduction in a warm surface temperature bias (see Fig. 12e-h) CONUS-wide when compared to NAMOC surface temperature bias. The fall and winter DSWRF differences also show an overall CONUS reduction in DSWRF for ThompsonMP, especially over the Upper Midwest and Texas in the fall, and the Ohio River Valley, South Florida and the southern states for Winter. However, these reductions are associated with a stronger cold bias in surface temperature for ThompsonMP compared to NAMOC when verified against observations (Fig. 12a-d).

6.3.2 Long-wave Radiation (LW)

For all seasons, spatial distributions are similar between the two configurations, but NAMOC typically has higher upward longwave radiation across much of the CONUS (Fig. 56-59). Since upward longwave radiation is closely related to the terrestrial, near-surface temperature, it is not surprising that when investigating the averaged 42-h forecasts from all 00 UTC initializations, signals in upward longwave radiation are also similar to those seen in 2 m temperature bias results; higher upward longwave radiation values may be indicative of higher near-surface temperatures, which is consistent with the results presented. This finding aligns well with the traditional verification where NAMOC, regardless of season, has higher median 2 m temperature bias values than ThompsonMP (i.e., NAMOC has warmer 2 m temperatures than ThompsonMP). The largest differences between the two configurations during the spring (Fig. 58) and are in the Upper Midwest and in the South, along the Gulf of Mexico Coast and extending up the eastern Atlantic Coast; the largest differences in the summer (Fig. 59) and fall (Fig. 56) are generally contained in the East region in the Southeast, extending up the Atlantic Coast. In spring, summer, and fall, there are large areas with differences greater than 20 W m^{-2}. Smaller differences are seen during the winter (Fig. 57) and are more isolated within the region along the Gulf Coast; differences in these areas are near or exceed 20 W m^{-2}. These areas are typically where the largest differences were observed in the point verification for 2 m temperature bias (see Fig. 12). In addition, these results align well with the above discussion on downward shortwave radiation. Recall that NAMOC typically had higher downward shortwave radiation values than ThompsonMP, and spatial distributions of the difference fields for upward longwave and downward shortwave radiation have similar areas of maxima.

Downward longwave radiation is strongly influenced by water vapor and aerosols in the atmosphere, where increased downward longwave radiation is generally indicative of increased cloudiness. Therefore, seeing areas of differences in downward longwave radiation is anticipated due to ThompsonMP being coupled to RRTM, whereas the Ferrier-Aligo scheme has constant values for cloud water droplets, cloud ice, and snow. In the winter, it is not surprising that large differences between the two configurations are seen in the Upper Midwest and parts of the Northern Plains, where cloudy regimes are typical during the winter season (Fig. 61). In these areas, ThompsonMP has larger downward longwave radiation values than NAMOC, with differences of 10 – 20 W m^{-2}. These areas of difference are not unexpected due to ThompsonMP being coupled to RRTM, whereas the Ferrier-Aligo scheme has constant values for cloud water droplets, cloud ice, and snow. The Rocky Mountain region also has enhanced areas of difference, where NAMOC has higher downward longwave radiation values than ThompsonMP (typically 10 – 20 W m^{-2}). In the fall season, there are also coherent structures in the difference field that have similarities to the winter (Fig. 60). The largest differences (~20 W m^{-2}) are seen over the Lower Mississippi Valley through the Ohio Valley and as well as over the upper Midwest and Northern Plains; in these areas, NAMOC has larger downward longwave radiation values than ThompsonMP, which is the same as seen in the winter. Areas where ThompsonMP has larger downward longwave radiation than NAMOC are seen within the Northwest CONUS and in areas of the Southeast up the Atlantic Coast as well as in the southern Midwest. In the summer aggregation, both configurations at the 42-h forecast lead time have maximum longwave radiation values in the southern portion of the East region (exceeding 450 W m^{-2}), with minimum values throughout the Rocky Mountain region and from the Great Basin into the Pacific Northwest (at and below 300 W m^{-2}; Fig. 63). Overall, while there are coherent structures in the difference field, they are typically isolated and not region-wide. In the spring season, distributions between the individual configurations are similar to the summer, but there is a general decrease in downward longwave radiation values; the difference field, like the summer, has isolated areas of enhanced differences, but no large-scale patterns emerge (Fig. 62).

Recall that in the vertical profiles for temperature bias, ThompsonMP typically had a larger median cold bias compared to NAMOC in the low-to-middle levels; however, there is a transition to NAMOC having lower warm biases than ThompsonMP in the middle-to-upper levels (see Fig. 5). The results discussed above for both upward and downward longwave radiation may be contributing to what is observed in the vertical distribution of temperature bias for the two configurations. In the low-to-middle levels, NAMOC has consistently higher temperatures and upward longwave radiation values than ThompsonMP; this result is in agreement between the relationship between radiation and temperature. In the middle-to-upper levels, ThompsonMP shifts to having larger warm median temperature biases than NAMOC, and in

the winter, this is also where ThompsonMP has higher downward longwave radiation values in the Upper Midwest and Northern Plains. Larger downward longwave radiation would potentially indicate more cloudiness in this area, and the enhanced cloudiness could increase the emittance of infrared radiation, which would increase warming.

7. Summary

An end-to-end sensitivity test was conducted to evaluate the resulting forecast performance when substituting the operational NAMOC Ferrier-hires microphysics scheme with the recently added Thompson microphysics scheme which is coupled to the RRTM radiation scheme using NEMS/NMMB. Each configuration was run over the same set of cases, spanning a 1-month period during each of the four seasons. The employed testing methodology allowed for pair-wise differences to be computed for several verification metrics, with an assessment of SS and PS pair-wise differences. Both traditional verification of upper air and surface variables as well as spatial comparisons between the two configurations were evaluated to get a better understanding on seasonal and regional differences.

Upper air verification of temperature showed that the shape of the distribution for both configurations was highly dependent on temporal aggregation, vertical level and forecast lead time; however, in the low-to-mid levels, ThompsonMP generally had lower median bias values while NAMOC had lower median bias values in the mid-to-upper-levels; a similar trend was noted for the full Alaska domain. At the lowest level, both configurations were typically warmer in the East CONUS compared to the West. When looking at vertical levels of dew point, the shape of the distribution was similar between the configurations with a consistent dry bias found near the surface for all but the winter aggregation. When differences were present, the favored configuration depended on vertical level and forecast lead time. For the Alaska domain, differences favored NAMOC for the summer aggregation, while ThompsonMP was favored for a majority of the lead times for all other seasons. When examining wind speed bias, a neutral-to-low bias was observed at the lowest level, increasing in magnitude up to 200 hPa. SS pair-wise differences tended to favor NAMOC more often in the East and low-to-mid levels in the West, while ThompsonMP was favored in the upper levels of the West. Similar to the East CONUS, for the Alaska domain, NAMOC was favored at the low-to-mid levels, while ThompsonMP was favored most at the highest levels.

Overall, when looking at the surface variables, a large number of SS and PS pair-wise differences were observed; however, a sensitivity in which configuration was favored was dependent on verification metric, temporal aggregation, initialization time, vertical level, lead time, and threshold. For 2 m temperature, a notable result showed both configurations exhibited warm biases during the summer that grew with increased forecast lead time; however an opposite signal was seen in the winter aggregation, where there were cold biases during the daytime hours. When differences were present, ThompsonMP typically had lower median bias values than NAMOC, leading to better performance by ThompsonMP in the summer when there was a warm bias and better performance by NAMOC in the winter when cold biases were present. A similar trend was observed in the Alaska domain, with NAMOC typically having a higher bias which translated to ThompsonMP being the better performer in the summer when biases remained high and for the other seasons the better performer depended on the sign of the bias. When looking at 2 m dew point temperature, both configurations showed dry biases increasing with forecast lead time during the summer and moist biases during the winter with ThompsonMP generally the better performer. The Alaska domain showed the same dry (moist) bias during summer (winter) with NAMOC generally favored in the winter and ThompsonMP generally favored in the summer. While no PS pair-wise differences were noted for 10 m wind speed bias, notable regional results showed the West typically having a neutral-to-low bias while the East had a consistent high bias regardless of season. Over Alaska, the summer aggregation had a high bias for most lead times favoring ThompsonMP, while NAMOC was favored more in the spring and few differences noted in the winter and fall. A look at daily precipitation accumulation over the CONUS showed minimal differences between the two configurations with few differences being SS. On the other hand, an examination of composite reflectivity showed NAMOC having consistently higher bias for all aggregations and forecast lead times. A number of SS differences were found, all favoring ThompsonMP.

Spatial distribution plots helped diagnose regional patterns that may not be captured in the time series plots. When examining 2 m temperature, all seasons showed NAMOC having a higher mean bias across the CONUS with the East having higher mean biases compared to the West. During the summer, a predominantly warm bias existed over the CONUS, while the winter displayed a cold bias over much of the CONUS, especially for the ThompsonMP configuration. Similar trends were noted over the full Alaska domain. For 2 m dew point temperature, NAMOC typically had higher mean biases, with moist biases observed during the winter in all regions except the SEC and West Coast regions and dry biases during the summer, with the strongest dry biases over the East. Over the Alaska domain, the summer dry bias was evident, increasing from west to east, while winter showed a dry bias in the south, increasing to moist in the north. Spatial differences in 10 m wind were small between the two configurations; a high bias across the East was found for all season except winter where an increase in low biases was seen. Over the West, a low bias was found over the NPL and NMT regions and a high bias along the West Coast for most seasons. The Alaska domain typically showed higher wind speed biases in the north compared to the south for all aggregations, especially during fall and winter.

A key result in this sensitivity study was the differences in shortwave and longwave radiation reaching the surface between the two configurations. Given that the ThompsonMP scheme is coupled with the RRTM scheme, which passes the cloud water droplet, cloud ice and snow sizes into the radiation scheme, impacts on both cloud-free and cloudy skies were expected. In general, this difference in microphysics schemes led to NAMOC having higher radiative values than ThompsonMP with more SW radiation reaching the surface, resulting in higher upward longwave radiation and higher near-surface temperatures CONUS-wide for all seasons.

8. References

Thompson, G., P. R. Field, R.M. Rasmussen, and W. D. Hall, 2008: Explicit Forecasts of winter precipitation using an improved bulk microphysics scheme. Part II: Implementation of a new snow parameterization. *Mon. Wea. Rev.,* **136,** 5095–5115.

Janjic, Z., and R.L. Gall, 2012: Scientific documentation of the NCEP nonhydrostatic multiscale model on the B grid (NMMB). Part 1 Dynamics. NCAR Technical Note NCAR/TN-489+STR, DOI: 10.5065/D6WH2MZX.

Table 6. SS (light shading) and PS (dark shading) pair-wise differences for the NAMOC and ThompsonMP configurations run with NEMSv0.9 (where the highlighted configuration is favored) for upper air temperature BCRMSE and bias by pressure level, season, and forecast lead time for the 00 UTC and 12 UTC initializations combined over the West verification domain.

Upper Air Temperature		Annual				Summer				Fall				Winter				Spring			
		f12	f24	f36	f48	f12	f24	f36	f48	f12	f24	f36	f48	f12	f24	f36	f48	f12	f24	f36	f48
BCRMSE	850	--	--	--	--	--	--	--	--	--	--	--	--	--	--	--	--	--	ThompMP	--	--
	700	--	--	--	--	--	--	--	--	--	--	--	--	--	--	--	--	--	--	--	--
	500	--	--	--	--	NAMOC	--	--	--	--	--	--	--	--	--	--	--	--	--	--	--
	400	--	--	--	--	--	--	--	--	--	--	--	--	--	--	--	--	--	--	--	--
	300	--	--	--	--	--	NAMOC	--	--	ThompMP	--	--	--	--	--	ThompMP	--	--	--	--	--
	200	--	--	--	--	--	--	--	--	--	--	--	ThompMP	--	ThompMP	--	--	--	--	--	--
	150	--	--	--	--	--	--	NAMOC	NAMOC	--	--	--	--	--	--	--	--	--	--	--	--
	100	--	--	--	--	ThompMP	--	--	--	--	--	--	--	--	--	--	--	--	--	--	--
Bias	850	NAMOC	NAMOC *	NAMOC *	NAMOC *	--	ThompMP *	ThompMP	ThompMP *	NAMOC	NAMOC *	NAMOC *	NAMOC *	NAMOC	NAMOC *	NAMOC *	NAMOC *	--	ThompMP *	ThompMP *	ThompMP *
	700	ThompMP	ThompMP *	ThompMP *	ThompMP *	ThompMP	ThompMP *	ThompMP *	ThompMP *	NAMOC	NAMOC	NAMOC *	NAMOC *	NAMOC	NAMOC	NAMOC *	NAMOC *	ThompMP	ThompMP *	ThompMP *	NAMOC *
	500	ThompMP	ThompMP	ThompMP *	ThompMP *	ThompMP *	ThompMP *	ThompMP *	ThompMP *	NAMOC	NAMOC	NAMOC	NAMOC	--	--	ThompMP	--	ThompMP	ThompMP	ThompMP	NAMOC *
	400	--	--	--	--	ThompMP *	ThompMP *	ThompMP *	ThompMP *	--	--	--	--	NAMOC	NAMOC	--	--	--	--	--	--
	300	NAMOC	NAMOC	NAMOC *	NAMOC *	--	NAMOC	NAMOC	ThompMP	NAMOC	NAMOC	NAMOC	NAMOC *	NAMOC	NAMOC *	NAMOC *	NAMOC *	NAMOC *	NAMOC *	NAMOC *	NAMOC *
	200	NAMOC	NAMOC	NAMOC	NAMOC	--	--	NAMOC	NAMOC	NAMOC	NAMOC	NAMOC	ThompMP	NAMOC	NAMOC	--	NAMOC *	NAMOC	NAMOC	NAMOC *	NAMOC *
	150	ThompMP	ThompMP	ThompMP	ThompMP	NAMOC	NAMOC *	NAMOC *	NAMOC *	ThompMP	ThompMP	ThompMP	ThompMP	--	--	--	--	ThompMP	--	--	--
	100	NAMOC	NAMOC	--	--	NAMOC	NAMOC	NAMOC	NAMOC *	NAMOC	--	--	--	--	--	--	--	NAMOC	--	ThompMP	--

Table 7. SS (light shading) and PS (dark shading) pair-wise differences for the NAMOC and ThompsonMP configurations run with NEMSv0.9 (where the highlighted configuration is favored) for upper air dew point temperature BCRMSE and bias by pressure level, season, and forecast lead time for the 00 UTC and 12 UTC initializations combined over the West verification domain.

Upper Air Dew Point Temperature		Annual				Summer				Fall				Winter				Spring			
		f12	f24	f36	f48	f12	f24	f36	f48	f12	f24	f36	f48	f12	f24	f36	f48	f12	f24	f36	f48
BCRMSE	850	--	--	ThompMP	ThompMP	--	--	--	--	--	--	ThompMP *	--	--	--	--	--	--	--	--	--
	700	--	--	--	--	--	--	--	--	--	--	--	--	--	--	--	--	--	--	--	--
	500	--	--	--	--	--	--	--	--	--	--	--	--	--	--	--	--	--	--	NAMOC *	--
	400	--	--	--	--	--	--	--	--	--	--	--	--	--	--	--	--	--	--	--	--
	300	--	--	--	--	--	--	--	--	--	--	--	--	--	--	--	--	--	--	--	--
Bias	850	--	--	--	--	--	--	--	--	--	ThompMP	--	--	--	--	--	--	--	--	--	--
	700	--	--	ThompMP	ThompMP	--	--	NAMOC	--	--	--	--	--	--	--	--	--	--	--	--	--
	500	--	--	NAMOC	--	--	NAMOC	--	--	--	--	--	--	--	--	--	--	--	--	--	--
	400	NAMOC	--	NAMOC *	NAMOC *	--	NAMOC *	NAMOC	--	--	NAMOC	--	--	--	--	--	--	--	--	NAMOC	--
	300	NAMOC *	NAMOC *	NAMOC *	ThompMP *	--	NAMOC *	--	--	ThompMP	ThompMP *	--	--	NAMOC *	ThompMP *	ThompMP *	NAMOC *	NAMOC *	NAMOC *	NAMOC *	NAMOC *

Table 8. SS (light shading) and PS (dark shading) pair-wise differences for the NAMOC and ThompsonMP configurations run with NEMSv0.9 (where the highlighted configuration is favored) for upper air wind BCRMSE and bias by pressure level, season, and forecast lead time for the 00 UTC and 12 UTC initializations combined over the West verification domain.

Upper Air Wind Speed		Annual				Summer				Fall				Winter				Spring			
		f12	f24	f36	f48	f12	f24	f36	f48	f12	f24	f36	f48	f12	f24	f36	f48	f12	f24	f36	f48
BCRMSE	850	--	--	--	--	--	ThompMP	--	--	--	--	--	--	--	--	--	--	--	--	--	--
	700	--	--	--	ThompMP	--	--	--	ThompMP	--	--	--	--	--	--	--	--	--	--	--	ThompMP
	500	--	--	ThompMP	--	--	--	--	--	--	--	--	--	NAMOC	--	--	--	--	--	--	--
	400	--	--	--	--	--	--	--	--	--	--	--	--	--	--	--	--	ThompMP	--	--	--
	300	--	--	--	--	--	--	--	--	--	--	--	ThompMP	ThompMP	--	--	--	--	--	--	--
	200	--	--	--	--	--	--	ThompMP	--	--	--	--	--	--	ThompMP	--	--	--	--	--	--
	150	--	--	--	--	--	--	ThompMP	ThompMP	--	--	--	--	--	--	--	--	--	NAMOC	--	NAMOC
	100	--	--	--	--	--	--	--	NAMOC	--	--	--	--	--	--	--	--	--	--	--	--
Bias	850	--	--	NAMOC	--	--	--	--	--	--	--	--	--	NAMOC	NAMOC	--	--	--	--	--	--
	700	--	--	--	NAMOC	--	--	--	--	--	--	--	--	--	--	ThompMP	--	--	--	--	--
	500	--	--	--	--	--	NAMOC	--	--	--	--	--	--	--	--	--	--	--	--	--	--
	400	--	--	--	--	--	--	--	--	--	--	--	--	--	--	--	NAMOC	--	--	--	ThompMP
	300	NAMOC	NAMOC	NAMOC	NAMOC	NAMOC	--	NAMOC	NAMOC	--	--	NAMOC	NAMOC	--	NAMOC	--	NAMOC	--	--	--	--
	200	ThompMP	--	--	--	--	--	NAMOC	NAMOC	--	NAMOC	--	--	ThompMP	--	ThompMP	--	ThompMP	--	ThompMP	ThompMP
	150	ThompMP	--	--	NAMOC	--	--	NAMOC	ThompMP	--	--	--	--	ThompMP	--	NAMOC	NAMOC	ThompMP	ThompMP	ThompMP	NAMOC
	100	ThompMP	--	--	--	--	ThompMP	NAMOC	ThompMP	--	--	--	--	ThompMP	--	--	--	ThompMP	NAMOC	NAMOC	NAMOC

Table 9. SS (light shading) and PS (dark shading) pair-wise differences for the NAMOC and ThompsonMP configurations run with NEMSv0.9 (where the highlighted configuration is favored) for surface temperature BCRMSE and bias by season and forecast lead time for the 00 UTC and 12 UTC initializations separately over the West verification domain.

Surface Temperature			f03	f06	f09	f12	f15	f18	f21	f24	f27	f30	f33	f36	f39	f42	f45	f48
BCRMSE	00 UTC Initializations	Annual	ThompMP	--	--	--	--	--	ThompMP	ThompMP	ThompMP	ThompMP	--	--	--	--	ThompMP	ThompMP
		Summer	ThompMP	--	--	--	--	--	ThompMP	--	ThompMP	--	--	--	--	--	ThompMP	ThompMP
		Fall	--	--	--	--	--	--	--	--	--	--	--	--	--	NAMOC	--	--
		Winter	ThompMP	--	--	--	--	ThompMP	ThompMP	ThompMP	--	--	--	--	--	--	ThompMP	ThompMP
		Spring	--	--	--	--	--	--	--	--	ThompMP	ThompMP	ThompMP	ThompMP	ThompMP	--	--	--
	12 UTC Initializations	Annual	--	--	ThompMP	ThompMP	ThompMP	--	--	--	--	--	ThompMP	ThompMP	--	--	--	--
		Summer	NAMOC	--	ThompMP	ThompMP	--	--	--	--	--	--	ThompMP	ThompMP	ThompMP	ThompMP	--	ThompMP
		Fall	--	--	--	ThompMP	--	--	NAMOC	--	--	--	NAMOC	--	--	--	--	--
		Winter	--	--	ThompMP	ThompMP	--	--	--	ThompMP	--	--	--	ThompMP	--	--	--	--
		Spring	--	--	ThompMP	ThompMP	ThompMP	ThompMP	--	--	--	ThompMP	ThompMP	--	--	--	--	--
Bias	00 UTC Initializations	Annual	--	--	--	--	ThompMP *	ThompMP *	ThompMP *	NAMOC *	ThompMP *	ThompMP *	ThompMP *	ThompMP	ThompMP *	ThompMP *	ThompMP *	NAMOC *
		Summer	--	NAMOC	NAMOC	NAMOC	ThompMP *	ThompMP *	ThompMP *	ThompMP	ThompMP	ThompMP *	ThompMP	ThompMP	ThompMP *	ThompMP *	ThompMP *	ThompMP *
		Fall	--	--	--	--	ThompMP	ThompMP *	ThompMP *	NAMOC *	ThompMP *	ThompMP	--	--	ThompMP *	ThompMP *	NAMOC *	NAMOC *
		Winter	--	--	--	--	--	NAMOC *	NAMOC *	NAMOC *	NAMOC *	NAMOC	ThompMP	--	NAMOC	NAMOC *	NAMOC *	NAMOC *
		Spring	NAMOC	NAMOC	NAMOC	NAMOC	ThompMP *	ThompMP *	ThompMP *	ThompMP *	NAMOC *	NAMOC *	NAMOC *	ThompMP *	ThompMP *	ThompMP *	ThompMP *	ThompMP *
	12 UTC Initializations	Annual	ThompMP	ThompMP *	ThompMP *	NAMOC *	ThompMP *	ThompMP *	ThompMP *	ThompMP	ThompMP *	ThompMP *	ThompMP *	NAMOC *	ThompMP *	ThompMP *	ThompMP *	ThompMP *
		Summer	ThompMP *	ThompMP *	ThompMP *	ThompMP *	ThompMP *	--	--	--	ThompMP *	ThompMP *	ThompMP *	ThompMP *	ThompMP *	ThompMP *	ThompMP *	ThompMP *
		Fall	ThompMP	NAMOC *	NAMOC *	NAMOC *	ThompMP *	ThompMP *	ThompMP *	ThompMP *	ThompMP *	ThompMP *	NAMOC *	NAMOC *	ThompMP *	ThompMP *	ThompMP *	ThompMP
		Winter	--	NAMOC *	NAMOC *	NAMOC *	--	--	--	--	--	NAMOC *	NAMOC *	NAMOC *	NAMOC *	NAMOC *	NAMOC	NAMOC
		Spring	ThompMP *	ThompMP *	ThompMP *	ThompMP *	NAMOC *	ThompMP *	NAMOC *	ThompMP *	ThompMP *	ThompMP *	ThompMP *	ThompMP *	ThompMP *	ThompMP *	NAMOC *	NAMOC *

Table 10. SS (light shading) and PS (dark shading) pair-wise differences for the NAMOC and ThompsonMP configurations run with NEMSv0.9 (where the highlighted configuration is favored) for surface dew point temperature BCRMSE and bias by season and forecast lead time for the 00 UTC and 12 UTC initializations separately over the West verification domain.

Surface Dew Point Temperature			f03	f06	f09	f12	f15	f18	f21	f24	f27	f30	f33	f36	f39	f42	f45	f48
BCRMSE	00 UTC Initializations	Annual	--	--	--	--	--	--	--	--	ThompMP	--	ThompMP	--	--	--	ThompMP	ThompMP
		Summer	ThompMP	ThompMP	--	--	NAMOC	--	ThompMP	--	ThompMP	ThompMP	ThompMP	ThompMP	--	--	ThompMP	ThompMP
		Fall	--	--	--	NAMOC	--	--	NAMOC	--	--	--	--	--	--	--	--	--
		Winter	--	--	--	--	--	--	--	--	--	--	--	--	--	--	--	--
		Spring	--	--	--	--	--	ThompMP	ThompMP	--	ThompMP	--	ThompMP	ThompMP	ThompMP	--	--	--
	12 UTC Initializations	Annual	--	--	--	--	ThompMP	--	--	ThompMP	--	--	ThompMP	ThompMP	--	--	--	--
		Summer	--	--	--	ThompMP	--	--	--	--	--	--	ThompMP	ThompMP	ThompMP	ThompMP	ThompMP	ThompMP
		Fall	--	--	NAMOC	--	--	--	--	--	--	--	--	--	--	--	--	--
		Winter	--	--	--	--	--	--	--	--	--	--	--	--	--	--	--	--
		Spring	--	--	--	--	ThompMP	--	--	--	--	--	ThompMP	--	--	ThompMP	ThompMP	ThompMP
Bias	00 UTC Initializations	Annual	NAMOC	NAMOC	--	--	NAMOC	ThompMP	ThompMP	ThompMP	ThompMP	--	ThompMP	ThompMP	ThompMP	ThompMP	ThompMP	--
		Summer	NAMOC	--	--	--	--	ThompMP	--	ThompMP	--	--	ThompMP	ThompMP	ThompMP	ThompMP	--	--
		Fall	NAMOC	NAMOC	NAMOC	NAMOC	NAMOC	NAMOC	NAMOC	--	ThompMP	ThompMP	ThompMP	ThompMP	--	ThompMP	--	ThompMP
		Winter	NAMOC	--	--	--	--	--	--	--	--	--	--	--	--	--	--	--
		Spring	NAMOC	--	--	--	--	ThompMP	ThompMP	ThompMP	--	--	--	--	--	--	ThompMP	ThompMP
	12 UTC Initializations	Annual	NAMOC	ThompMP	ThompMP	ThompMP	--	--	--	ThompMP	ThompMP	ThompMP	ThompMP	ThompMP	ThompMP	ThompMP	--	--
		Summer	ThompMP	ThompMP	ThompMP	ThompMP	--	--	--	ThompMP	ThompMP	ThompMP	ThompMP	--	--	--	--	--
		Fall	--	--	--	--	--	--	--	--	--	ThompMP	ThompMP	ThompMP	ThompMP	ThompMP	--	--
		Winter	--	--	--	--	--	--	--	--	--	--	--	NAMOC	--	--	--	--
		Spring	--	ThompMP	ThompMP	ThompMP	--	--	--	--	--	ThompMP	ThompMP *	ThompMP	ThompMP	--	--	--

Table 11. SS (light shading) and PS (dark shading) pair-wise differences for the NAMOC and ThompsonMP configurations run with NEMSv0.9 (where the highlighted configuration is favored) for surface wind BCRMSE and bias by season and forecast lead time for the 00 UTC and 12 UTC initializations separately over the West verification domain.

Surface Wind Speed			f03	f06	f09	f12	f15	f18	f21	f24	f27	f30	f33	f36	f39	f42	f45	f48
BCRMSE	00 UTC Initializations	Annual	--	--	--	--	--	ThompMP	ThompMP	--	--	--	ThompMP	--	--	--	--	--
		Summer	--	--	--	--	--	--	--	ThompMP	ThompMP	--	--	--	--	--	ThompMP	--
		Fall	--	--	--	NAMOC	--	ThompMP	ThompMP	--	--	--	ThompMP	--	ThompMP	--	--	--
		Winter	--	--	--	--	--	--	ThompMP	--	--	--	--	--	--	--	--	--
		Spring	--	NAMOC	NAMOC	--	--	--	--	--	--	--	--	--	--	--	--	--
	12 UTC Initializations	Annual	--	--	--	--	--	--	--	--	--	--	--	--	--	--	--	--
		Summer	ThompMP	ThompMP	ThompMP	--	--	--	--	--	--	--	--	ThompMP	ThompMP	--	--	--
		Fall	ThompMP	--	--	--	--	--	--	--	--	--	--	--	--	--	--	--
		Winter	--	--	--	--	--	--	--	--	--	--	--	--	--	--	--	--
		Spring	--	--	--	--	ThompMP	--	--	--	--	--	--	--	--	--	--	--
Bias	00 UTC Initializations	Annual	--	--	--	--	ThompMP	NAMOC	NAMOC	NAMOC	NAMOC	NAMOC	--	--	NAMOC	NAMOC	NAMOC	NAMOC
		Summer	NAMOC	--	NAMOC	--	--	NAMOC	NAMOC	ThompMP	NAMOC	NAMOC	--	--	ThompMP	ThompMP	--	NAMOC
		Fall	--	--	--	--	--	--	--	NAMOC	--	--	--	--	--	NAMOC	NAMOC	--
		Winter	--	--	--	--	--	--	NAMOC	NAMOC	NAMOC	NAMOC	--	--	--	NAMOC	NAMOC	NAMOC
		Spring	--	--	NAMOC	--	NAMOC	NAMOC	NAMOC	NAMOC	--	--	--	--	NAMOC	NAMOC	NAMOC	NAMOC
	12 UTC Initializations	Annual	NAMOC	NAMOC	NAMOC	NAMOC	NAMOC	NAMOC	--	--	ThompMP	NAMOC	NAMOC	NAMOC	NAMOC	--	--	--
		Summer	ThompMP	ThompMP	NAMOC	NAMOC	NAMOC	--	--	NAMOC	ThompMP	ThompMP	NAMOC	NAMOC	NAMOC	--	--	--
		Fall	ThompMP	NAMOC	NAMOC	--	--	--	ThompMP	--	ThompMP	NAMOC	NAMOC	--	--	--	--	--
		Winter	NAMOC	NAMOC	NAMOC	--	--	--	--	--	--	NAMOC	NAMOC	--	--	--	--	--
		Spring	NAMOC	NAMOC	NAMOC	NAMOC	NAMOC	--	NAMOC	--	NAMOC	NAMOC	NAMOC	NAMOC	NAMOC	NAMOC	--	--

Table 12. SS differences for the NAMOC and ThompsonMP configurations run with NEMSv0.9 (where the highlighted configuration is favored) for 24-hour QPF GSS and frequency bias by season, forecast lead time, and threshold for the 00 UTC and 12 UTC initializations separately over the West verification domain.

Daily QPF				>0.01	>0.25	>0.5	>0.75	>1	>1.25	>1.5	>2	>3
Gilbert Skill Score	00 UTC Initializations	Annual	f36	ThompMP	--	--	--	--	--	--	--	--
		Summer	f36	--	--	--	--	--	--	--	--	--
		Fall	f36	--	--	--	--	--	--	--	--	--
		Winter	f36	--	--	--	--	--	--	--	--	--
		Spring	f36	--	--	--	--	--	--	--	--	--
	12 UTC Initializations	Annual	f24	--	--	--	--	--	--	--	--	--
			f48	--	--	--	--	--	--	--	--	--
		Summer	f24	--	--	--	--	--	--	--	--	--
			f48	ThompMP	--	--	--	--	--	--	--	--
		Fall	f24	--	--	--	--	--	--	--	--	--
			f48	--	--	--	--	--	--	--	--	--
		Winter	f24	--	--	--	--	--	--	--	--	--
			f48	--	--	--	--	--	--	--	--	--
		Spring	f24	--	--	--	--	--	--	--	--	--
			f48	--	--	--	--	--	--	--	--	--
Frequency Bias	00 UTC Initializations	Annual	f36	--	--	--	--	--	--	--	--	--
		Summer	f36	--	--	--	--	--	--	--	--	--
		Fall	f36	--	--	--	--	--	--	--	--	--
		Winter	f36	--	--	--	--	--	--	--	--	--
		Spring	f36	--	--	--	--	--	--	--	--	--
	12 UTC Initializations	Annual	f24	--	--	--	--	--	--	--	--	--
			f48	--	--	--	--	--	--	--	--	--
		Summer	f24	--	--	--	--	--	--	--	--	--
			f48	ThompMP	--	--	--	--	--	--	--	--
		Fall	f24	--	--	--	--	--	--	--	--	--
			f48	--	--	--	--	--	--	--	--	--
		Winter	f24	--	--	--	--	--	--	--	--	--
			f48	--	--	--	--	--	--	--	--	--
		Spring	f24	--	--	--	--	--	--	--	--	--
			f48	--	--	--	--	--	--	--	--	--

Table 13. SS differences for the NAMOC and ThompsonMP configurations run with NEMSv0.9 (where the highlighted configuration is favored) for reflectivity GSS and frequency bias by season, threshhold and forecast lead time for the 00 UTC and 12 UTC initializations separately over the West verification domain.

REFC				f03	f06	f09	f12	f15	f18	f21	f24	f27	f30	f33	f36	f39	f42	f45	f48
GSS	00 UTC Initializations	≥10	Annual	--	--	ThompMP	--	--	ThompMP	--	--	--	--	ThompMP	--	ThompMP	--	--	--
			Summer	--	--	--	--	--	--	--	--	--	--	--	--	--	--	--	--
			Fall	--	--	--	--	--	--	--	--	--	--	--	--	--	--	--	--
			Winter	--	--	--	--	--	--	--	--	--	--	--	--	--	--	--	--
			Spring	--	--	--	--	--	--	--	--	--	--	--	--	--	--	--	--
		≥20	Annual	--	--	--	--	--	--	--	--	--	--	--	--	--	--	--	--
			Summer	--	--	--	--	--	--	--	--	--	--	--	--	--	--	--	--
			Fall	--	--	--	--	--	--	--	--	--	--	--	--	--	--	--	--
			Winter	--	--	--	--	--	--	--	--	--	--	--	--	--	--	--	--
			Spring	--	--	--	--	--	--	--	--	--	--	--	--	--	--	--	--
	12 UTC Initializations	≥10	Annual	ThompMP	--	--	--	--	--	--	--	--	--	--	--	--	--	--	--
			Summer	--	--	--	--	--	--	--	--	--	--	--	--	--	--	--	--
			Fall	--	--	--	--	--	--	--	--	--	--	--	--	--	--	--	--
			Winter	--	--	--	--	--	--	--	--	--	--	--	--	--	--	--	--
			Spring	--	--	--	--	--	--	--	--	--	--	--	--	--	--	--	--
		≥20	Annual	ThompMP	--	--	--	--	--	--	--	--	--	--	--	--	--	--	--
			Summer	--	--	--	--	--	--	--	--	--	--	--	--	--	--	--	--
			Fall	--	--	--	--	--	--	--	--	--	--	--	--	--	--	--	--
			Winter	--	--	--	--	--	--	--	--	--	--	--	--	--	--	--	--
			Spring	--	--	--	--	--	--	--	--	--	--	--	--	--	--	--	--
Frequency Bias	00 UTC Initializations	≥10	Annual	ThompMP	ThompMP	ThompMP	ThompMP	ThompMP	ThompMP	ThompMP	ThompMP	ThompMP	ThompMP	ThompMP	ThompMP	ThompMP	ThompMP	ThompMP	ThompMP
			Summer	--	--	--	--	--	--	ThompMP	--	--	--	--	--	--	--	--	--
			Fall	--	--	--	--	ThompMP	--	--	--	--	--	--	ThompMP	--	--	--	ThompMP
			Winter	ThompMP	ThompMP	ThompMP	--	--	--	--	ThompMP	ThompMP	ThompMP	ThompMP	ThompMP	ThompMP	ThompMP	ThompMP	ThompMP
			Spring	ThompMP	ThompMP	ThompMP	ThompMP	ThompMP	ThompMP	ThompMP	ThompMP	ThompMP	ThompMP	ThompMP	ThompMP	ThompMP	ThompMP	ThompMP	ThompMP
		≥20	Annual	ThompMP	--	--	--	--	ThompMP	ThompMP	ThompMP	--	--	ThompMP	ThompMP	ThompMP	ThompMP	ThompMP	ThompMP
			Summer	--	--	--	--	--	--	--	--	--	--	--	--	--	--	--	--
			Fall	--	--	--	--	--	--	--	--	--	--	--	--	--	--	--	--
			Winter	ThompMP	--	--	--	--	--	--	ThompMP	--	ThompMP	--	ThompMP	--	ThompMP	ThompMP	ThompMP
			Spring	--	--	--	ThompMP	--	--	ThompMP	--	--	--	--	ThompMP	--	ThompMP	--	--
	12 UTC Initializations	≥10	Annual	ThompMP	ThompMP	ThompMP	ThompMP	ThompMP	ThompMP	ThompMP	ThompMP	ThompMP	ThompMP	ThompMP	ThompMP	ThompMP	ThompMP	ThompMP	ThompMP
			Summer	--	--	--	--	--	--	--	--	--	--	--	--	--	--	--	--
			Fall	ThompMP	ThompMP	ThompMP	ThompMP	--	--	--	--	--	--	--	--	--	--	--	--
			Winter	ThompMP	ThompMP	ThompMP	ThompMP	ThompMP	--	--	--	ThompMP	--	--	ThompMP	ThompMP	ThompMP	ThompMP	--
			Spring	--	ThompMP	ThompMP	ThompMP	--	--	ThompMP	ThompMP	ThompMP	ThompMP	ThompMP	--	--	--	--	ThompMP
		≥20	Annual	ThompMP	ThompMP	ThompMP	ThompMP	ThompMP	--	--	--	ThompMP	--	--	--	--	--	ThompMP	--
			Summer	--	--	--	--	--	--	--	--	--	--	--	--	--	--	--	--
			Fall	--	--	--	--	--	--	--	--	--	--	--	--	--	--	--	--
			Winter	ThompMP	ThompMP	--	ThompMP	--	--	--	--	--	--	--	--	--	ThompMP	ThompMP	--
			Spring	--	--	ThompMP	--	--	--	--	ThompMP	ThompMP	ThompMP	ThompMP	--	--	--	--	ThompMP

Table 14. SS (light shading) and PS (dark shading) pair-wise differences for the NAMOC and ThompsonMP configurations run with NEMSv0.9 (where the highlighted configuration is favored) for upper air temperature BCRMSE and bias by pressure level, season, and forecast lead time for the 00 UTC and 12 UTC initializations combined over the East verification domain.

Upper Air Temperature		Annual				Summer				Fall				Winter				Spring			
		f12	f24	f36	f48	f12	f24	f36	f48	f12	f24	f36	f48	f12	f24	f36	f48	f12	f24	f36	f48
BCRMSE	850	--	NAMOC	NAMOC	--	--	--	--	--	--	NAMOC	NAMOC	--	--	--	NAMOC	--	--	--	--	--
	700	--	--	--	--	--	--	--	--	--	--	--	--	--	--	--	--	--	--	--	--
	500	--	--	--	--	--	--	--	--	--	--	--	--	--	--	--	--	--	--	--	--
	400	--	--	--	--	--	--	--	--	--	--	--	--	--	--	--	--	--	--	--	--
	300	--	--	--	--	--	--	--	--	--	--	--	--	--	--	ThompMP	--	--	--	--	--
	200	--	NAMOC	--	--	--	--	--	--	--	NAMOC	--	--	--	--	ThompMP	--	--	--	--	--
	150	--	--	--	--	--	--	NAMOC	NAMOC	NAMOC	--	--	--	--	--	--	--	--	--	--	--
	100	--	ThompMP	--	ThompMP	--	--	--	--	--	--	--	ThompMP	--	--	--	--	--	--	ThompMP	--
Bias	850	ThompMP	ThompMP *	ThompMP *	ThompMP *	--	ThompMP *	ThompMP *	ThompMP *	ThompMP	ThompMP *	ThompMP *	ThompMP *	ThompMP	NAMOC *	NAMOC *	NAMOC *	ThompMP	ThompMP *	ThompMP *	ThompMP *
	700	ThompMP	ThompMP *	ThompMP *	NAMOC *	ThompMP	ThompMP *	ThompMP *	ThompMP *	NAMOC	NAMOC	NAMOC *	NAMOC *	NAMOC	NAMOC	NAMOC	NAMOC *	ThompMP	ThompMP *	ThompMP *	ThompMP *
	500	NAMOC	NAMOC *	NAMOC	NAMOC *	ThompMP *	NAMOC *	NAMOC *	NAMOC *	NAMOC	NAMOC	--	NAMOC	NAMOC	NAMOC	--	--	NAMOC	NAMOC *	NAMOC	NAMOC *
	400	ThompMP	NAMOC	--	--	ThompMP	NAMOC *	NAMOC *	NAMOC *	NAMOC	--	--	--	--	NAMOC	NAMOC	NAMOC	--	--	--	--
	300	NAMOC	NAMOC	NAMOC	NAMOC *	ThompMP	--	--	--	--	NAMOC	ThompMP	ThompMP	NAMOC	NAMOC	NAMOC	NAMOC *	NAMOC	NAMOC	NAMOC *	NAMOC *
	200	NAMOC	NAMOC	NAMOC	NAMOC	--	NAMOC	NAMOC	NAMOC	NAMOC	NAMOC	NAMOC	--	NAMOC	--	NAMOC	--	NAMOC	NAMOC *	NAMOC	NAMOC
	150	NAMOC	NAMOC	ThompMP	NAMOC	NAMOC	NAMOC *	NAMOC *	NAMOC *	NAMOC	NAMOC	NAMOC	NAMOC	ThompMP	--	NAMOC	--	ThompMP	NAMOC	ThompMP	--
	100	NAMOC	NAMOC	NAMOC	--	ThompMP	NAMOC	--	NAMOC	NAMOC	NAMOC	NAMOC	--	NAMOC	--	--	NAMOC	--	--	--	--

Table 15. SS (light shading) and PS (dark shading) pair-wise differences for the NAMOC and ThompsonMP configurations run with NEMSv0.9 (where the highlighted configuration is favored) for upper air dew point temperature BCRMSE and bias by pressure level, season, and forecast lead time for the 00 UTC and 12 UTC initializations combined over the East verification domain.

Upper Air Dew Point Temperature		Annual				Summer				Fall				Winter				Spring			
		f12	f24	f36	f48	f12	f24	f36	f48	f12	f24	f36	f48	f12	f24	f36	f48	f12	f24	f36	f48
BCRMSE	850	--	--	--	--	--	--	--	--	--	--	--	--	--	--	--	--	--	ThompMP	--	--
	700	--	--	--	--	--	--	--	--	--	--	--	--	--	--	--	--	--	--	--	--
	500	--	--	--	--	--	--	--	--	--	--	--	--	--	--	--	--	--	--	--	--
	400	--	--	--	--	--	--	--	--	--	--	--	--	--	--	--	--	--	--	--	--
	300	--	--	--	--	--	--	--	--	--	NAMOC	--	--	--	--	NAMOC	--	NAMOC	--	--	--
Bias	850	ThompMP	--	--	--	ThompMP *	--	ThompMP	ThompMP *	--	--	--	--	ThompMP	--	--	--	--	--	--	--
	700	NAMOC	--	NAMOC	--	--	--	--	--	--	--	--	ThompMP	--	NAMOC	NAMOC	--	--	NAMOC	--	--
	500	--	--	--	--	--	ThompMP	--	--	--	--	--	--	--	NAMOC *	--	--	--	--	--	--
	400	NAMOC	NAMOC	NAMOC	NAMOC *	--	--	--	NAMOC *	NAMOC	NAMOC	NAMOC *	--	--	--	--	ThompMP *	--	--	--	NAMOC *
	300	NAMOC *	NAMOC *	ThompMP *	ThompMP *	--	NAMOC	NAMOC	--	ThompMP	--	--	ThompMP *	NAMOC *	--	ThompMP *	ThompMP *	--	NAMOC *	NAMOC *	--

Table 16. SS (light shading) and PS (dark shading) pair-wise differences for the NAMOC and ThompsonMP configurations run with NEMSv0.9 (where the highlighted configuration is favored) for upper air wind BCRMSE and bias by pressure level, season, and forecast lead time for the 00 UTC and 12 UTC initializations combined over the East verification domain.

Upper Air Wind Speed		Annual				Summer				Fall				Winter				Spring			
		f12	f24	f36	f48	f12	f24	f36	f48	f12	f24	f36	f48	f12	f24	f36	f48	f12	f24	f36	f48
BCRMSE	850	--	--	--	--	--	--	--	--	--	--	--	--	--	--	--	--	--	--	--	--
	700	--	--	--	--	--	--	--	--	--	--	--	--	--	--	--	--	--	--	--	--
	500	--	--	--	--	--	--	--	--	--	--	--	--	--	--	--	--	--	--	--	--
	400	--	--	--	--	--	--	--	--	--	--	--	--	--	--	--	--	--	--	--	--
	300	--	--	--	--	--	--	--	--	--	--	--	--	--	--	--	--	--	--	--	--
	200	--	--	--	--	--	--	--	--	--	--	--	--	--	--	--	--	--	--	--	--
	150	--	--	--	--	--	--	--	--	--	--	--	--	--	--	--	--	--	--	--	--
	100	--	--	ThompMP	--	--	--	--	--	--	--	--	--	ThompMP	--	--	--	--	--	ThompMP	--
Bias	850	--	NAMOC	--	NAMOC	--	NAMOC	NAMOC	NAMOC	--	--	--	--	--	NAMOC	--	--	--	--	--	--
	700	--	ThompMP	ThompMP	--	--	--	--	--	--	--	--	--	--	ThompMP	ThompMP	--	--	--	--	ThompMP
	500	--	--	--	--	--	--	--	--	--	--	--	--	--	--	--	--	--	ThompMP	--	--
	400	NAMOC	--	--	NAMOC	--	--	--	--	NAMOC	--	--	--	--	--	--	--	--	--	--	--
	300	NAMOC	NAMOC	NAMOC	NAMOC	--	NAMOC	--	--	NAMOC	NAMOC	NAMOC	NAMOC	--	--	--	--	--	NAMOC	--	--
	200	NAMOC	NAMOC	--	--	--	--	--	--	NAMOC	--	NAMOC	NAMOC	--	--	--	--	NAMOC	--	--	--
	150	NAMOC	--	--	--	--	--	--	--	NAMOC	--	--	--	NAMOC	--	--	--	--	ThompMP	--	--
	100	--	ThompMP	--	--	--	--	--	--	--	ThompMP	--	--	--	--	NAMOC	--	--	--	--	--

Table 17. SS (light shading) and PS (dark shading) pair-wise differences for the NAMOC and ThompsonMP configurations run with NEMSv0.9 (where the highlighted configuration is favored) for surface temperature BCRMSE and bias by season and forecast lead time for the 00 UTC and 12 UTC initializations separately over the East verification domain.

Surface Temperature			f03	f06	f09	f12	f15	f18	f21	f24	f27	f30	f33	f36	f39	f42	f45	f48
BCRMSE	00 UTC Initializations	Annual	--	--	--	--	NAMOC	--	--	--	--	--	--	--	NAMOC	--	--	--
		Summer	--	--	--	ThompMP	--	--	ThompMP	ThompMP	--	ThompMP	ThompMP	ThompMP	NAMOC	--	--	--
		Fall	--	--	--	--	NAMOC	--	--	--	--	--	--	--	--	--	--	--
		Winter	--	--	--	--	--	--	--	--	NAMOC	--	--	--	--	--	--	--
		Spring	--	--	--	--	NAMOC	--	--	--	--	NAMOC	--	--	--	--	--	--
	12 UTC Initializations	Annual	--	ThompMP	ThompMP	--	--	--	--	--	NAMOC	NAMOC	--	--	NAMOC	NAMOC	NAMOC	NAMOC
		Summer	--	--	ThompMP	--	ThompMP	--	ThompMP	NAMOC	--	--	ThompMP	ThompMP	--	--	--	--
		Fall	--	--	ThompMP	--	--	--	--	--	--	NAMOC	--	NAMOC	NAMOC	NAMOC	NAMOC	--
		Winter	--	ThompMP	--	--	--	--	NAMOC	NAMOC	--	--	--	--	NAMOC	--	--	--
		Spring	--	--	--	--	NAMOC	NAMOC	NAMOC	--	--	--	--	--	--	--	--	--
Bias	00 UTC Initializations	Annual	--	NAMOC	NAMOC	--	ThompMP *	ThompMP *	ThompMP *	ThompMP *	ThompMP *	ThompMP *	ThompMP *	ThompMP *	ThompMP *	ThompMP *	ThompMP *	ThompMP *
		Summer	ThompMP	NAMOC	NAMOC	ThompMP	ThompMP *	ThompMP *	ThompMP *	ThompMP *	ThompMP *	ThompMP *	ThompMP	ThompMP *	ThompMP *	ThompMP *	ThompMP *	ThompMP *
		Fall	NAMOC	NAMOC	--	--	ThompMP *	ThompMP *	ThompMP *	ThompMP *	ThompMP *	ThompMP *	ThompMP *	ThompMP *	ThompMP *	ThompMP *	ThompMP *	ThompMP *
		Winter	ThompMP	ThompMP	ThompMP	--	NAMOC	NAMOC *	NAMOC *	NAMOC *	NAMOC *	NAMOC	ThompMP	--	NAMOC *	NAMOC *	NAMOC *	NAMOC *
		Spring	--	--	--	ThompMP	ThompMP *	ThompMP *	ThompMP *	ThompMP *	ThompMP *	ThompMP *	ThompMP *	ThompMP *	ThompMP *	ThompMP *	ThompMP *	ThompMP *
	12 UTC Initializations	Annual	ThompMP *	ThompMP *	ThompMP *	ThompMP *	ThompMP *	ThompMP *	ThompMP *	ThompMP *	ThompMP *	ThompMP *	ThompMP *	ThompMP *	ThompMP *	ThompMP *	ThompMP *	ThompMP *
		Summer	ThompMP *	ThompMP *	ThompMP *	ThompMP *	--	--	--	ThompMP	ThompMP *	ThompMP *	ThompMP *	ThompMP *	ThompMP *	ThompMP *	ThompMP *	ThompMP *
		Fall	ThompMP *	ThompMP *	ThompMP *	ThompMP *	ThompMP *	ThompMP *	ThompMP *	ThompMP *	ThompMP *	ThompMP *	ThompMP *	ThompMP *	ThompMP *	ThompMP *	ThompMP *	ThompMP *
		Winter	--	NAMOC *	NAMOC *	NAMOC	--	--	--	--	NAMOC	NAMOC *	NAMOC *	NAMOC *	NAMOC *	--	--	--
		Spring	ThompMP *	ThompMP *	ThompMP *	ThompMP *	ThompMP *	ThompMP *	ThompMP *	ThompMP *	ThompMP *	ThompMP *	ThompMP *	ThompMP *	ThompMP *	ThompMP *	ThompMP *	ThompMP *

Table 18. SS (light shading) and PS (dark shading) pair-wise differences for the NAMOC and ThompsonMP configurations run with NEMSv0.9 (where the highlighted configuration is favored) for surface dew point temperature BCRMSE and bias by season and forecast lead time for the 00 UTC and 12 UTC initializations separately over the East verification domain.

Surface Dew Point Temperature			f03	f06	f09	f12	f15	f18	f21	f24	f27	f30	f33	f36	f39	f42	f45	f48
BCRMSE	00 UTC Initializations	Annual	--	--	--	NAMOC	--	--	--	ThompMP	ThompMP	ThompMP	ThompMP	--	--	ThompMP	ThompMP	ThompMP
		Summer	ThompMP	--	--	--	NAMOC	--	--	ThompMP	ThompMP	ThompMP	ThompMP	--	--	--	ThompMP	ThompMP *
		Fall	NAMOC	--	--	NAMOC	--	--	--	--	--	ThompMP	--	ThompMP	--	--	--	--
		Winter	--	--	--	--	--	--	--	--	--	--	--	--	--	--	--	ThompMP
		Spring	--	--	NAMOC	--	--	--	--	ThompMP	--	ThompMP	ThompMP	ThompMP	ThompMP	ThompMP	ThompMP	ThompMP
	12 UTC Initializations	Annual	ThompMP	--	--	--	--	--	--	--	--	--	ThompMP	ThompMP	--	--	--	--
		Summer	ThompMP	--	--	ThompMP	--	--	--	--	NAMOC	--	ThompMP	ThompMP	--	--	--	--
		Fall	--	--	--	ThompMP	--	--	--	--	--	--	--	--	ThompMP	ThompMP	ThompMP	--
		Winter	--	--	--	--	--	NAMOC	NAMOC	--	--	--	ThompMP	--	--	--	--	--
		Spring	ThompMP	--	--	--	--	ThompMP	--	--	--	--	--	ThompMP	--	--	--	--
Bias	00 UTC Initializations	Annual	NAMOC	NAMOC	NAMOC	NAMOC	ThompMP	ThompMP	ThompMP	ThompMP	ThompMP	ThompMP	ThompMP	ThompMP	ThompMP	ThompMP	ThompMP	--
		Summer	NAMOC	NAMOC	ThompMP	ThompMP *	ThompMP *	ThompMP *	ThompMP *	ThompMP *	ThompMP *	ThompMP *	ThompMP	ThompMP *	ThompMP *	ThompMP *	ThompMP *	ThompMP *
		Fall	--	NAMOC	NAMOC	--	--	ThompMP	ThompMP	ThompMP	ThompMP	--	--	--	--	--	ThompMP *	ThompMP
		Winter	NAMOC	NAMOC	NAMOC	NAMOC	--	--	--	--	--	NAMOC	NAMOC	--	--	ThompMP	ThompMP *	--
		Spring	--	--	--	--	ThompMP	ThompMP	ThompMP	ThompMP	--	--	--	--	--	ThompMP	--	--
	12 UTC Initializations	Annual	--	--	--	--	ThompMP	--	ThompMP	ThompMP	ThompMP	ThompMP	ThompMP	--	--	--	--	--
		Summer	ThompMP	ThompMP *	ThompMP *	ThompMP	ThompMP *	ThompMP *	ThompMP *	ThompMP *	ThompMP *	ThompMP *	ThompMP *	ThompMP *	ThompMP	ThompMP	ThompMP	ThompMP
		Fall	--	--	ThompMP	--	ThompMP	ThompMP	--	--	--	ThompMP	ThompMP	ThompMP	ThompMP	ThompMP	ThompMP	ThompMP
		Winter	ThompMP	ThompMP	ThompMP	--	--	--	--	--	--	ThompMP	ThompMP	--	--	--	--	--
		Spring	--	ThompMP	--	--	--	--	--	--	--	--	--	--	--	--	--	--

Table 19. SS (light shading) and PS (dark shading) pair-wise differences for the NAMOC and ThompsonMP configurations run with NEMSv0.9 (where the highlighted configuration is favored) for surface wind BCRMSE and bias by season and forecast lead time for the 00 UTC and 12 UTC initializations separately over the East verification domain.

Surface Wind Speed			f03	f06	f09	f12	f15	f18	f21	f24	f27	f30	f33	f36	f39	f42	f45	f48
BCRMSE	00 UTC Initializations	Annual	ThompMP	--	--	--	--	--	ThompMP	--	--	--	--	--	--	--	--	--
		Summer	--	ThompMP	--	ThompMP	ThompMP	ThompMP	ThompMP	--	--	--	--	ThompMP	--	--	--	ThompMP
		Fall	ThompMP	--	ThompMP	--	ThompMP	--	NAMOC	--	--	--	--	--	--	--	--	--
		Winter	--	--	--	--	--	--	--	--	--	--	--	--	--	--	--	--
		Spring	--	--	--	--	--	--	ThompMP	--	ThompMP	--	--	--	--	--	--	--
	12 UTC Initializations	Annual	ThompMP	--	--	--	--	--	--	NAMOC	--	--	--	--	--	--	--	--
		Summer	ThompMP	ThompMP	--	ThompMP	--	--	--	--	--	--	--	ThompMP	ThompMP	--	--	--
		Fall	ThompMP	--	--	--	--	--	--	--	--	--	--	--	--	--	--	--
		Winter	ThompMP	--	NAMOC	NAMOC	--	--	NAMOC	NAMOC	--	--	--	--	--	--	--	NAMOC
		Spring	--	--	--	ThompMP	--	--	--	--	--	--	--	--	--	--	--	--
Bias	00 UTC Initializations	Annual	ThompMP	--	--	--	ThompMP	ThompMP	ThompMP	ThompMP	--	--	--	--	ThompMP	ThompMP	ThompMP	ThompMP
		Summer	ThompMP	--	--	ThompMP	ThompMP	ThompMP	ThompMP	ThompMP	ThompMP	--	--	ThompMP	ThompMP	ThompMP	ThompMP	ThompMP
		Fall	--	--	--	--	ThompMP	ThompMP	ThompMP	ThompMP	--	--	--	--	ThompMP	ThompMP	ThompMP	--
		Winter	--	NAMOC	--	--	ThompMP	NAMOC	NAMOC	--	--	--	--	--	--	NAMOC	NAMOC	--
		Spring	ThompMP	ThompMP	ThompMP	ThompMP	ThompMP	ThompMP	ThompMP	ThompMP	--	--	--	--	ThompMP	ThompMP	ThompMP	ThompMP
	12 UTC Initializations	Annual	ThompMP	ThompMP	ThompMP	ThompMP	--	NAMOC	--	--	ThompMP	ThompMP	ThompMP	--	--	--	NAMOC	--
		Summer	ThompMP	ThompMP	ThompMP	ThompMP	--	--	--	--	--	ThompMP	ThompMP	ThompMP	ThompMP	--	--	--
		Fall	ThompMP	ThompMP	ThompMP	--	--	--	--	--	ThompMP	ThompMP	ThompMP	--	--	--	--	--
		Winter	ThompMP	NAMOC	NAMOC	--	--	NAMOC	--	--	--	NAMOC	--	--	--	--	NAMOC	NAMOC
		Spring	ThompMP	ThompMP	ThompMP	ThompMP	--	NAMOC	--	--	ThompMP	ThompMP	ThompMP	ThompMP	--	--	--	--

Table 20. SS differences for the NAMOC and ThompsonMP configurations run with NEMSv0.9 (where the highlighted configuration is favored) for 24-hour QPF GSS and frequency bias by season, forecast lead time, and threshold for the 00 UTC and 12 UTC initializations separately over the East verification domain.

Daily QPF				>0.01	>0.25	>0.5	>0.75	>1	>1.25	>1.5	>2	>3
Gilbert Skill Score	00 UTC Initializations	Annual	f36	--	--	--	--	--	--	--	--	--
		Summer	f36	--	--	--	--	--	--	--	--	--
		Fall	f36	--	--	--	--	--	--	--	NAMOC	--
		Winter	f36	--	--	--	--	--	--	--	--	--
		Spring	f36	--	--	--	--	--	--	--	--	--
	12 UTC Initializations	Annual	f24	--	--	--	--	--	--	--	--	--
			f48	--	--	--	--	--	--	--	--	--
		Summer	f24	--	--	--	--	--	--	--	--	--
			f48	--	--	--	--	--	--	--	--	--
		Fall	f24	--	--	--	--	--	--	--	--	--
			f48	--	--	--	--	--	--	--	--	--
		Winter	f24	--	--	--	--	--	--	--	--	--
			f48	--	--	--	--	--	--	--	--	--
		Spring	f24	--	--	--	--	--	--	--	--	--
			f48	--	--	--	--	--	--	--	--	--
Frequency Bias	00 UTC Initializations	Annual	f36	--	--	--	--	--	--	--	--	--
		Summer	f36	--	--	--	--	--	--	--	--	--
		Fall	f36	--	--	--	--	--	--	--	--	--
		Winter	f36	--	--	--	--	--	--	--	--	ThompMP
		Spring	f36	--	--	--	--	--	--	--	--	--
	12 UTC Initializations	Annual	f24	--	--	--	--	--	--	--	--	--
			f48	--	--	--	--	--	--	--	--	--
		Summer	f24	--	--	--	--	--	--	--	--	--
			f48	--	--	--	--	--	--	--	--	--
		Fall	f24	--	--	--	--	--	--	--	--	--
			f48	--	--	--	--	--	--	--	--	--
		Winter	f24	--	--	--	--	--	--	--	--	--
			f48	--	--	--	--	--	--	--	--	--
		Spring	f24	--	--	--	--	--	--	--	--	--
			f48	--	--	--	--	--	--	--	--	--

Table 21. SS differences for the NAMOC and ThompsonMP configurations run with NEMSv0.9 (where the highlighted configuration is favored) for reflectivity GSS and frequency bias by season, threshhold and forecast lead time for the 00 UTC and 12 UTC initializations separately over the East verification domain.

REFC				f03	f06	f09	f12	f15	f18	f21	f24	f27	f30	f33	f36	f39	f42	f45	f48
GSS	00 UTC Initializations	≥10	Annual	ThompMP	ThompMP	ThompMP	ThompMP	--	--	--	--	--	--	--	--	--	--	--	--
			Summer	--	--	--	--	--	--	--	--	--	--	--	--	--	--	--	NAMOC
			Fall	--	--	--	--	--	--	--	--	--	--	--	--	--	--	--	--
			Winter	--	--	--	--	--	--	--	--	--	--	--	--	--	--	--	--
			Spring	--	--	--	--	--	--	--	--	--	--	--	--	--	--	--	--
		≥20	Annual	--	--	--	--	--	--	--	--	--	--	--	--	--	--	--	--
			Summer	--	--	--	--	--	--	--	--	--	--	--	--	--	--	--	NAMOC
			Fall	--	--	--	--	--	--	--	--	--	--	--	--	--	--	--	--
			Winter	--	--	--	--	--	--	--	--	--	--	--	--	--	--	--	--
			Spring	--	--	--	--	--	--	--	--	--	--	--	--	--	--	--	--
	12 UTC Initializations	≥10	Annual	ThompMP	--	--	--	--	--	ThompMP	ThompMP	--	--	--	--	--	--	--	--
			Summer	--	--	--	--	--	--	--	--	--	--	--	--	--	--	--	--
			Fall	--	--	--	--	--	--	--	--	--	--	--	--	--	--	--	--
			Winter	--	--	--	--	--	--	--	--	--	--	--	--	--	--	--	--
			Spring	--	--	--	--	--	--	--	--	--	--	--	--	--	--	--	--
		≥20	Annual	--	--	--	--	--	--	--	--	--	--	--	--	--	--	--	--
			Summer	--	--	--	--	--	--	--	--	--	--	--	--	--	--	--	--
			Fall	--	--	--	--	--	--	--	--	--	--	--	--	--	--	--	--
			Winter	--	--	--	--	--	--	--	--	--	--	--	--	--	--	--	--
			Spring	--	--	--	--	--	--	--	--	--	--	--	--	--	--	--	--
Frequency Bias	00 UTC Initializations	≥10	Annual	ThompMP	ThompMP	ThompMP	ThompMP	ThompMP	ThompMP	ThompMP	ThompMP	ThompMP	ThompMP	ThompMP	ThompMP	ThompMP	ThompMP	ThompMP	ThompMP
			Summer	ThompMP	ThompMP	ThompMP	ThompMP	ThompMP	ThompMP	ThompMP	ThompMP	--	--	--	--	--	--	--	--
			Fall	--	--	ThompMP	ThompMP	ThompMP	ThompMP	ThompMP	ThompMP	--	--	--	--	--	ThompMP	--	ThompMP
			Winter	ThompMP	ThompMP	ThompMP	ThompMP	ThompMP	ThompMP	ThompMP	ThompMP	ThompMP	ThompMP	ThompMP	ThompMP	ThompMP	ThompMP	ThompMP	ThompMP
			Spring	ThompMP	--	--	--	--	--	--	ThompMP	--	--	ThompMP	ThompMP	ThompMP	--	ThompMP	ThompMP
		≥20	Annual	ThompMP	ThompMP	ThompMP	ThompMP	ThompMP	ThompMP	ThompMP	ThompMP	ThompMP	--	--	--	--	ThompMP	ThompMP	ThompMP
			Summer	--	--	--	--	--	--	--	--	--	--	--	--	--	--	--	--
			Fall	--	--	ThompMP	--	--	--	--	--	--	--	--	--	--	--	ThompMP	ThompMP
			Winter	--	ThompMP	ThompMP	ThompMP	ThompMP	ThompMP	ThompMP	ThompMP	ThompMP	ThompMP	ThompMP	--	ThompMP	ThompMP	ThompMP	ThompMP
			Spring	--	--	--	--	--	--	--	--	--	--	--	--	--	--	--	--
	12 UTC Initializations	≥10	Annual	ThompMP	ThompMP	ThompMP	ThompMP	ThompMP	ThompMP	ThompMP	ThompMP	ThompMP	ThompMP	ThompMP	ThompMP	ThompMP	ThompMP	ThompMP	ThompMP
			Summer	--	--	--	ThompMP	--	--	--	--	--	--	ThompMP	ThompMP	--	--	--	ThompMP
			Fall	ThompMP	ThompMP	ThompMP	ThompMP	--	ThompMP	--	ThompMP	ThompMP	ThompMP	ThompMP	ThompMP	--	--	ThompMP	ThompMP
			Winter	ThompMP	ThompMP	ThompMP	ThompMP	ThompMP	ThompMP	ThompMP	ThompMP	ThompMP	ThompMP	ThompMP	ThompMP	ThompMP	ThompMP	--	ThompMP
			Spring	ThompMP	--	--	ThompMP	ThompMP	ThompMP	ThompMP	--	ThompMP	ThompMP	ThompMP	ThompMP	--	--	--	--
		≥20	Annual	ThompMP	ThompMP	ThompMP	ThompMP	ThompMP	ThompMP	ThompMP	ThompMP	ThompMP	ThompMP	ThompMP	ThompMP	ThompMP	--	--	--
			Summer	--	--	--	--	--	--	--	--	--	--	--	ThompMP	--	--	--	--
			Fall	--	--	--	--	--	--	--	--	--	--	--	--	--	--	--	--
			Winter	ThompMP	ThompMP	ThompMP	ThompMP	ThompMP	ThompMP	ThompMP	ThompMP	ThompMP	ThompMP	ThompMP	ThompMP	ThompMP	ThompMP	--	ThompMP
			Spring	--	--	--	ThompMP	--	--	--	--	--	--	--	--	--	--	--	--

Table 22. SS (light shading) and PS (dark shading) pair-wise differences for the NAMOC and ThompsonMP configurations run with NEMSv0.9 (where the highlighted configuration is favored) for upper air temperature BCRMSE and bias by pressure level, season, and forecast lead time for the 00 UTC and 12 UTC initializations combined over the full Alaska verification domain.

Upper Air Temperature		Annual				Summer				Fall				Winter				Spring			
		f12	f24	f36	f48	f12	f24	f36	f48	f12	f24	f36	f48	f12	f24	f36	f48	f12	f24	f36	f48
BCRMSE	850	--	--	--	--	--	--	ThompMP	--	--	--	--	--	--	--	--	--	--	--	--	NAMOC
	700	--	--	--	--	--	--	--	--	--	--	--	--	--	--	--	--	--	--	--	--
	500	--	--	--	--	--	--	--	--	--	--	--	--	--	--	--	--	--	--	--	--
	400	--	--	--	--	--	--	--	--	--	--	--	--	--	--	--	--	--	--	--	--
	300	ThompMP	ThompMP	ThompMP	ThompMP	--	ThompMP	--	--	ThompMP	ThompMP	ThompMP	--	--	--	--	--	ThompMP	ThompMP	ThompMP	--
	200	--	--	--	--	--	--	--	--	--	ThompMP	ThompMP	--	--	--	--	--	--	--	--	--
	150	--	--	--	--	--	--	--	--	--	--	--	--	--	--	--	--	--	--	--	--
	100	--	--	--	--	--	--	--	--	ThompMP	--	--	--	--	--	--	--	--	--	--	--
Bias	850	NAMOC *	NAMOC *	NAMOC *	NAMOC *	ThompMP *	ThompMP *	ThompMP *	ThompMP *	NAMOC	NAMOC *	NAMOC *	NAMOC *	NAMOC	NAMOC *	NAMOC *	NAMOC *	NAMOC	NAMOC *	NAMOC *	NAMOC *
	700	NAMOC *	NAMOC *	NAMOC *	NAMOC *	NAMOC *	ThompMP *	ThompMP *	ThompMP *	NAMOC	NAMOC *	NAMOC *	NAMOC *	ThompMP	NAMOC	NAMOC *	NAMOC *	NAMOC	NAMOC *	NAMOC *	NAMOC *
	500	ThompMP	ThompMP	ThompMP	ThompMP	ThompMP	ThompMP *	ThompMP *	ThompMP *	ThompMP	--	ThompMP	--	--	--	--	--	ThompMP	ThompMP	ThompMP	ThompMP
	400	NAMOC	NAMOC	NAMOC	NAMOC	ThompMP	ThompMP	--	ThompMP	NAMOC	--	--	NAMOC	NAMOC	NAMOC *	NAMOC *	NAMOC *	NAMOC	NAMOC	NAMOC	NAMOC
	300	NAMOC	NAMOC *	NAMOC *	NAMOC *	NAMOC *	NAMOC *	NAMOC *	NAMOC *	NAMOC	NAMOC *	NAMOC *	NAMOC *	--	NAMOC	NAMOC	NAMOC	NAMOC	NAMOC *	NAMOC *	NAMOC *
	200	NAMOC	NAMOC	ThompMP	ThompMP	NAMOC	ThompMP	ThompMP	ThompMP	--	NAMOC	--	ThompMP	NAMOC	--	--	--	NAMOC	NAMOC	--	--
	150	ThompMP	ThompMP	ThompMP	ThompMP	ThompMP	ThompMP	ThompMP	ThompMP	NAMOC	ThompMP	ThompMP	--	--	ThompMP	ThompMP	ThompMP	ThompMP	ThompMP	ThompMP	ThompMP
	100	ThompMP	ThompMP	ThompMP	ThompMP	ThompMP	--	ThompMP	ThompMP	--	--	ThompMP	--	--	ThompMP	ThompMP	--	NAMOC	ThompMP	ThompMP	ThompMP

Table 23. SS (light shading) and PS (dark shading) pair-wise differences for the NAMOC and ThompsonMP configurations run with NEMSv0.9 (where the highlighted configuration is favored) for upper air dew point temperature BCRMSE and bias by pressure level, season, and forecast lead time for the 00 UTC and 12 UTC initializations combined over the full Alaska verification domain.

Upper Air Dew Point Temperature		Annual				Summer				Fall				Winter				Spring			
		f12	f24	f36	f48	f12	f24	f36	f48	f12	f24	f36	f48	f12	f24	f36	f48	f12	f24	f36	f48
BCRMSE	850	--	--	ThompMP	--	--	--	--	--	--	--	--	--	--	--	--	--	--	--	ThompMP	--
	700	--	--	--	--	--	--	ThompMP *	--	--	--	--	--	--	--	--	--	ThompMP	--	--	--
	500	--	--	--	--	--	--	--	--	--	--	--	--	NAMOC	--	--	--	--	--	--	--
	400	--	--	--	NAMOC	--	--	--	--	--	--	--	--	--	--	--	--	--	--	--	--
	300	--	--	NAMOC *	--	--	--	--	--	--	NAMOC	--	NAMOC *	--	--	NAMOC *	--	--	--	NAMOC	--
Bias	850	NAMOC	NAMOC *	ThompMP	--	--	--	NAMOC	--	--	ThompMP *	ThompMP	--	NAMOC	NAMOC	--	ThompMP	--	NAMOC	NAMOC	--
	700	NAMOC	--	--	--	NAMOC	NAMOC	--	--	--	--	--	--	--	--	--	--	--	--	--	--
	500	NAMOC	--	NAMOC	--	--	NAMOC	--	--	--	NAMOC	NAMOC	--	NAMOC	--	--	--	--	--	--	NAMOC
	400	NAMOC *	NAMOC *	NAMOC *	NAMOC *	--	NAMOC	--	--	ThompMP *	--	ThompMP *	ThompMP	ThompMP	NAMOC *	ThompMP *	ThompMP *	NAMOC	--	NAMOC *	--
	300	ThompMP *	ThompMP *	ThompMP *	ThompMP *	NAMOC *	NAMOC *	NAMOC *	NAMOC *	ThompMP *	ThompMP *	ThompMP *	ThompMP *	ThompMP *	ThompMP *	--	ThompMP *	ThompMP *	ThompMP *	ThompMP *	ThompMP *

Table 24. SS (light shading) and PS (dark shading) pair-wise differences for the NAMOC and ThompsonMP configurations run with NEMSv0.9 (where the highlighted configuration is favored) for upper air wind BCRMSE and bias by pressure level, season, and forecast lead time for the 00 UTC and 12 UTC initializations combined over the full Alaska verification domain.

Upper Air Wind Speed		Annual				Summer				Fall				Winter				Spring			
		f12	f24	f36	f48	f12	f24	f36	f48	f12	f24	f36	f48	f12	f24	f36	f48	f12	f24	f36	f48
BCRMSE	850	--	--	--	--	--	--	--	--	--	--	--	--	--	--	--	--	--	--	--	--
	700	--	--	--	--	--	--	--	--	--	--	--	NAMOC	--	--	--	--	--	--	--	--
	500	--	NAMOC	--	--	--	--	--	--	--	--	--	--	--	NAMOC	--	--	--	--	--	--
	400	--	--	--	--	--	--	--	ThompMP	--	--	--	--	--	ThompMP	--	--	--	--	--	--
	300	--	--	--	--	--	--	--	ThompMP	--	--	--	--	--	--	--	--	--	--	--	--
	200	--	--	--	--	--	--	--	--	--	--	--	--	--	--	--	--	--	--	--	--
	150	--	--	--	--	--	--	--	--	--	--	--	--	--	--	--	--	--	--	--	--
	100	--	--	--	--	--	--	--	--	--	--	--	ThompMP	--	--	--	--	--	--	--	--
Bias	850	--	--	NAMOC	--	--	NAMOC	NAMOC	--	--	--	NAMOC	--	NAMOC	--	--	--	--	--	--	--
	700	--	--	--	--	--	--	NAMOC	--	--	--	--	--	--	--	--	--	--	--	--	--
	500	NAMOC	--	NAMOC	NAMOC	--	--	--	--	--	--	--	--	--	--	--	--	--	--	--	NAMOC
	400	NAMOC	NAMOC	NAMOC	NAMOC	--	--	NAMOC	--	--	--	NAMOC	NAMOC	--	--	--	--	--	NAMOC	--	NAMOC
	300	--	NAMOC	NAMOC	--	--	--	--	--	--	--	--	NAMOC	--	--	--	--	--	--	--	NAMOC
	200	ThompMP	ThompMP	--	--	--	ThompMP	--	--	ThompMP	--	--	NAMOC	--	--	--	--	ThompMP	ThompMP	--	--
	150	ThompMP	--	--	ThompMP	--	--	NAMOC	NAMOC	--	--	--	--	ThompMP	--	NAMOC	--	NAMOC	ThompMP	--	NAMOC
	100	--	--	ThompMP	--	--	--	ThompMP	--	--	--	--	--	--	--	--	--	ThompMP	--	--	--

Table 25. SS (light shading) and PS (dark shading) pair-wise differences for the NAMOC and ThompsonMP configurations run with NEMSv0.9 (where the highlighted configuration is favored) for surface temperature BCRMSE and bias by season and forecast lead time for the 00 UTC and 12 UTC initializations separately over the full Alaska verification domain.

Surface Temperature			f03	f06	f09	f12	f15	f18	f21	f24	f27	f30	f33	f36	f39	f42	f45	f48
BCRMSE	00 UTC Initializations	Annual	ThompMP	--	--	--	--	--	--	--	--	--	--	--	--	--	--	--
		Summer	ThompMP	ThompMP	--	--	ThompMP	--	ThompMP	ThompMP	ThompMP	ThompMP	--	--	ThompMP	--	ThompMP	ThompMP
		Fall	--	--	--	--	--	--	--	NAMOC	--	--	--	--	--	--	--	--
		Winter	--	--	--	--	--	NAMOC	--	NAMOC	--	NAMOC *	NAMOC *	NAMOC *	NAMOC *	NAMOC *	NAMOC	NAMOC
		Spring	--	--	--	--	--	--	--	--	--	--	--	--	--	--	--	--
	12 UTC Initializations	Annual	--	--	--	--	--	--	--	--	--	--	--	--	--	--	--	--
		Summer	ThompMP	ThompMP	--	ThompMP	ThompMP	--	ThompMP	ThompMP	ThompMP	--	ThompMP	--	ThompMP	ThompMP	--	ThompMP
		Fall	--	--	NAMOC	--	--	--	--	--	--	--	--	NAMOC	--	--	--	--
		Winter	--	NAMOC	--	--	--	--	--	--	NAMOC	--	--	--	--	--	NAMOC	NAMOC
		Spring	--	--	--	--	--	--	--	--	--	--	--	--	--	--	ThompMP	ThompMP
Bias	00 UTC Initializations	Annual	ThompMP	ThompMP	ThompMP	--	ThompMP	ThompMP *	NAMOC *	NAMOC *	NAMOC *	ThompMP *	ThompMP *	ThompMP *	ThompMP *	ThompMP *	NAMOC *	NAMOC *
		Summer	ThompMP *	ThompMP	ThompMP	ThompMP	ThompMP *	ThompMP *	ThompMP *	ThompMP *	ThompMP *	ThompMP *	ThompMP *	ThompMP *	ThompMP *	ThompMP *	ThompMP *	ThompMP *
		Fall	--	--	--	--	--	NAMOC	NAMOC *	NAMOC *	NAMOC	ThompMP	ThompMP *	ThompMP	ThompMP	NAMOC	NAMOC *	NAMOC *
		Winter	--	--	--	NAMOC	NAMOC	--	--	NAMOC	--	--	--	--	--	--	NAMOC	NAMOC
		Spring	NAMOC *	ThompMP	ThompMP	--	ThompMP *	NAMOC *	NAMOC *	NAMOC *	NAMOC *	ThompMP *	ThompMP *	ThompMP *	ThompMP *	NAMOC *	NAMOC *	NAMOC *
	12 UTC Initializations	Annual	--	ThompMP	NAMOC *	NAMOC *	ThompMP *	ThompMP *	ThompMP *	ThompMP *	ThompMP *	ThompMP *	NAMOC *	NAMOC *	NAMOC *	ThompMP *	ThompMP *	ThompMP *
		Summer	ThompMP *	ThompMP *	ThompMP *	ThompMP *	ThompMP *	ThompMP *	ThompMP *	ThompMP *	ThompMP *	ThompMP *	ThompMP *	ThompMP *	ThompMP *	ThompMP *	ThompMP *	ThompMP *
		Fall	NAMOC	--	NAMOC	NAMOC *	ThompMP	ThompMP *	ThompMP *	ThompMP *	ThompMP	NAMOC *	NAMOC *	NAMOC *	ThompMP *	ThompMP *	ThompMP *	ThompMP *
		Winter	--	--	--	--	--	--	--	--	--	--	--	--	--	--	--	--
		Spring	--	NAMOC *	NAMOC *	NAMOC *	NAMOC *	NAMOC *	ThompMP *	ThompMP *	ThompMP *	NAMOC *	NAMOC *	NAMOC *	NAMOC *	ThompMP *	ThompMP *	ThompMP *

Table 26. SS (light shading) and PS (dark shading) pair-wise differences for the NAMOC and ThompsonMP configurations run with NEMSv0.9 (where the highlighted configuration is favored) for surface dew point temperature BCRMSE and bias by season and forecast lead time for the 00 UTC and 12 UTC initializations separately over the full Alaska verification domain.

Surface Dew Point Temperature			f03	f06	f09	f12	f15	f18	f21	f24	f27	f30	f33	f36	f39	f42	f45	f48
BCRMSE	00 UTC Initializations	Annual	ThompMP	--	--	--	--	--	--	--	--	--	--	--	--	--	--	--
		Summer	ThompMP	ThompMP	ThompMP	--	--	--	--	--	--	--	--	ThompMP	--	ThompMP	ThompMP	ThompMP
		Fall	--	--	--	--	--	--	--	--	--	--	--	--	--	--	--	--
		Winter	--	--	--	--	--	NAMOC	--	--	--	NAMOC	NAMOC *	NAMOC *	NAMOC *	NAMOC *	NAMOC *	NAMOC
		Spring	--	--	--	--	--	--	--	--	ThompMP	--	--	--	--	--	--	--
	12 UTC Initializations	Annual	--	--	--	--	--	--	--	NAMOC	--	--	--	--	--	--	--	--
		Summer	--	--	--	--	--	--	ThompMP	ThompMP	ThompMP	--	--	--	--	ThompMP	--	--
		Fall	--	--	--	--	--	--	NAMOC	NAMOC	--	--	--	--	--	--	--	--
		Winter	--	--	--	--	--	NAMOC	--	NAMOC *	NAMOC	NAMOC	--	--	--	NAMOC	NAMOC *	NAMOC *
		Spring	--	--	--	--	--	--	--	--	--	NAMOC	--	--	--	--	--	--
Bias	00 UTC Initializations	Annual	--	--	--	NAMOC	NAMOC	NAMOC	--	--	--	--	--	--	--	--	--	--
		Summer	ThompMP	--	--	--	ThompMP	ThompMP	ThompMP	--	--	--	--	--	NAMOC	--	--	--
		Fall	--	NAMOC	NAMOC	NAMOC	NAMOC	NAMOC	--	--	--	--	NAMOC	--	--	--	--	--
		Winter	--	--	NAMOC	NAMOC *	NAMOC *	NAMOC *	--	--	--	--	--	NAMOC	NAMOC	--	--	--
		Spring	ThompMP	ThompMP	--	--	--	ThompMP	--	--	--	ThompMP	--	--	--	ThompMP	ThompMP	ThompMP
	12 UTC Initializations	Annual	NAMOC	NAMOC	--	--	--	--	--	--	--	--	--	ThompMP	ThompMP	ThompMP	--	--
		Summer	--	ThompMP	ThompMP	ThompMP	ThompMP	--	--	--	--	--	--	--	--	--	--	--
		Fall	NAMOC	NAMOC	--	--	--	--	--	--	--	--	ThompMP	--	ThompMP	ThompMP	--	--
		Winter	NAMOC	--	--	--	--	--	NAMOC	--	--	--	--	--	--	--	--	NAMOC
		Spring	--	--	--	--	--	--	--	--	--	--	--	ThompMP	ThompMP	ThompMP	ThompMP	--

Table 27. SS (light shading) and PS (dark shading) pair-wise differences for the NAMOC and ThompsonMP configurations run with NEMSv0.9 (where the highlighted configuration is favored) for surface wind BCRMSE and bias by season and forecast lead time for the 00 UTC and 12 UTC initializations separately over the full Alaska verification domain.

Surface Wind Speed			f03	f06	f09	f12	f15	f18	f21	f24	f27	f30	f33	f36	f39	f42	f45	f48
BCRMSE	00 UTC Initializations	Annual	ThompMP	--	--	--	--	--	--	--	--	--	--	--	--	--	--	--
		Summer	ThompMP	--	ThompMP	--	--	ThompMP	--	--	--	--	--	--	--	--	--	--
		Fall	ThompMP	--	--	--	--	--	--	--	--	--	--	--	--	--	--	--
		Winter	--	--	--	--	--	--	ThompMP	--	--	--	--	--	--	--	--	--
		Spring	--	--	ThompMP	--	--	--	--	--	--	--	--	--	--	--	--	--
	12 UTC Initializations	Annual	--	--	--	--	--	--	--	--	--	--	ThompMP	--	--	--	--	--
		Summer	ThompMP	ThompMP	ThompMP	--	--	--	--	--	ThompMP	--	--	--	ThompMP	ThompMP	--	--
		Fall	--	--	--	--	--	--	--	ThompMP	--	--	--	--	--	--	--	--
		Winter	--	--	--	NAMOC	--	--	--	NAMOC	--	--	--	--	--	--	NAMOC	--
		Spring	--	--	--	--	--	--	--	--	NAMOC	--	--	--	--	--	--	--
Bias	00 UTC Initializations	Annual	ThompMP	--	ThompMP	--	--	ThompMP	NAMOC	NAMOC	NAMOC	--	--	--	--	--	NAMOC	NAMOC
		Summer	ThompMP	ThompMP	ThompMP	--	ThompMP	ThompMP	NAMOC	ThompMP	ThompMP	ThompMP	ThompMP	--	--	ThompMP	ThompMP	ThompMP
		Fall	ThompMP	--	--	--	--	--	--	--	--	--	--	--	--	--	--	--
		Winter	--	--	--	--	--	--	--	--	--	--	--	--	--	--	--	--
		Spring	NAMOC	--	--	--	--	NAMOC	NAMOC	NAMOC	--	--	--	--	--	--	NAMOC	NAMOC
	12 UTC Initializations	Annual	ThompMP	ThompMP	NAMOC	NAMOC	ThompMP	--	--	--	ThompMP	ThompMP	NAMOC	NAMOC	ThompMP	ThompMP	ThompMP	ThompMP
		Summer	ThompMP	ThompMP	NAMOC	NAMOC	ThompMP	ThompMP	ThompMP	ThompMP	ThompMP	ThompMP	NAMOC	NAMOC	ThompMP	ThompMP	ThompMP	ThompMP
		Fall	--	--	ThompMP	--	--	--	--	--	--	--	--	NAMOC	ThompMP	--	ThompMP	ThompMP
		Winter	--	--	--	--	--	--	--	ThompMP	--	--	--	--	--	--	--	--
		Spring	--	NAMOC	--	NAMOC	NAMOC	--	--	--	--	NAMOC	NAMOC	NAMOC	NAMOC	--	ThompMP	--

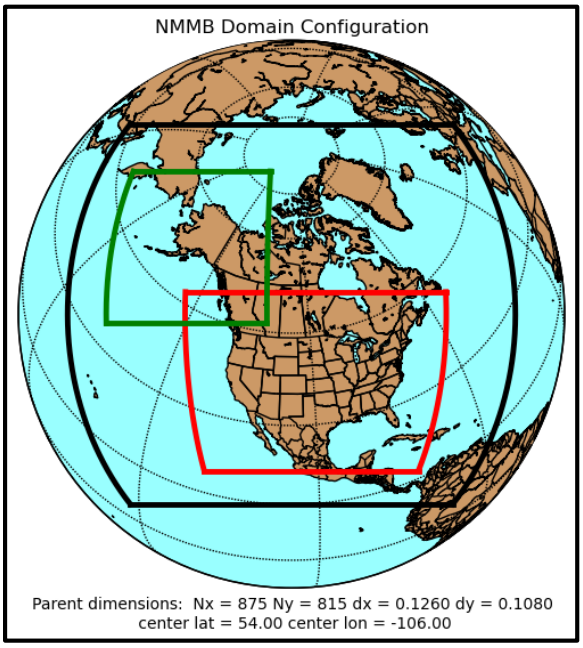

Figure 1. Map showing the boundary of the NEMS-NMMB computational domains. The parent domain (12 km) is outlined by the black line, the CONUS nest (3 km) is outlined by the red line, and the Alaska nest (3 km) is outlined by the green line.

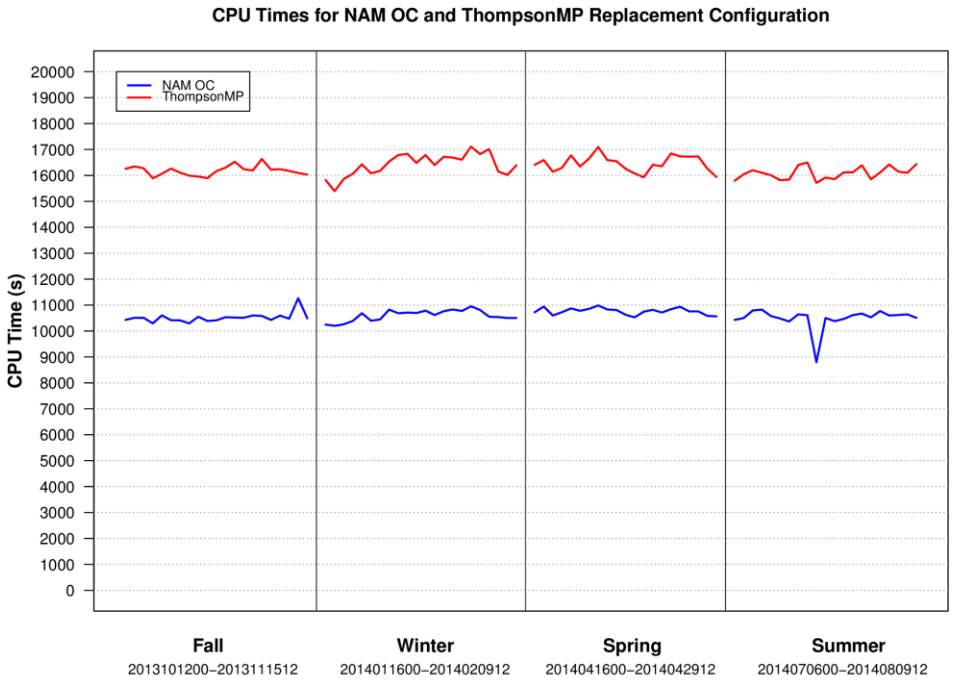

Figure 1. Time series run times (s) for all initializations used in this test, with the start and end initializations given for each season. The 84 total initializations that ran to completion are included in this graph; forecasts were initialized every 36 hours and run out to 48 hours. The NAMOC configuration is in blue, and the ThompsonMP configuration is in red.

Figure 3. Map showing the locations of the a) CONUS-West, CONUS-East, b) 14 CONUS regional, and c) 2 Alaska verification domains. The outermost outline of the regional CONUS domains depict the full CONUS verification domain.

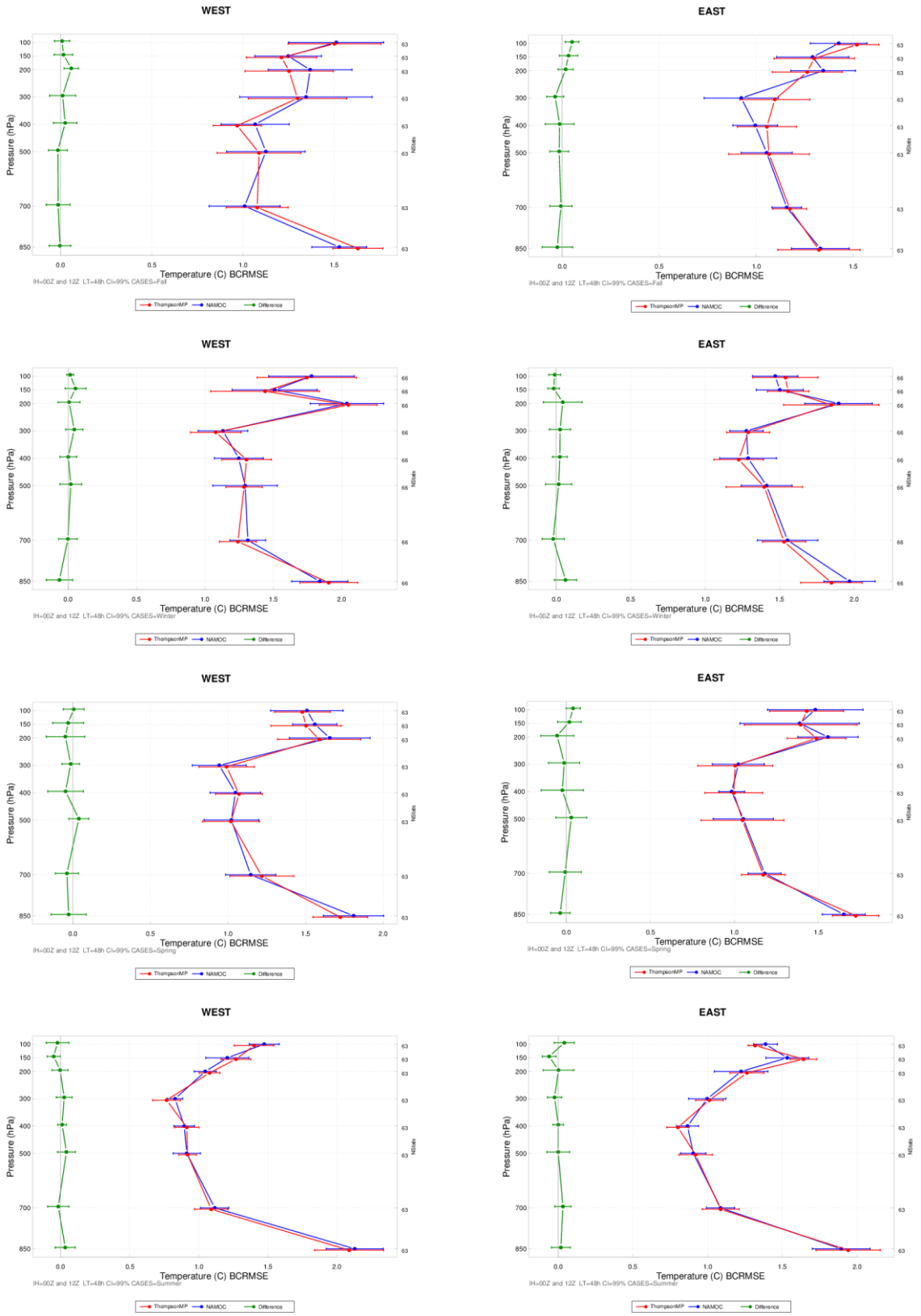

Figure 4. Vertical profiles of the median BCRMSE for temperature (°C) for the 48-h forecast lead time. The left column is aggregated over the CONUS West domain, and the right column is aggregated across the CONUS East domain. The first row is the fall aggregation, the second row is the winter aggregation, the third row is the spring aggregation, and the fourth row is the summer aggregation. NAMOC is in blue, ThompsonMP in red, and the differences (NAMOC-ThompsonMP) in green. The vertical bars attached to the median represent the 99% CIs.

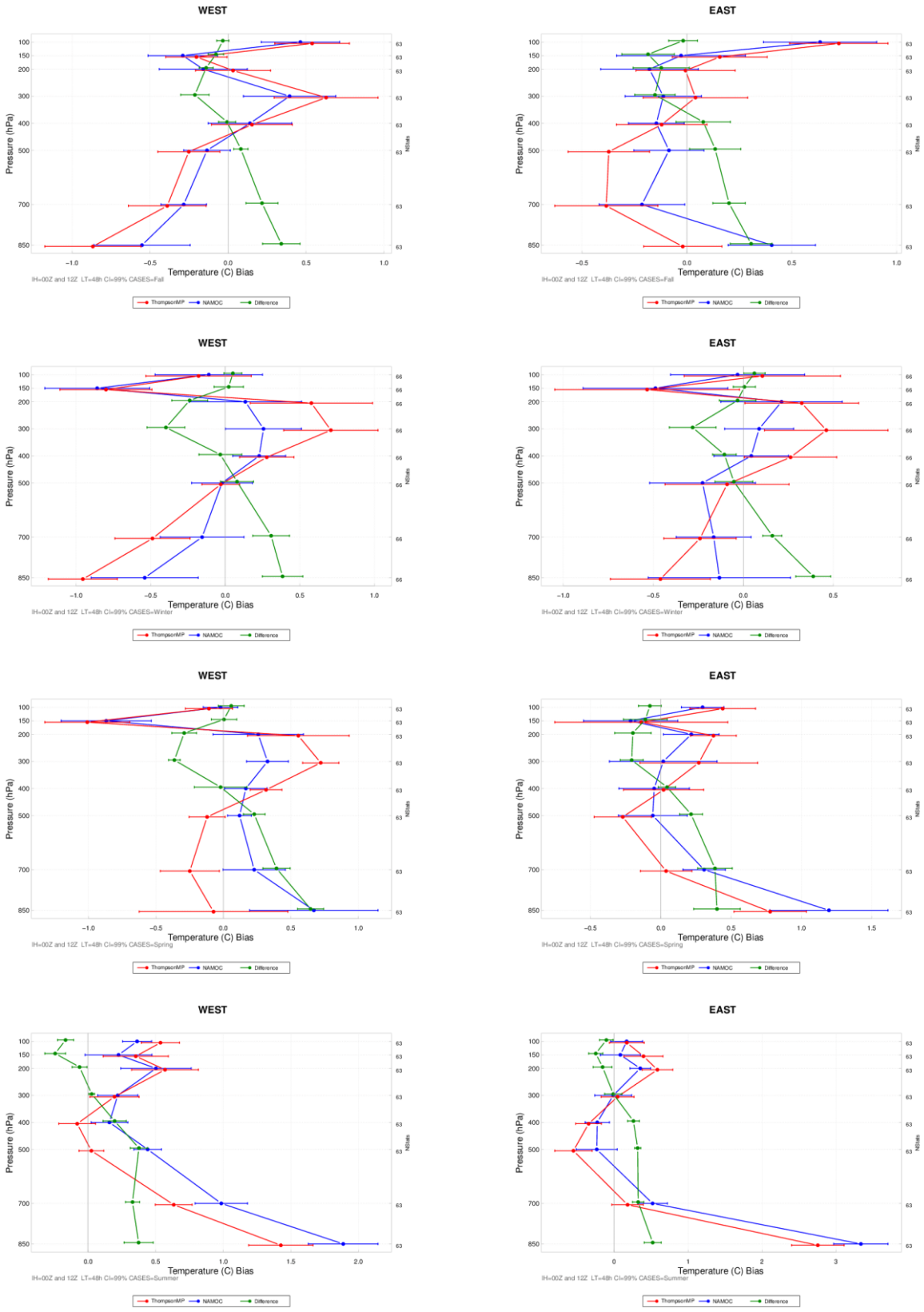

Figure 5. Vertical profiles of the median bias for temperature (°C) for the 48-h forecast lead time. The left column is aggregated over the CONUS West domain, and the right column is aggregated across the CONUS East domain. The first row is the fall aggregation, the second row is the winter aggregation, the third row is the spring aggregation, and the fourth row is the summer aggregation. NAMOC is in blue, ThompsonMP in red, and the differences (NAMOC-ThompsonMP) in green. The vertical bars attached to the median represent the 99% CIs.

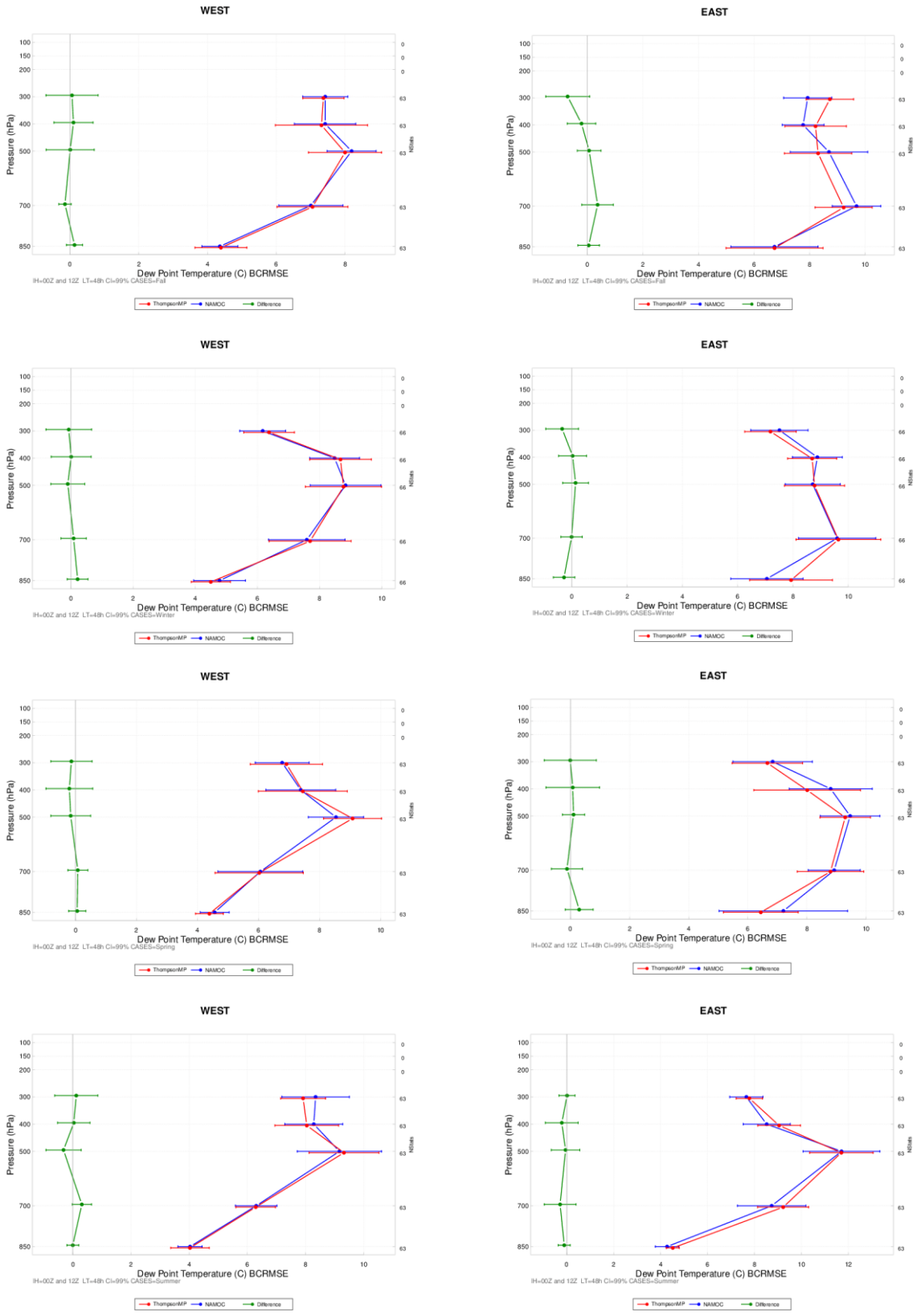

Figure 6. Vertical profiles of the median BCRMSE for dew point temperature (°C) for the 48-h forecast lead time. The left column is aggregated over the CONUS West domain, and the right column is aggregated across the CONUS East domain. The first row is the fall aggregation, the second row is the winter aggregation, the third row is the spring aggregation, and the fourth row is the summer aggregation. NAMOC is in blue, ThompsonMP in red, and the differences (NAMOC-ThompsonMP) in green. The vertical bars attached to the median represent the 99% CIs.

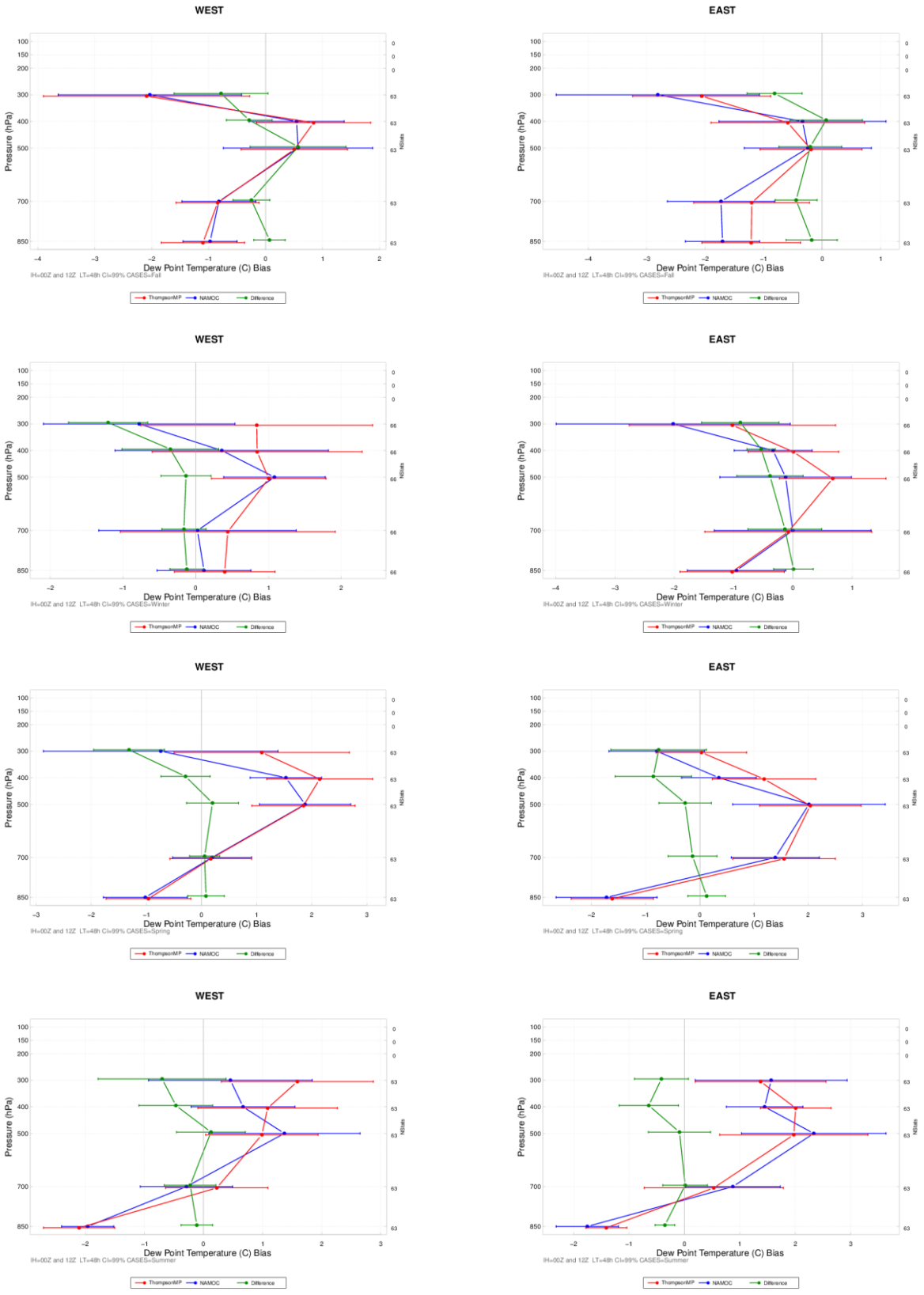

Figure 7. Vertical profiles of the median bias for dew point temperature (°C) for the 48-h forecast lead time. The left column is aggregated over the CONUS West domain, and the right column is aggregated across the CONUS East domain. The first row is the fall aggregation, the second row is the winter aggregation, the third row is the spring aggregation, and the fourth row is the summer aggregation. NAMOC is in blue, ThompsonMP in red, and the differences (NAMOC-ThompsonMP) in green. The vertical bars attached to the median represent the 99% CIs.

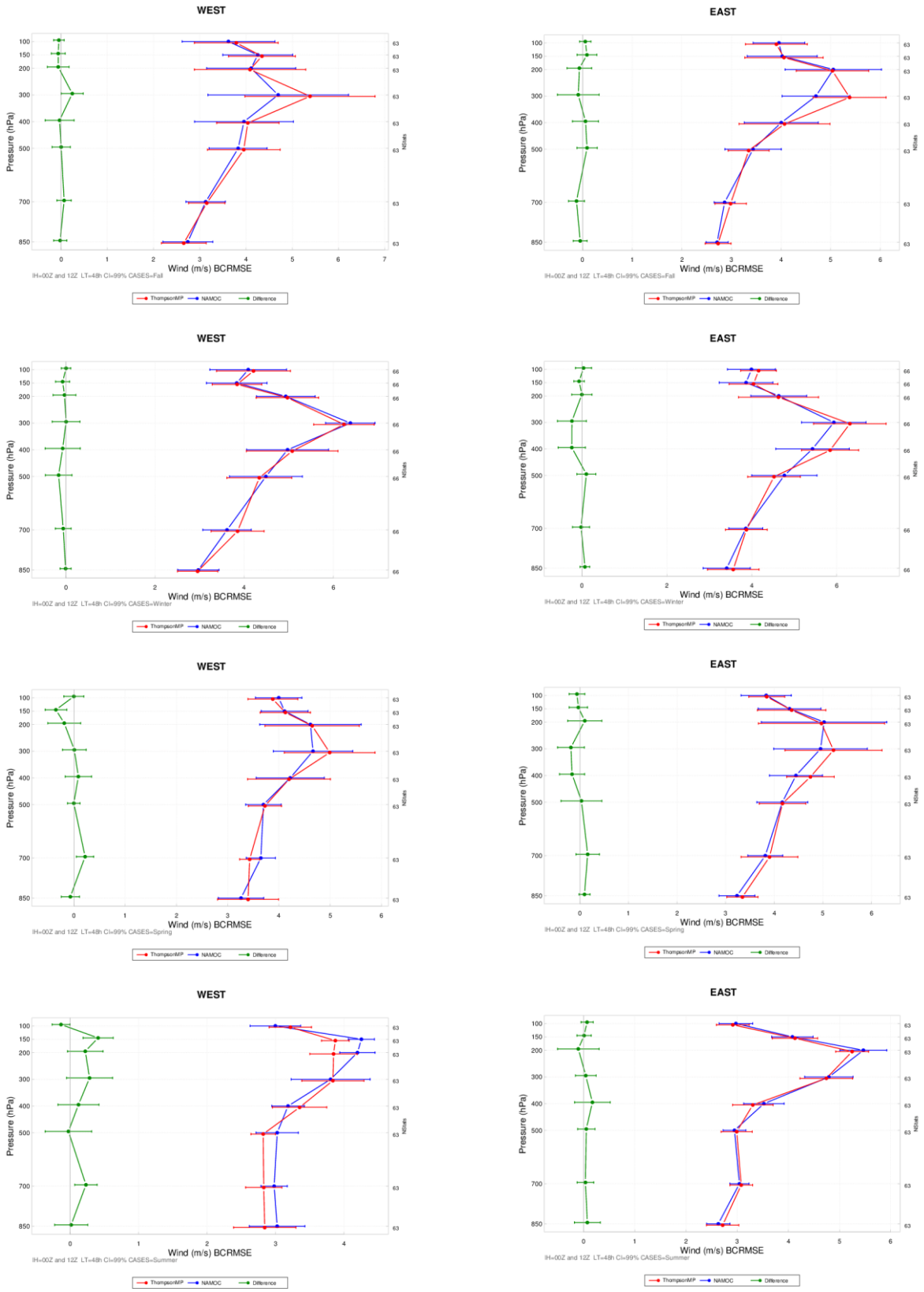

Figure 8. Vertical profiles of the median BCRMSE for wind speed (m s^{-1}) for the 48-h forecast lead time. The left column is aggregated over the CONUS West domain, and the right column is aggregated across the CONUS East domain. The first row is the fall aggregation, the second row is the winter aggregation, the third row is the spring aggregation, and the fourth row is the summer aggregation. NAMOC is in blue, ThompsonMP in red, and the differences (NAMOC-ThompsonMP) in green. The vertical bars attached to the median represent the 99% CIs.

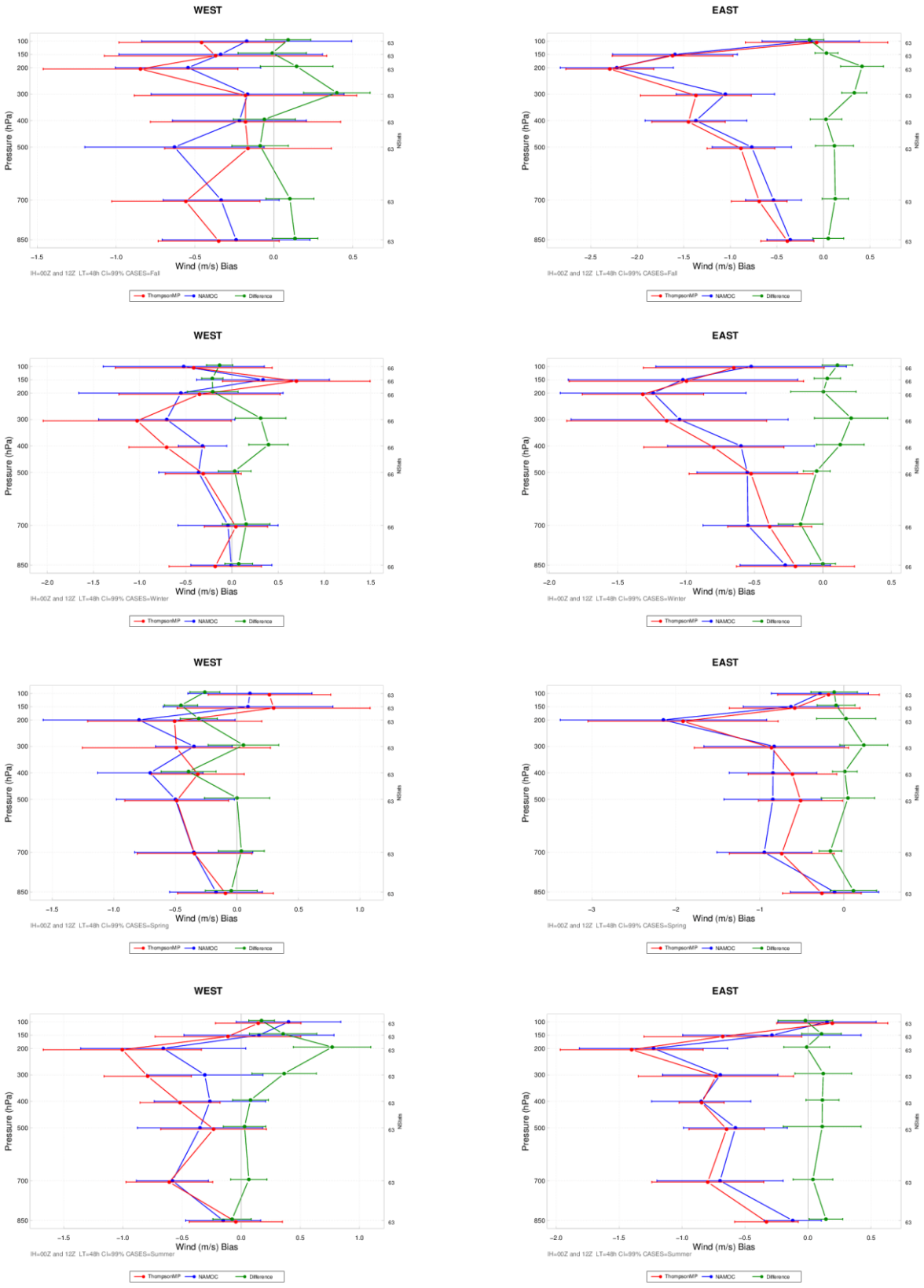

Figure 9. Vertical profiles of the median bias for wind speed (m s^{-1}) for the 48-h forecast lead time. The left column is aggregated over the CONUS West domain, and the right column is aggregated across the CONUS East domain. The first row is the fall aggregation, the second row is the winter aggregation, the third row is the spring aggregation, and the fourth row is the summer aggregation. NAMOC is in blue, ThompsonMP in red, and the differences (NAMOC-ThompsonMP) in green. The vertical bars attached to the median represent the 99% CIs.

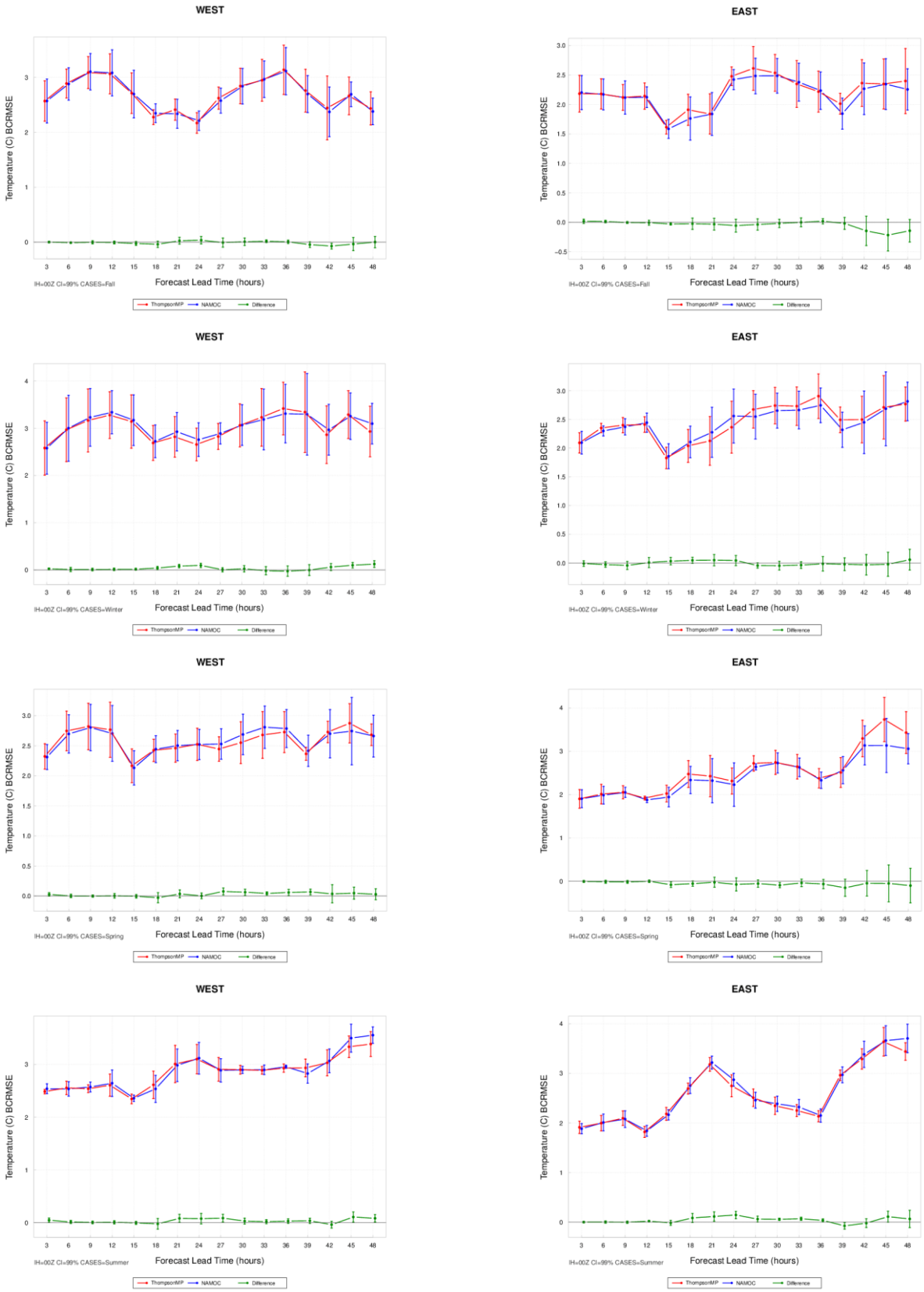

Figure 10. Time series plots of the 2 m AGL temperature (°C) for median BCRMSE for all 00 UTC initializations. The left column is aggregated over the CONUS West domain, and the right column is aggregated across the CONUS East domain. The first row is the fall aggregation, the second row is the winter aggregation, the third row is the spring aggregation, and the fourth row is the summer aggregation. NAMOC is in blue, ThompsonMP in red, and the differences (NAMOC-ThompsonMP) in green. The vertical bars attached to the median represent the 99% CIs.

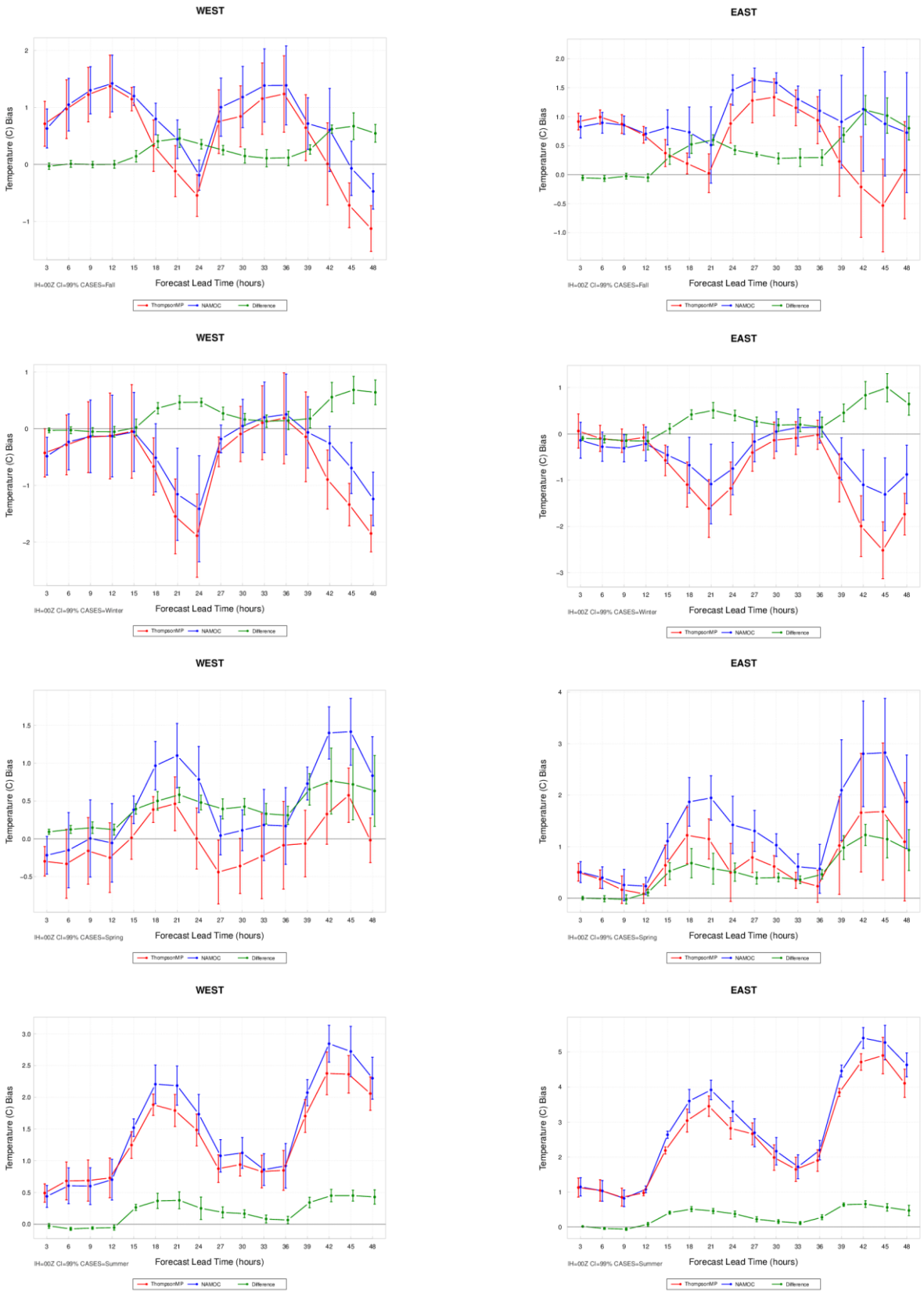

Figure 11. Time series plots of the 2 m AGL temperature (°C) for median bias for all 00 UTC initializations. The left column is aggregated over the CONUS West domain, and the right column is aggregated across the CONUS East domain. The first row is the fall aggregation, the second row is the winter aggregation, the third row is the spring aggregation, and the fourth row is the summer aggregation. NAMOC is in blue, ThompsonMP in red, and the differences (NAMOC-ThompsonMP) in green. The vertical bars attached to the median represent the 99% CIs.

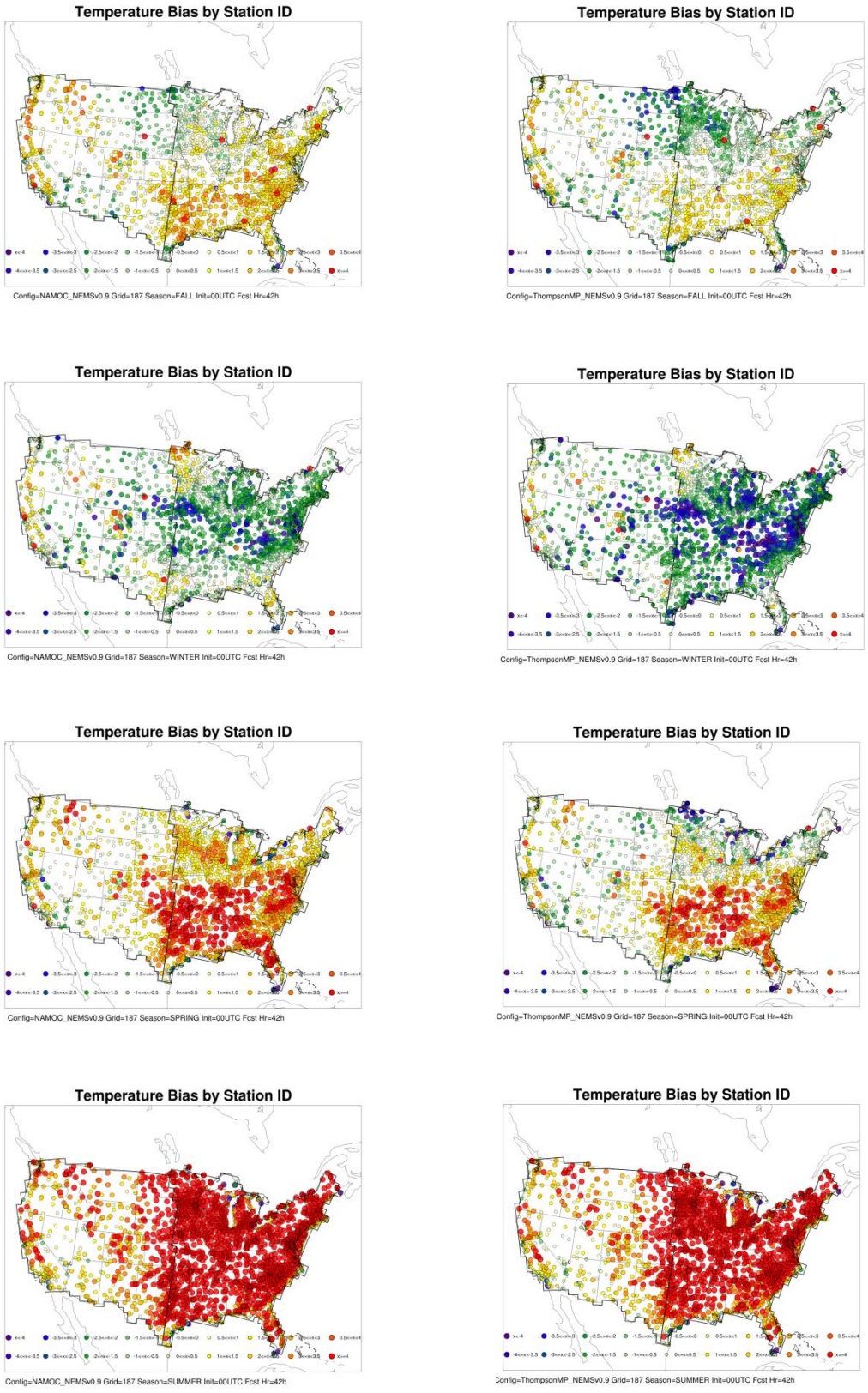

Figure 12. Spatial plots of the 2 m AGL temperature (°C) for mean bias for the 42-h forecast lead time for all 00 UTC initializations over the CONUS domain. The left column is NAMOC, and the right column is ThompsonMP. The first row is the fall aggregation, the second row is the winter aggregation, the third row is the spring aggregation, and the fourth row is the summer aggregation.

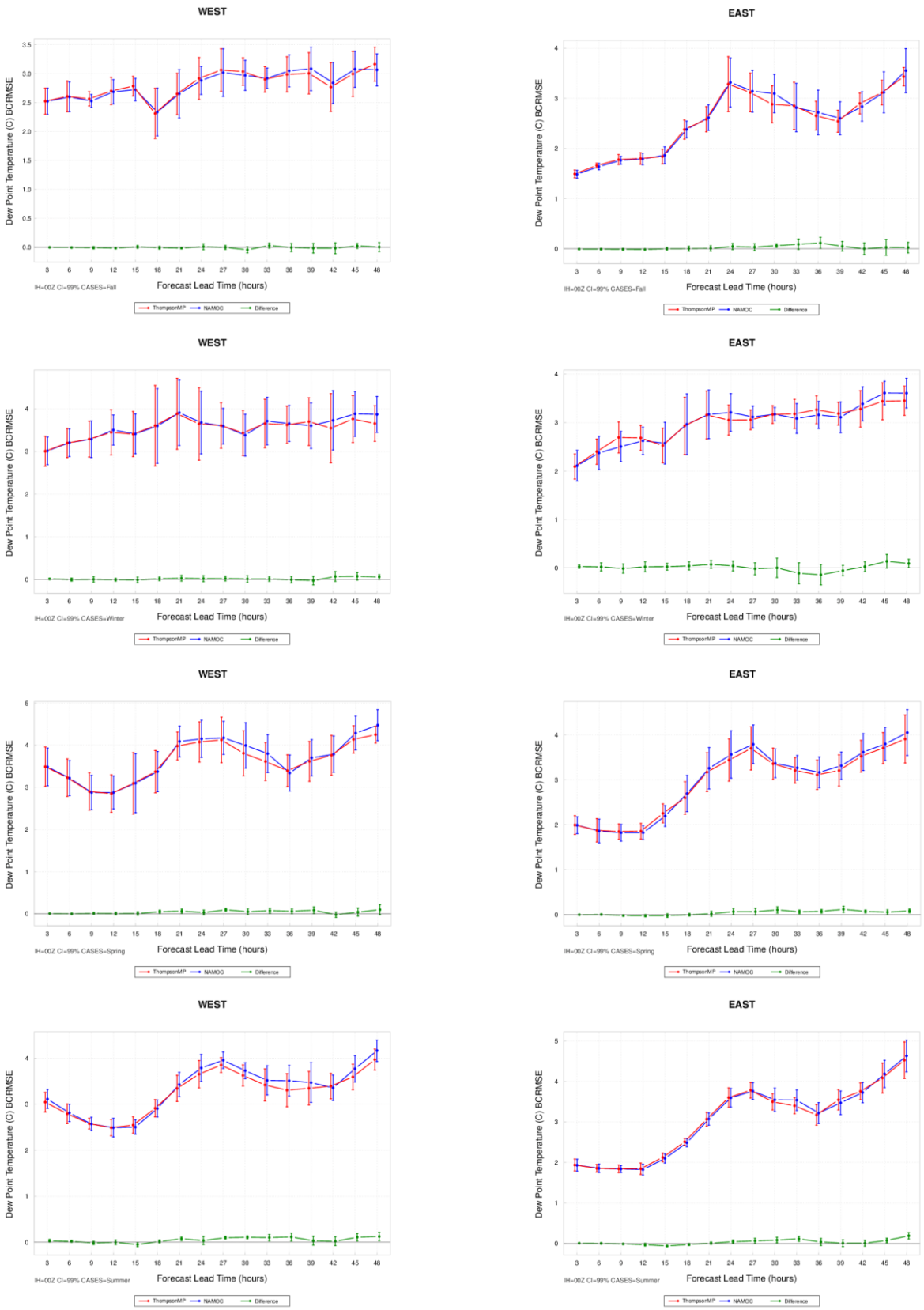

Figure 13. Time series plots of the 2 m AGL dew point temperature (°C) for median BCRMSE for all 00 UTC initializations. The left column is aggregated over the CONUS West domain, and the right column is aggregated across the CONUS East domain. The first row is the fall aggregation, the second row is the winter aggregation, the third row is the spring aggregation, and the fourth row is the summer aggregation. NAMOC is in blue, ThompsonMP in red, and the differences (NAMOC-ThompsonMP) in green. The vertical bars attached to the median represent the 99% CIs.

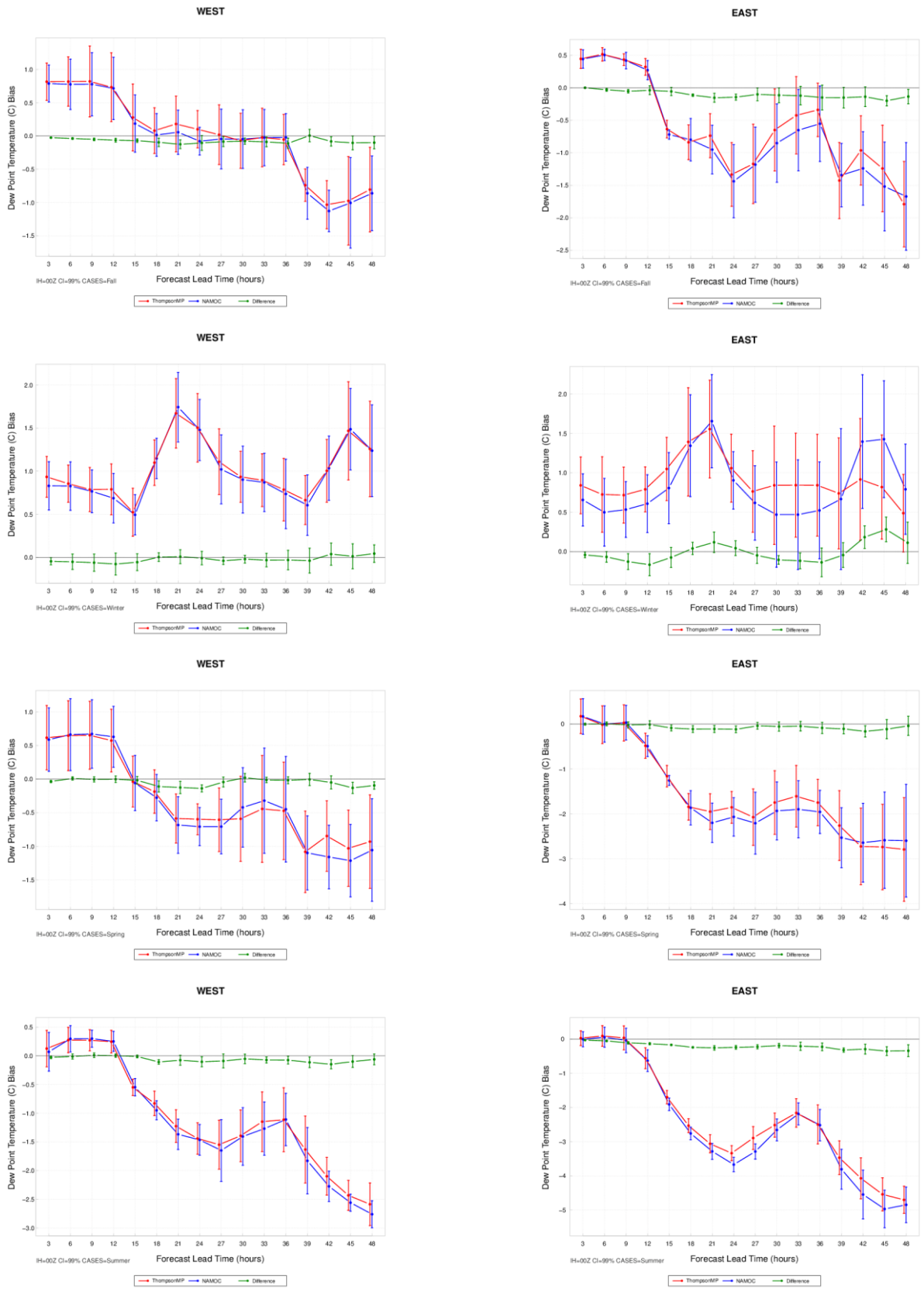

Figure 14. Time series plots of the 2 m AGL dew point temperature (°C) for median bias for all 00 UTC initializations. The left column is aggregated over the CONUS West domain, and the right column is aggregated across the CONUS East domain. The first row is the fall aggregation, the second row is the winter aggregation, the third row is the spring aggregation, and the fourth row is the summer aggregation. NAMOC is in blue, ThompsonMP in red, and the differences (NAMOC-ThompsonMP) in green. The vertical bars attached to the median represent the 99% CIs.

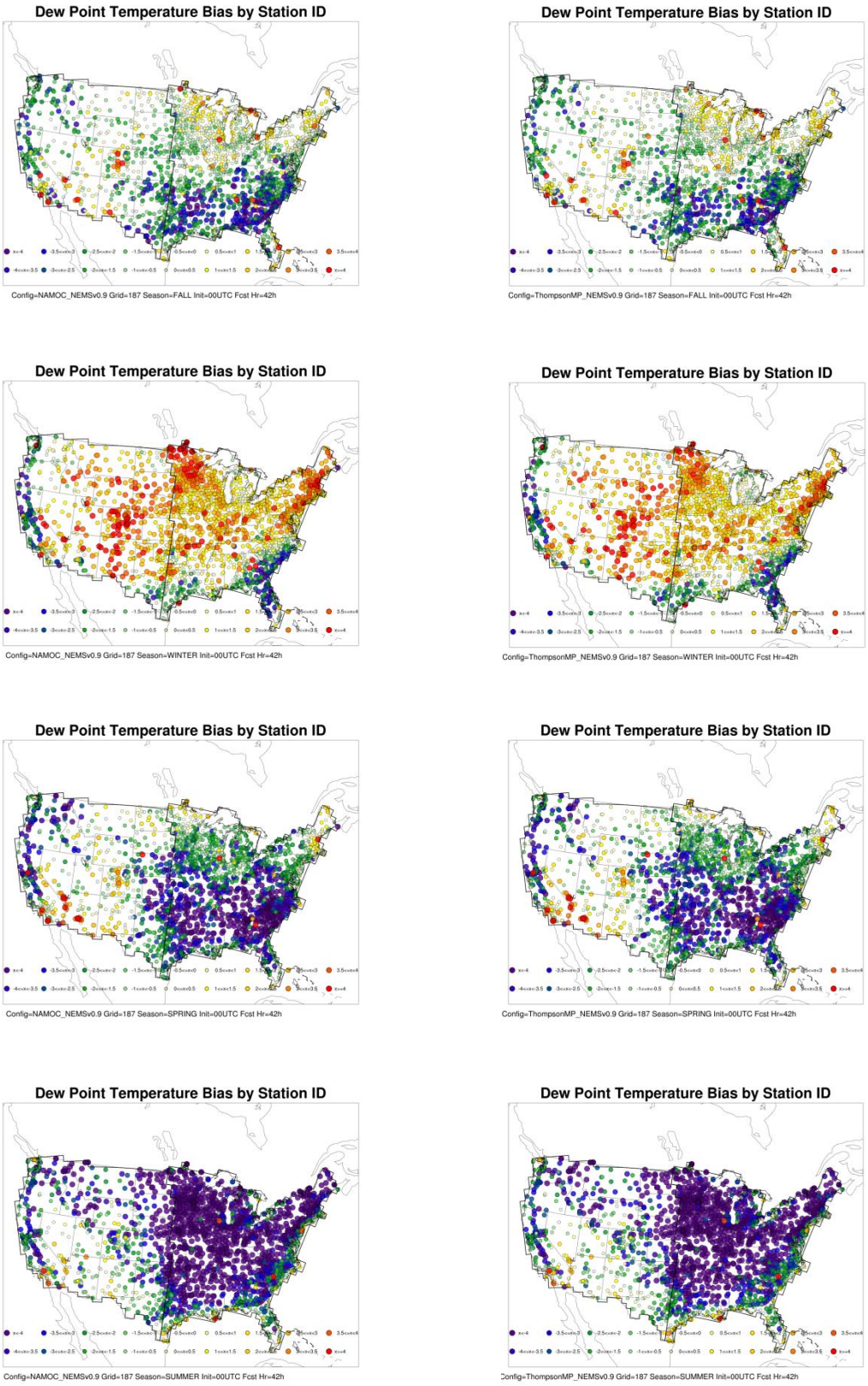

Figure 15. Spatial plots of the 2 m AGL dew point temperature (°C) for mean bias for the 42-h forecast lead time for all 00 UTC initializations over the CONUS domain. The left column is NAMOC, and the right column is ThompsonMP. The first row is the fall aggregation, the second row is the winter aggregation, the third row is the spring aggregation, and the fourth row is the summer aggregation.

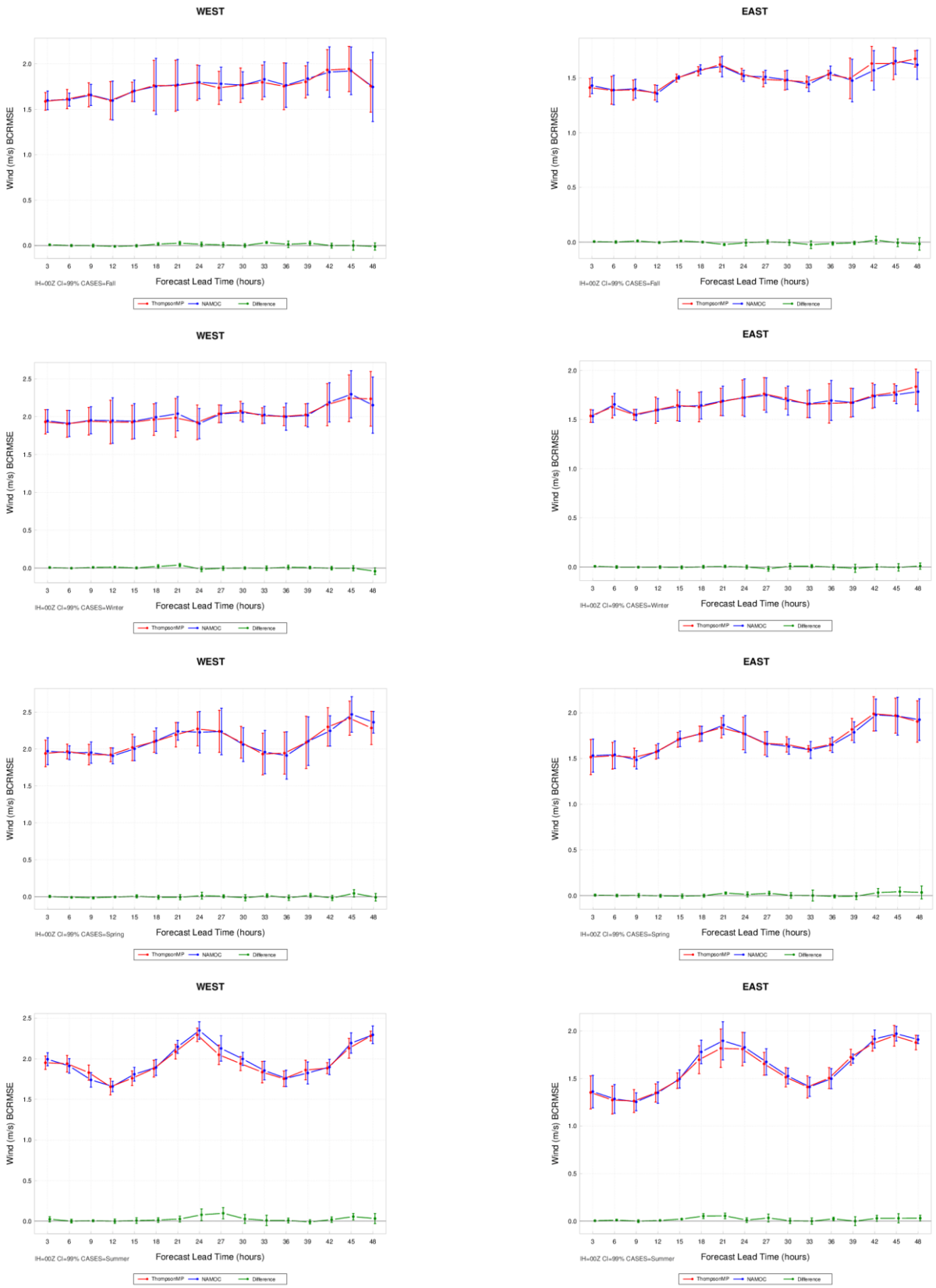

Figure 16. Time series plots of the 10 m AGL wind speed (m s^{-1}) for median BCRMSE for all 00 UTC initializations. The left column is aggregated over the CONUS West domain, and the right column is aggregated across the CONUS East domain. The first row is the fall aggregation, the second row is the winter aggregation, the third row is the spring aggregation, and the fourth row is the summer aggregation. NAMOC is in blue, ThompsonMP in red, and the differences (NAMOC-ThompsonMP) in green. The vertical bars attached to the median represent the 99% CIs.

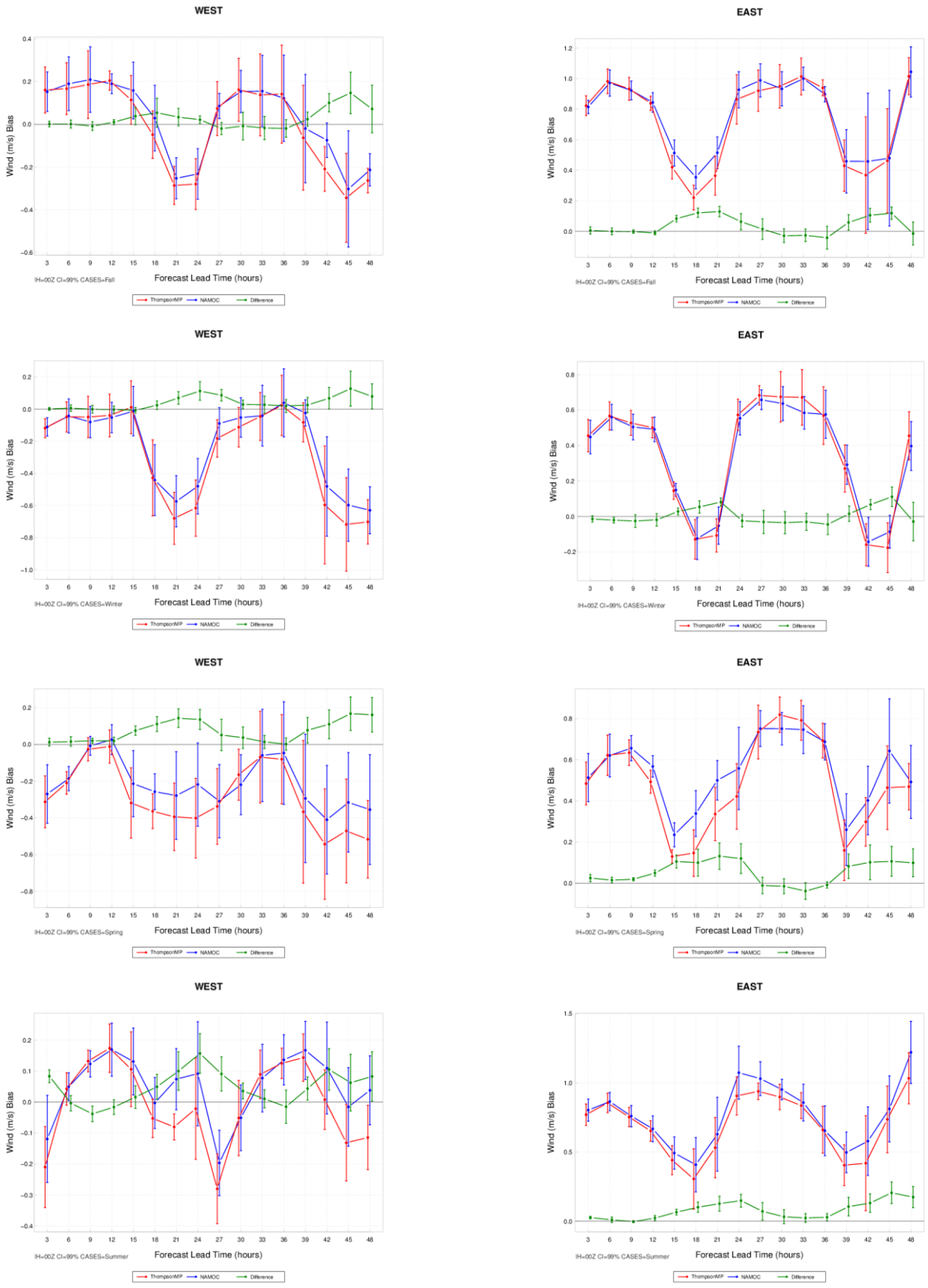

Figure 17. Time series plots of the 10 m AGL wind speed (m s^{-1}) for median bias for all 00 UTC initializations. The left column is aggregated over the CONUS West domain, and the right column is aggregated across the CONUS East domain. The first row is the fall aggregation, the second row is the winter aggregation, the third row is the spring aggregation, and the fourth row is the summer aggregation. NAMOC is in blue, ThompsonMP in red, and the differences (NAMOC-ThompsonMP) in green. The vertical bars attached to the median represent the 99% CIs.

Figure 18. Spatial plots of the 10 m AGL wind speed (m s^{-1}) for mean bias for the 42-h forecast lead time for all 00 UTC initializations over the CONUS domain. The left column is NAMOC, and the right column is ThompsonMP. The first row is the fall aggregation, the second row is the winter aggregation, the third row is the spring aggregation, and the fourth row is the summer aggregation.

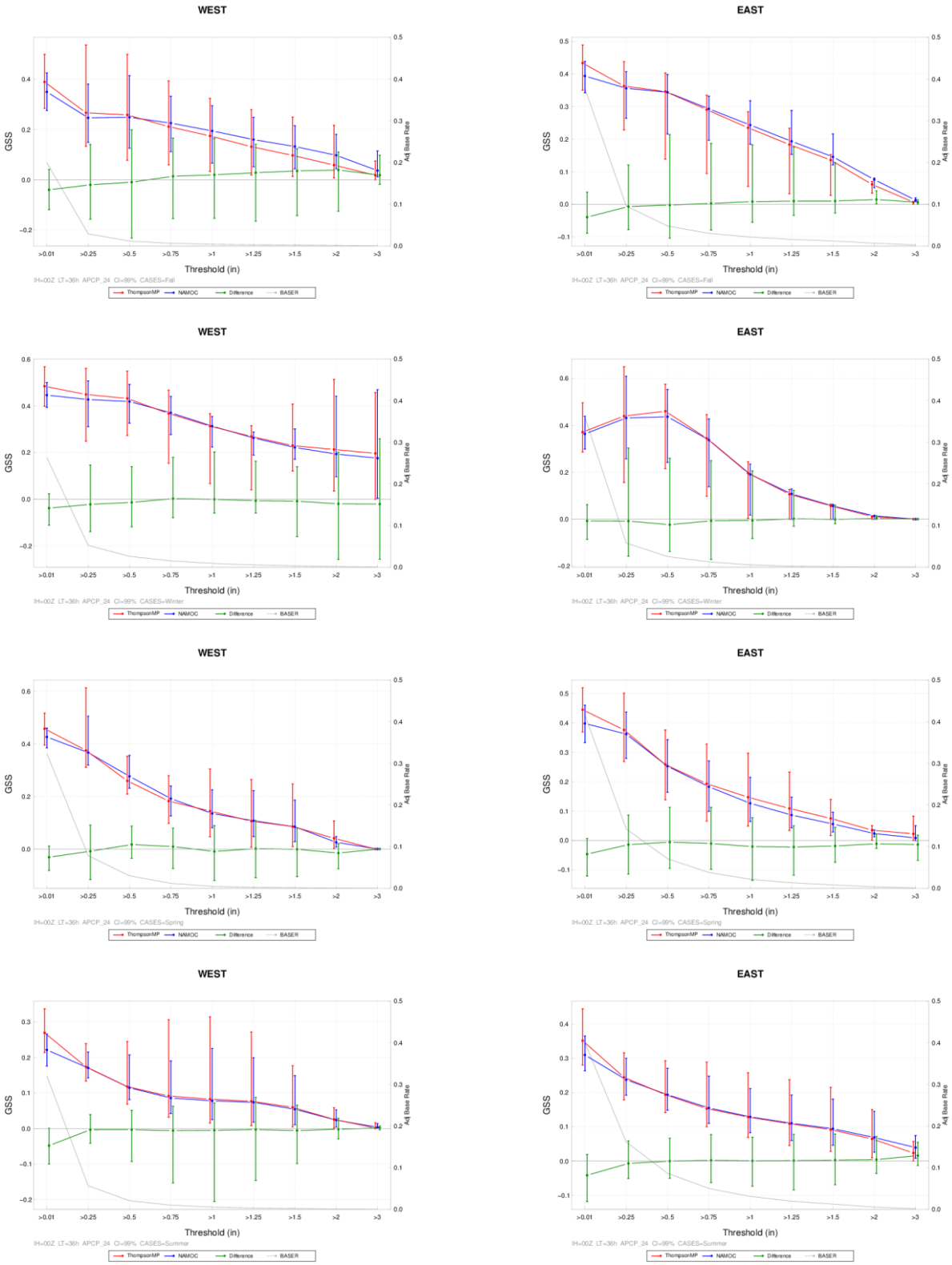

Figure 19. Threshold series plot of 24-h accumulated precipitation (in) for aggregated GSS for the East and West regions of the CONUS domain across all 00 UTC initializations for the 36-h forecast lead time for the fall, winter, spring and summer aggregations. NAMOC is in blue and ThompsonMP in red. The base rate, in grey, is associated with the second y-axis. The vertical bars attached to the aggregated value represent the 99% CIs.

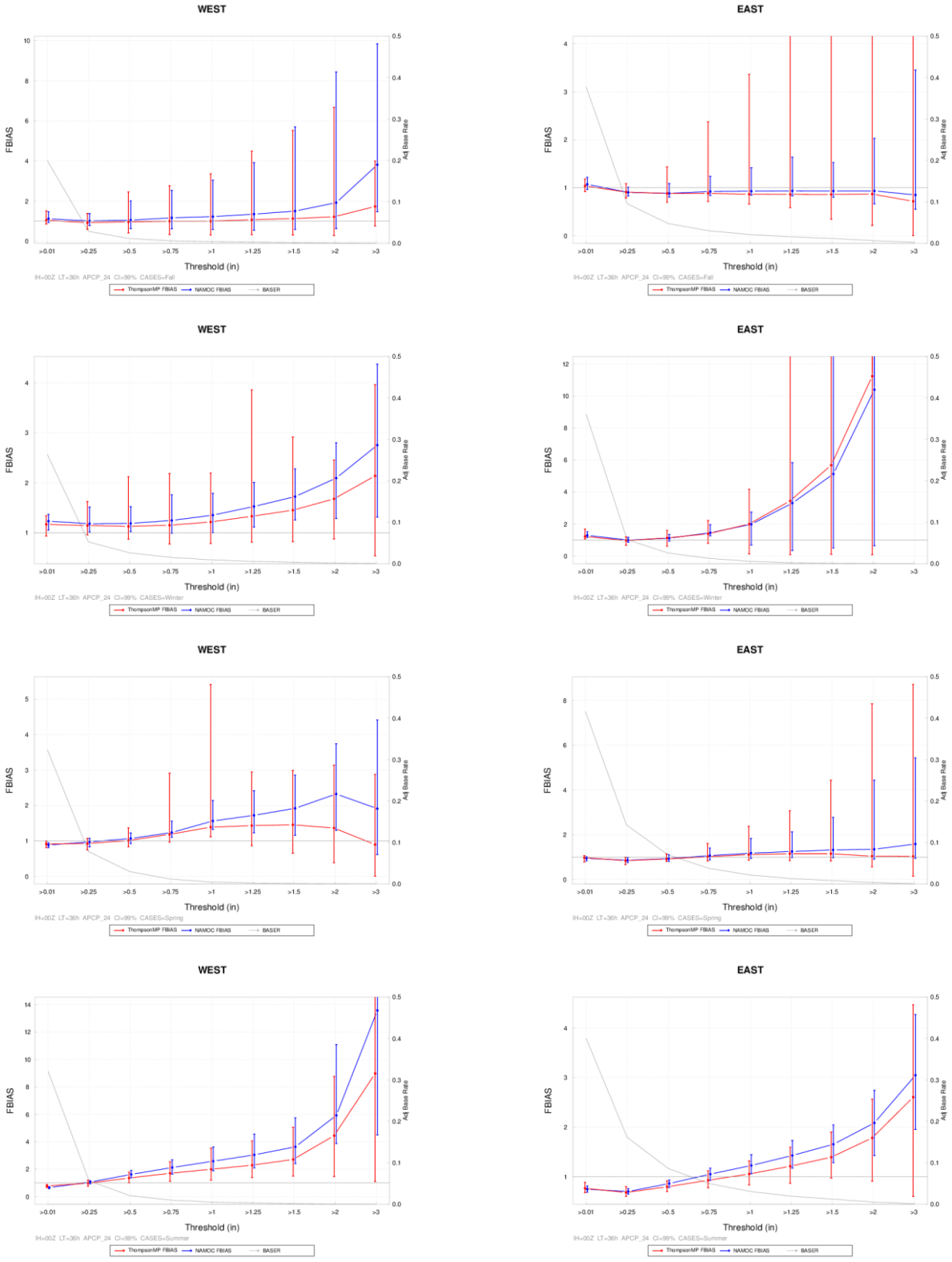

Figure 20. Threshold series plot of 24-h accumulated precipitation (in) for aggregated frequency bias for the East and West regions of the CONUS domain across all 00 UTC initializations for the 36-h forecast lead time for the fall, winter, spring and summer aggregations. NAMOC is in blue and ThompsonMP in red. The base rate, in grey, is associated with the second y-axis. The vertical bars attached to the aggregated value represent the 99% CIs.

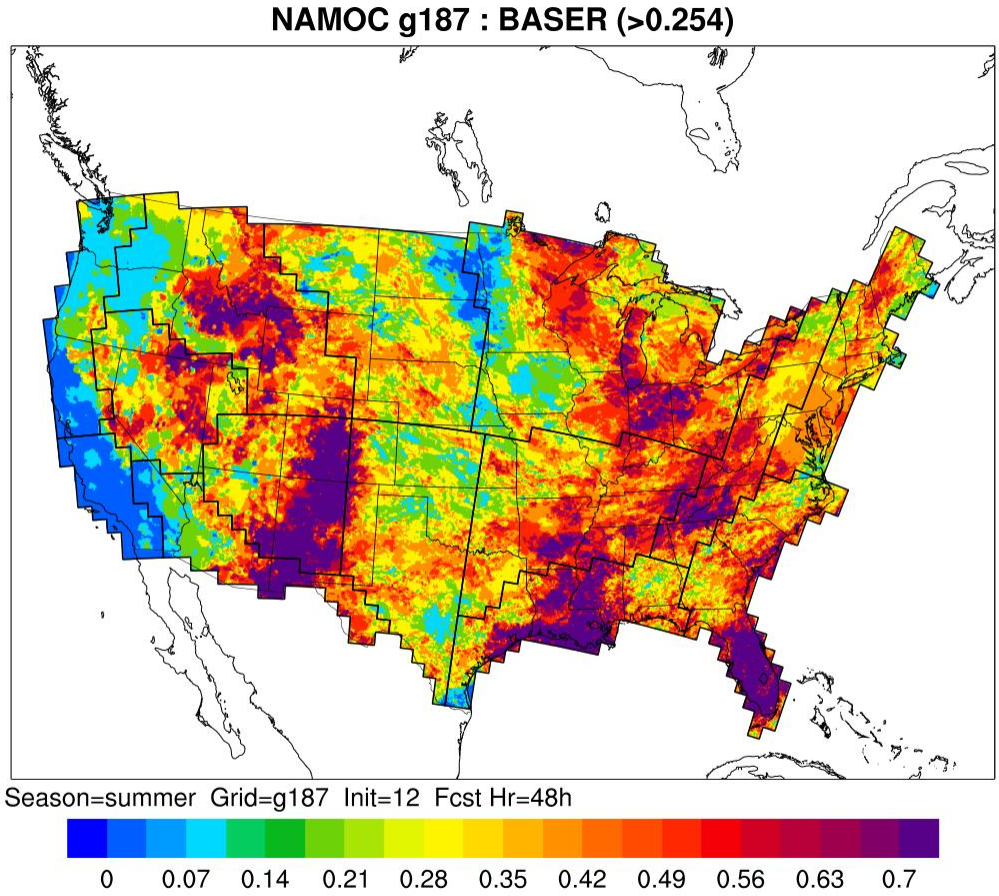

Figure 21. Base rate for the summer aggregation across all 12 UTC initializations at the 48-hour forecast lead time for 0.01". The base rate is the measurement of observed grid box events to the total number of grid boxes in the domain.

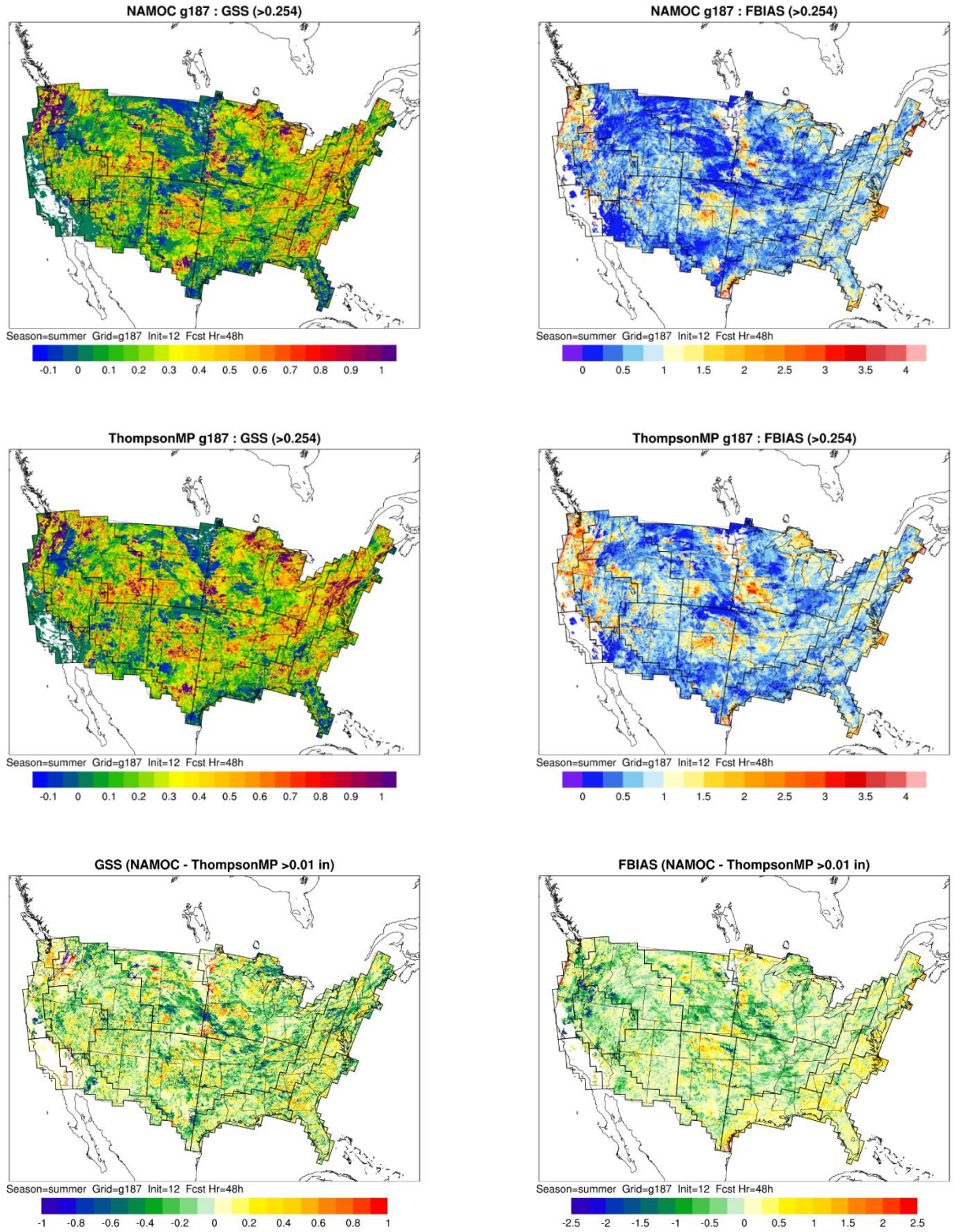

Figure 22. Gilbert skill score for (a), (b) NAMOC, (c), (d) ThompsonMP and (e), (f) differences (NAMOC-ThompsonMP) for GSS (left column) and Frequency bias(right column) at the 0.01" threshold during the summer aggregation across all 12 UTC initializations at the 48-hour forecast lead time.

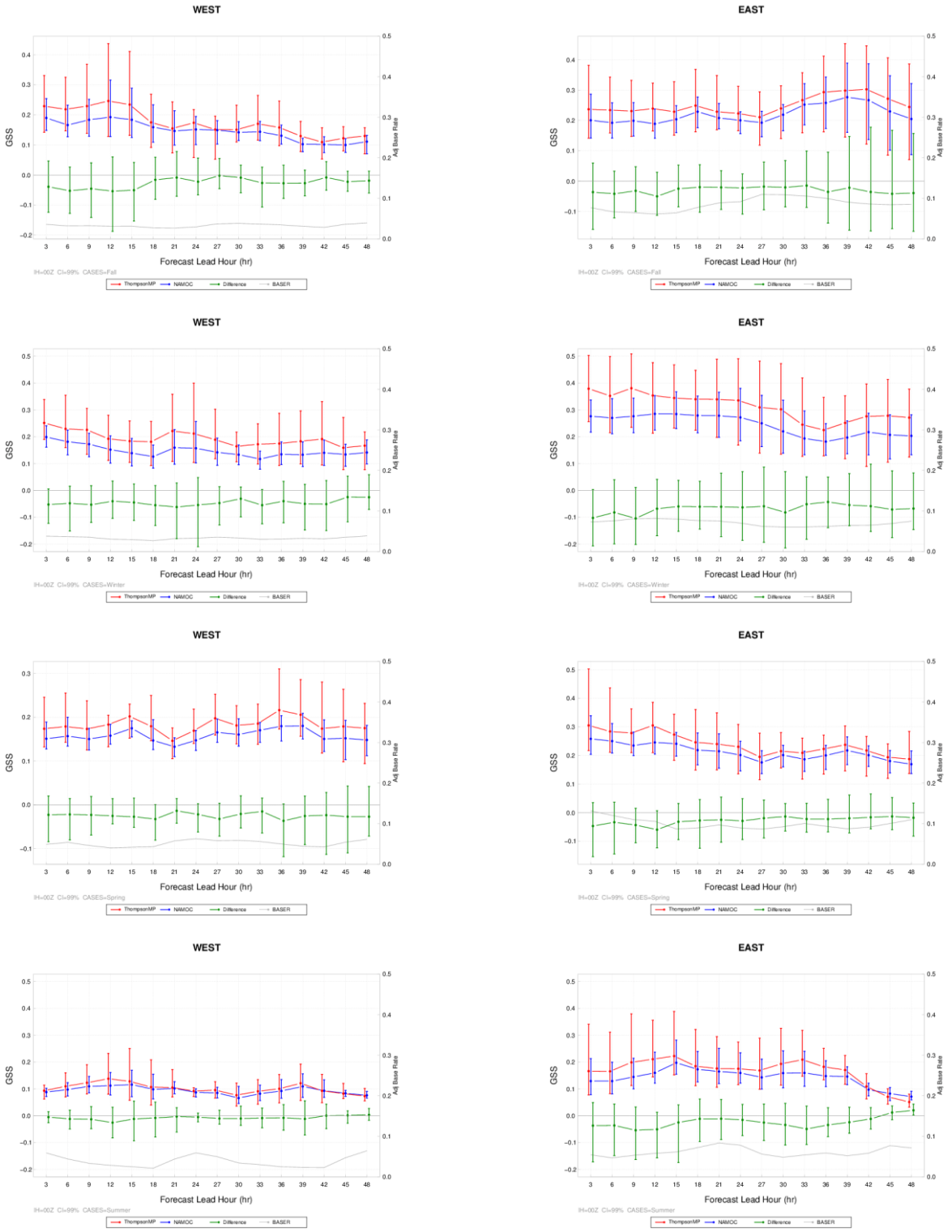

Figure 23. Lead series plots of composite reflectivity (dBZ) for aggregated GSS for the East and West regions of the CONUS domain across all 00 UTC initializations at the ≥10 threshold for the fall, winter, spring and summer aggregations. NAMOC is in blue, ThompsonMP in red, and the differences (NAMOC-ThompsonMP) in green. The base rate, in grey, is associated with the second y-axis. The vertical bars attached to the aggregated value represent the 99% CIs.

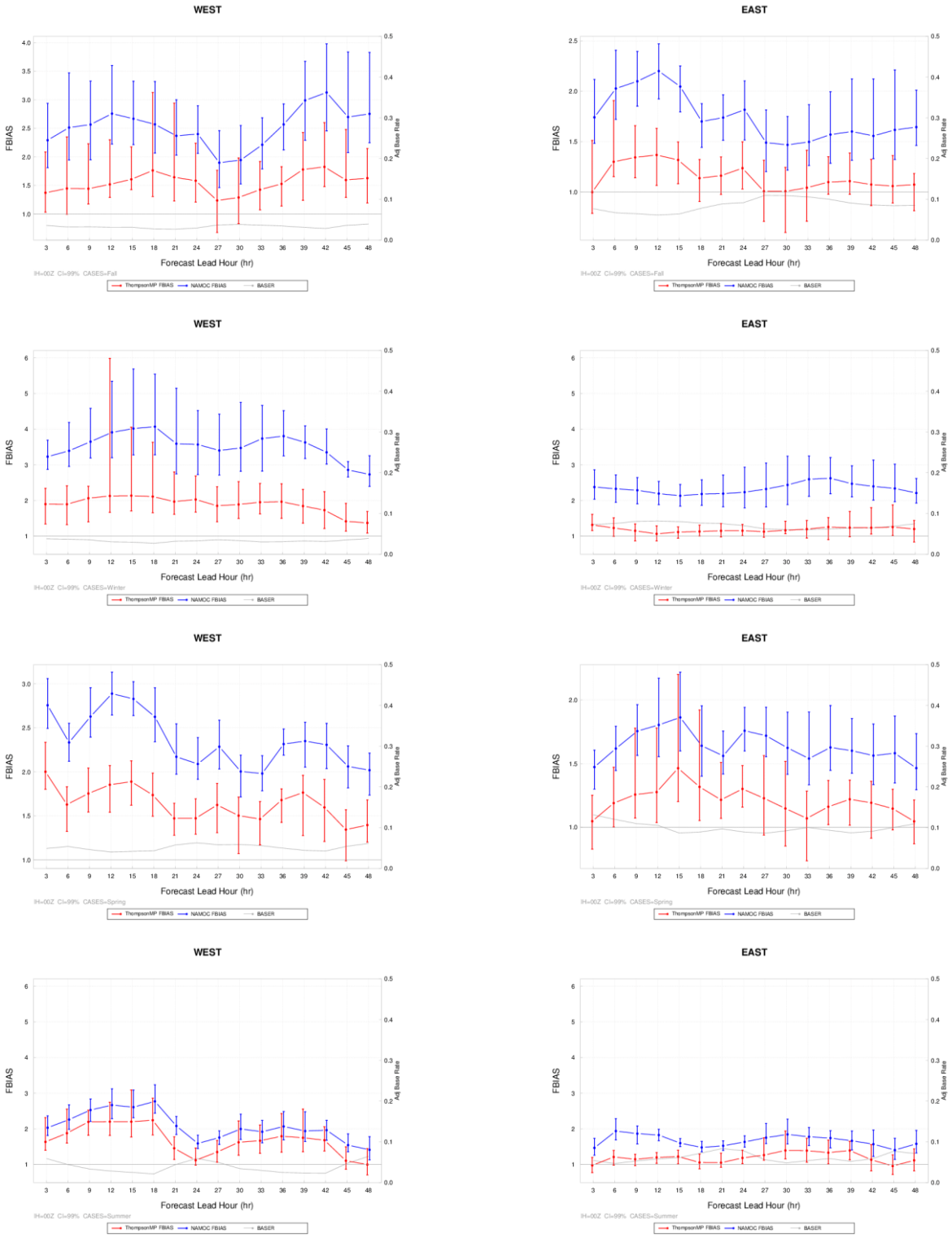

Figure 24. Lead series plots of composite reflectivity (dBZ) for aggregated frequency bias for the East and West regions of the CONUS domain across all 00 UTC initializations at the ≥10 threshold for the fall, winter, spring and summer aggregations. NAMOC is in blue and ThompsonMP in red. The base rate, in grey, is associated with the second y-axis. The vertical bars attached to the aggregated value represent the 99% CIs.

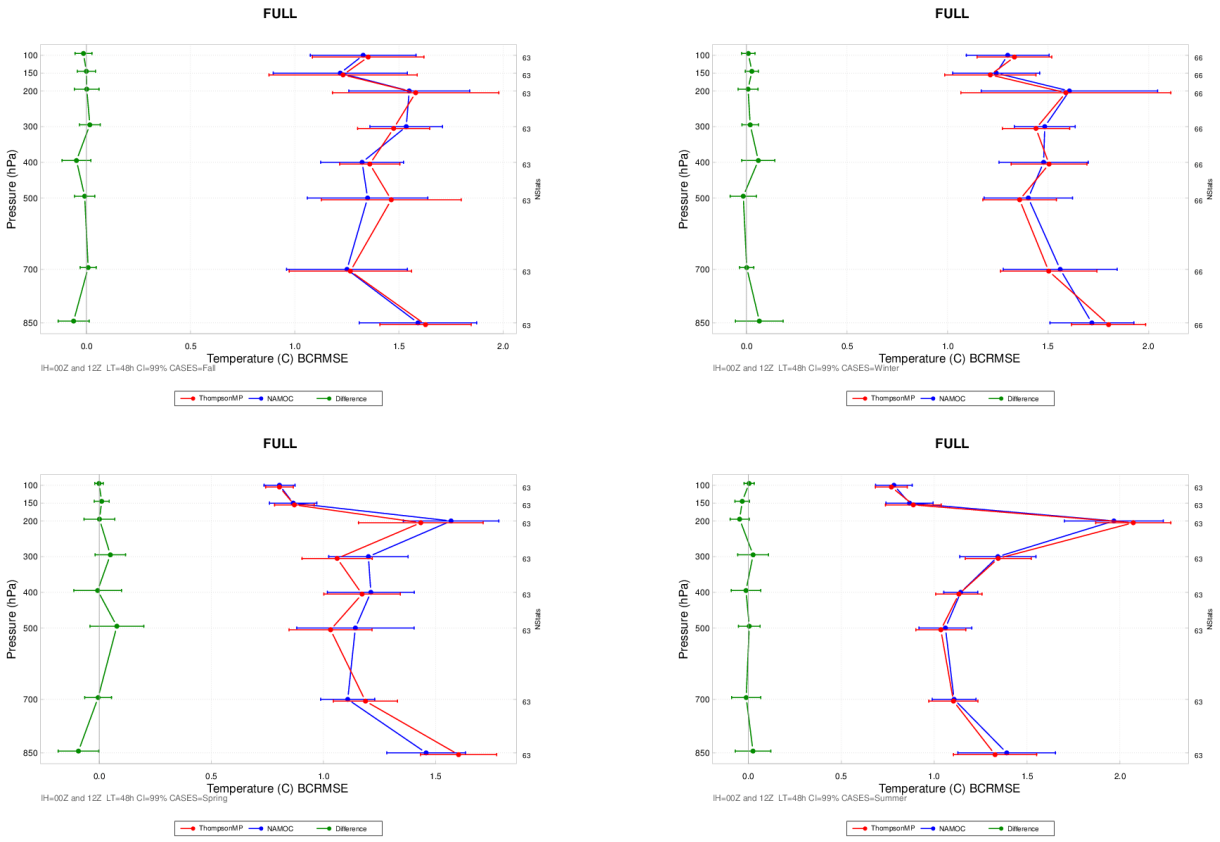

Figure 25. Vertical profiles of the median BCRMSE for temperature (°C) for the full Alaska domain for the 48-h forecast lead time for the (a) fall aggregation, (b) winter aggregation, (c) spring aggregation, and (d) summer aggregation. NAMOC is in blue, ThompsonMP in red, and the differences (NAMOC-ThompsonMP) in green. The vertical bars attached to the median represent

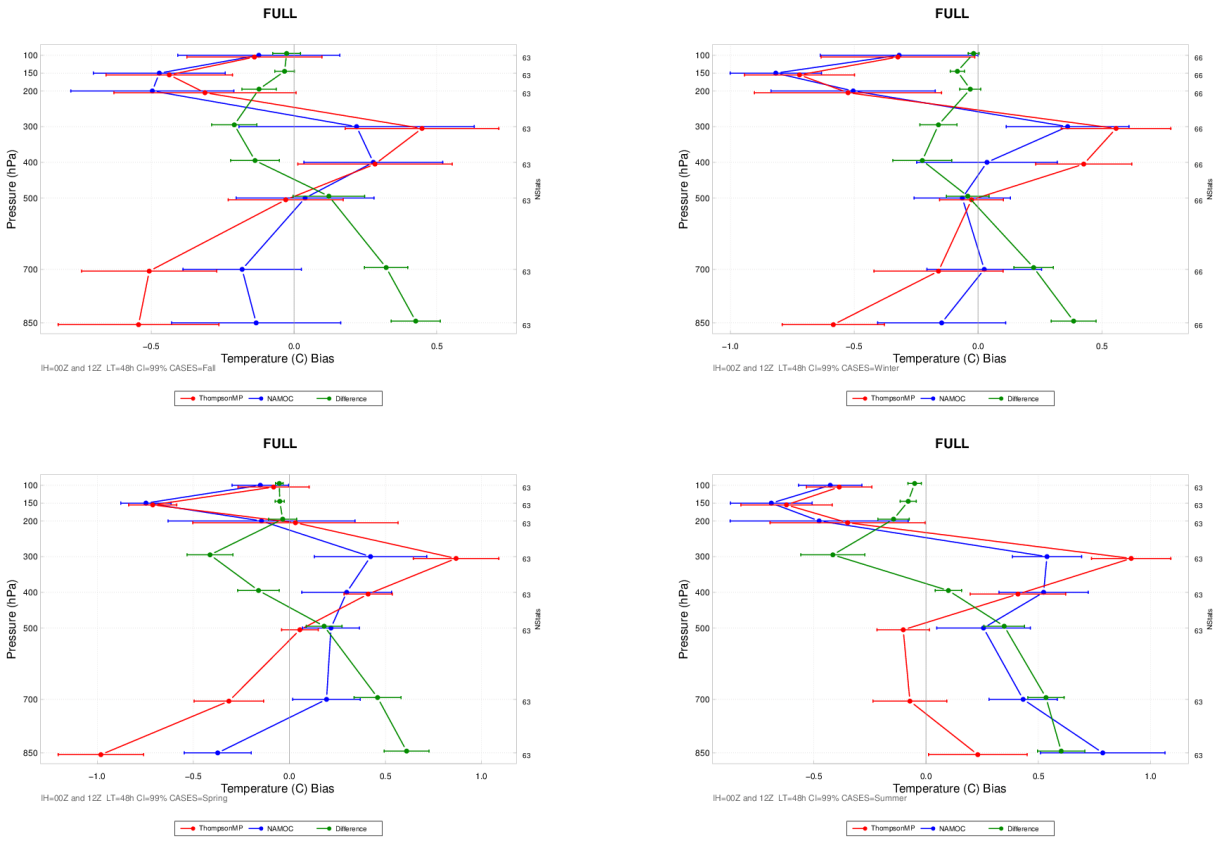

Figure 26. Vertical profiles of the median bias for temperature (°C) for the full Alaska domain for the 48-h forecast lead time for the (a) fall aggregation, (b) winter aggregation, (c) spring aggregation, and (d) summer aggregation. NAMOC is in blue, ThompsonMP in red, and the differences (NAMOC-ThompsonMP) in green. The vertical bars attached to the median represent the 99% CIs.

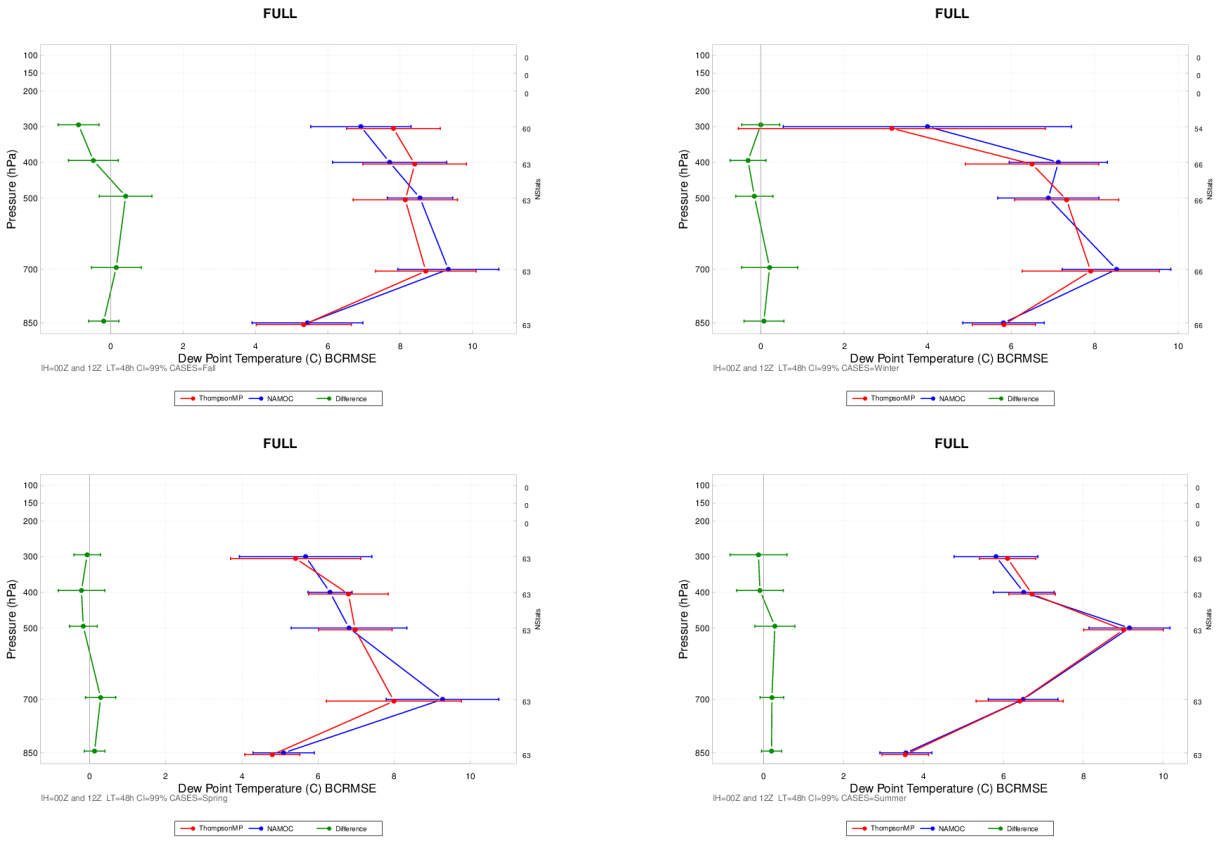

Figure 27. Vertical profiles of the median BCRMSE for dew point temperature (°C) for the full Alaska domain for the 48-h forecast lead time for the (a) fall aggregation, (b) winter aggregation, (c) spring aggregation, and (d) summer aggregation. NAMOC is in blue, ThompsonMP in red, and the differences (NAMOC-ThompsonMP) in green. The vertical bars attached to the median represent the 99% CIs.

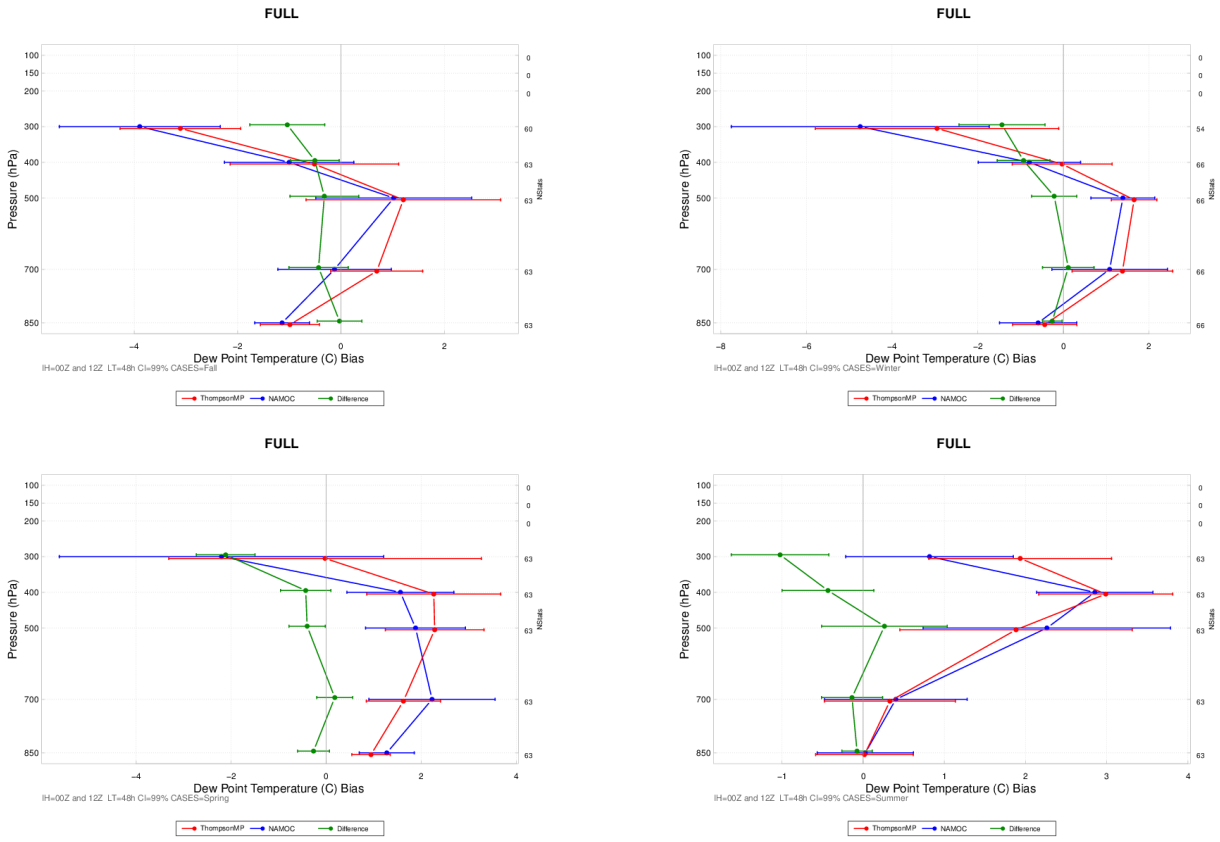

Figure 28. Vertical profiles of the median bias for dew point temperature (°C) for the full Alaska domain for the 48-h forecast lead time for the (a) fall aggregation, (b) winter aggregation, (c) spring aggregation, and (d) summer aggregation. NAMOC is in blue, ThompsonMP in red, and the differences (NAMOC-ThompsonMP) in green. The vertical bars attached to the median represent the 99% CIs.

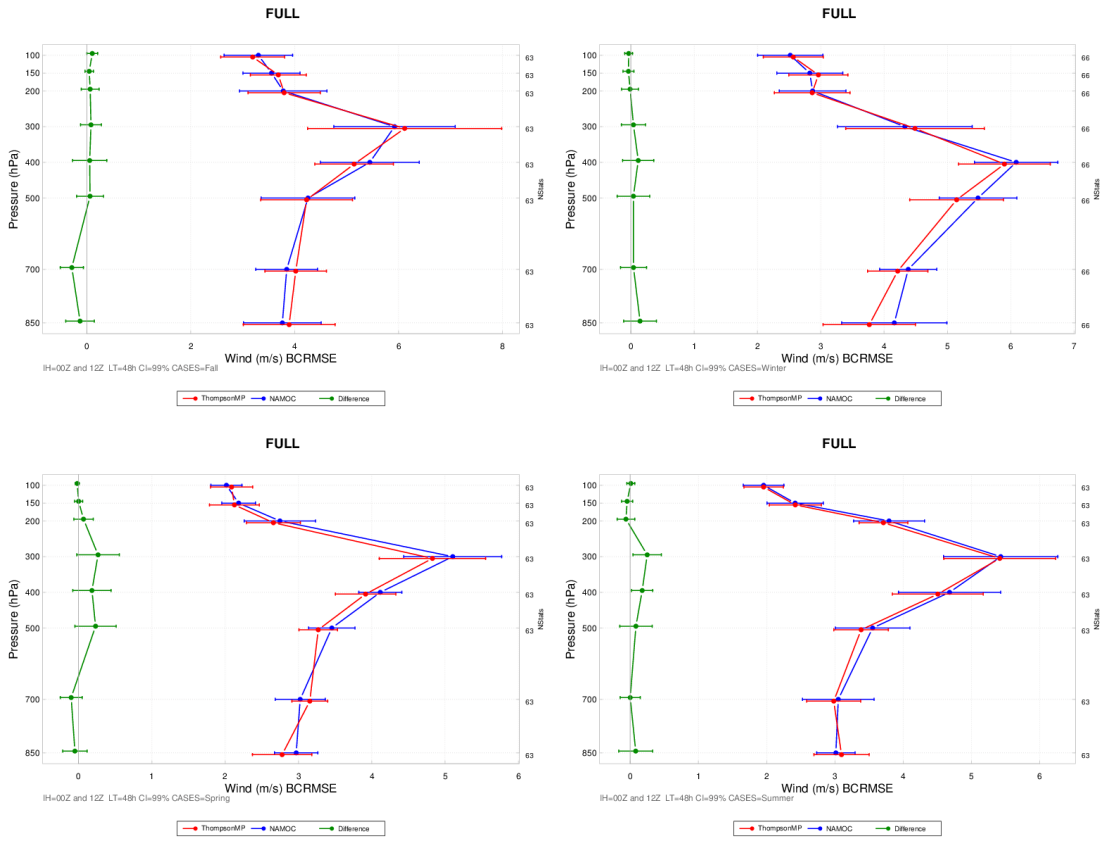

Figure 29. Vertical profiles of the median BCRMSE for wind (m/s) for the full Alaska domain for the 48-h forecast lead time for the (a) fall aggregation, (b) winter aggregation, (c) spring aggregation, and (d) summer aggregation. NAMOC is in blue, ThompsonMP in red, and the differences (NAMOC-ThompsonMP) in green. The vertical bars attached to the median represent the 99% CIs.

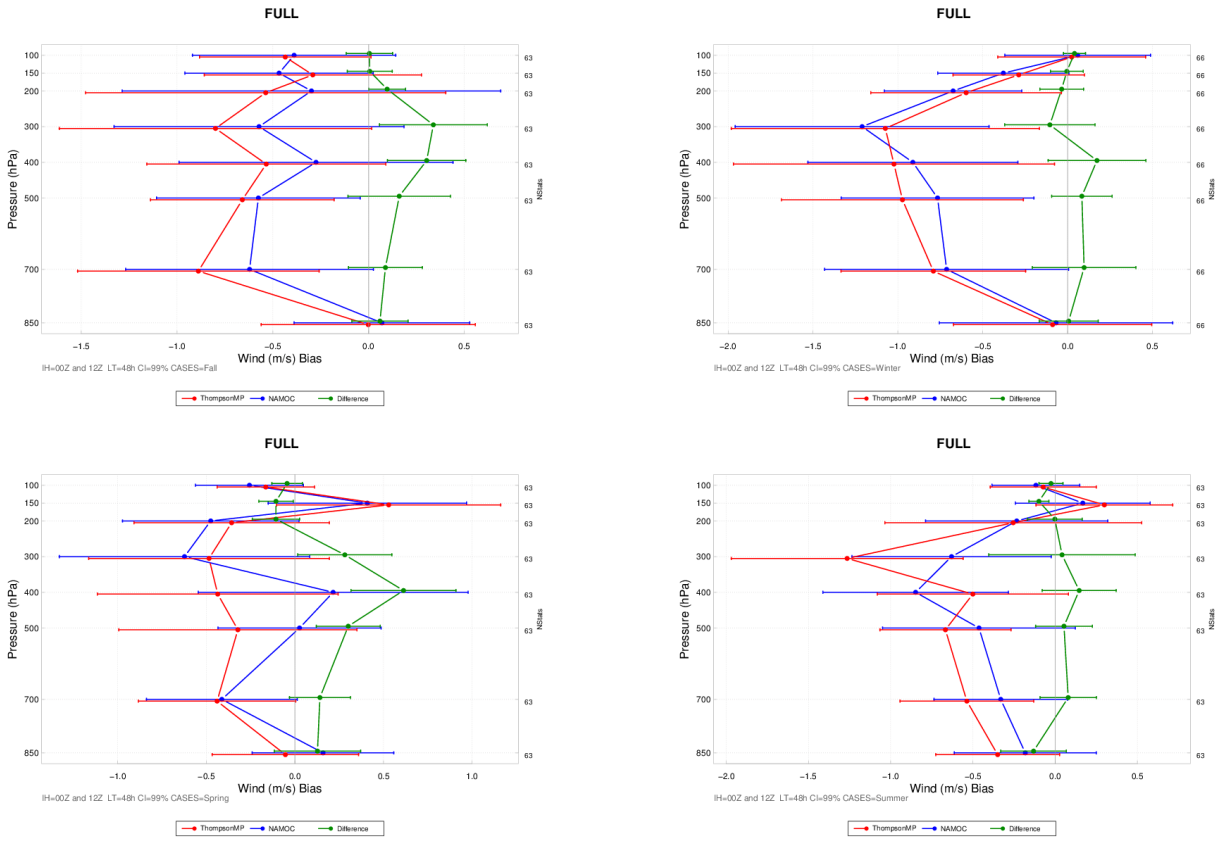

Figure 30. Vertical profiles of the median bias for wind (m/s) for the full Alaska domain for the 48-h forecast lead time for the (a) fall aggregation, (b) winter aggregation, (c) spring aggregation, and (d) summer aggregation. NAMOC is in blue, ThompsonMP in red, and the differences (NAMOC-ThompsonMP) in green. The vertical bars attached to the median represent the 99% CIs.

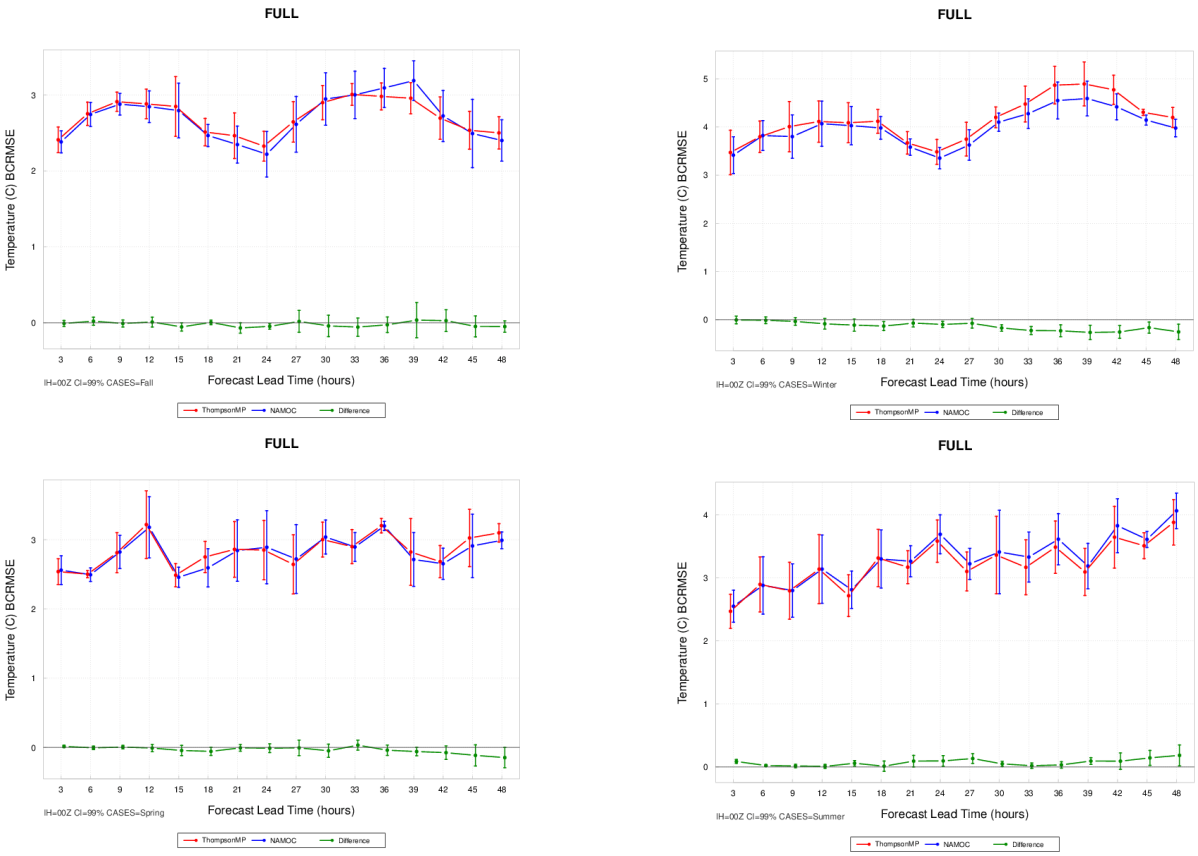

Figure 31. Time series plots of the 2 m AGL temperature (°C) for median BCRMSE for all 00 UTC initializations over the full Alaska domain aggregated over the (a) fall aggregation, (b) winter aggregation, (c) spring aggregation, and (d) summer aggregation. NAMOC is in blue, ThompsonMP in red, and the differences (NAMOC-ThompsonMP) in green. The vertical bars attached to the median represent the 99% CIs.

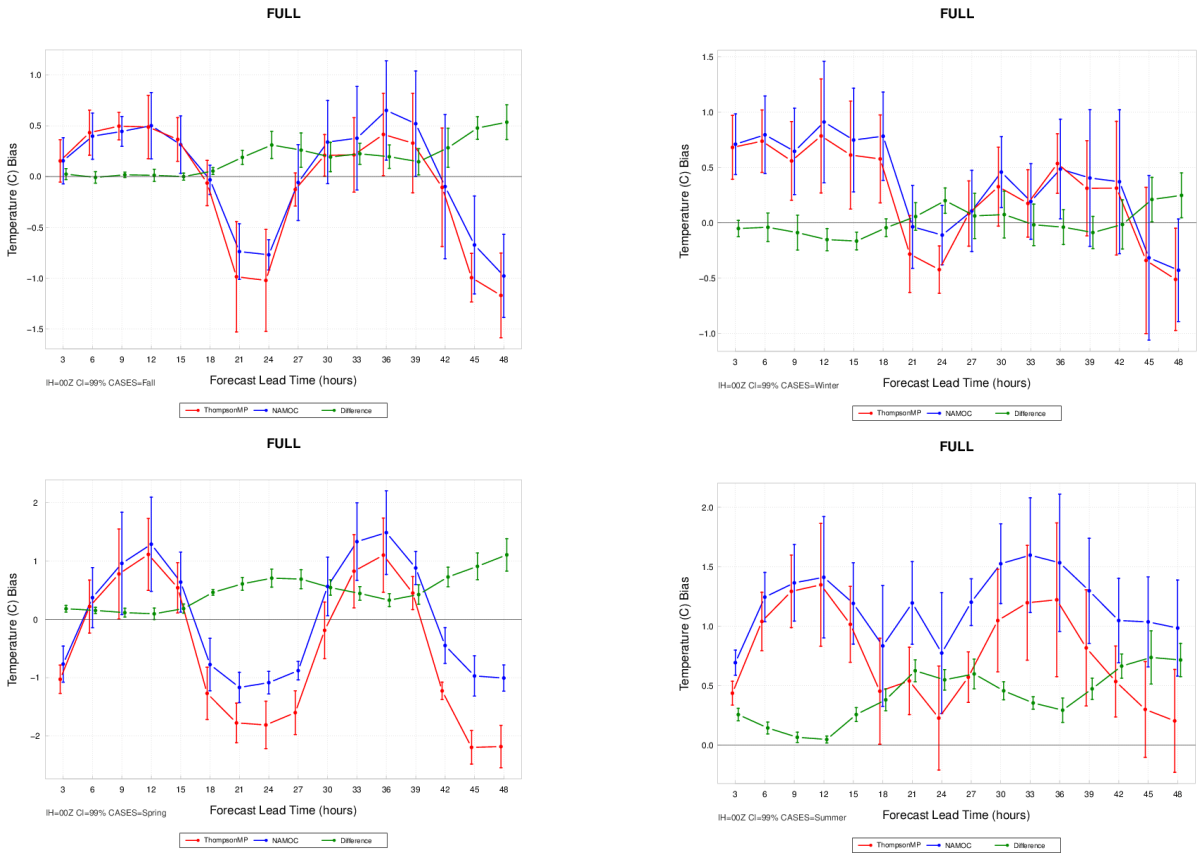

Figure 32. Time series plots of the 2 m AGL temperature (°C) for median bias for all 00 UTC initializations over the full Alaska domain aggregated over the (a) fall aggregation, (b) winter aggregation, (c) spring aggregation, and (d) summer aggregation. NAMOC is in blue, ThompsonMP in red, and the differences (NAMOC-ThompsonMP) in green. The vertical bars attached to the median represent the 99% CIs.

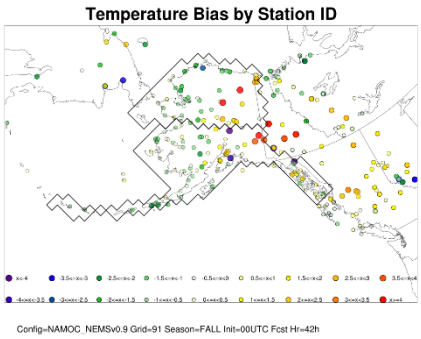

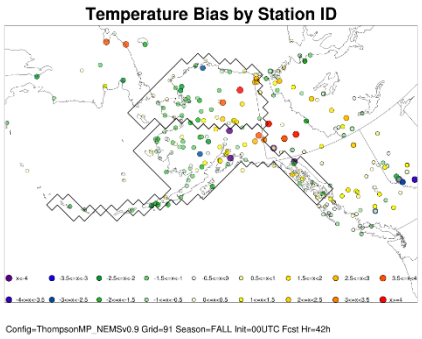

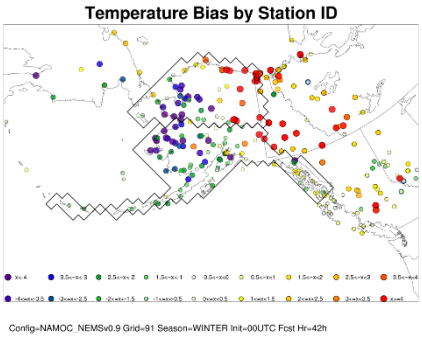

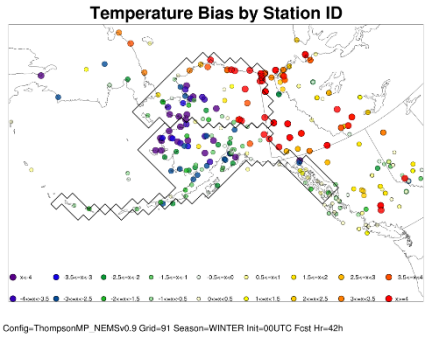

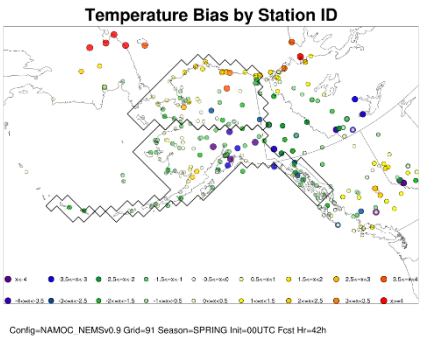

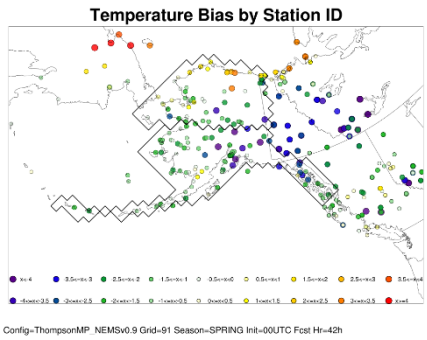

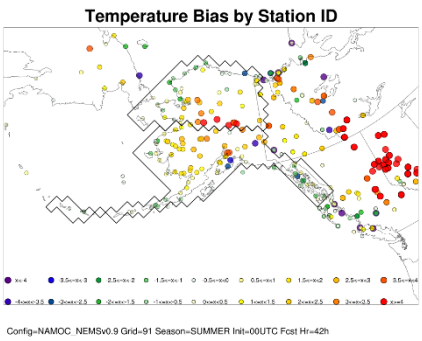

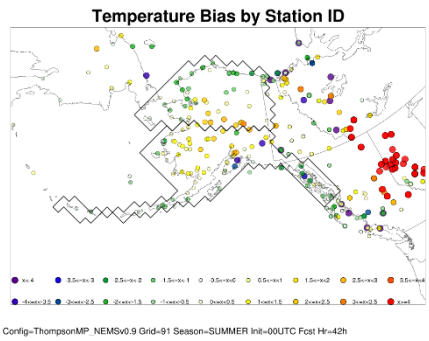

Figure 33. Spatial plots of the 2 m AGL temperature (°C) for mean bias for the 42-h forecast lead time for all 00 UTC initializations over the full Alaska domain. The left column is NAMOC, and the right column is ThompsonMP. The first row is the fall aggregation, the second row is the winter aggregation, the third row is the spring aggregation, and the fourth row is the summer aggregation.

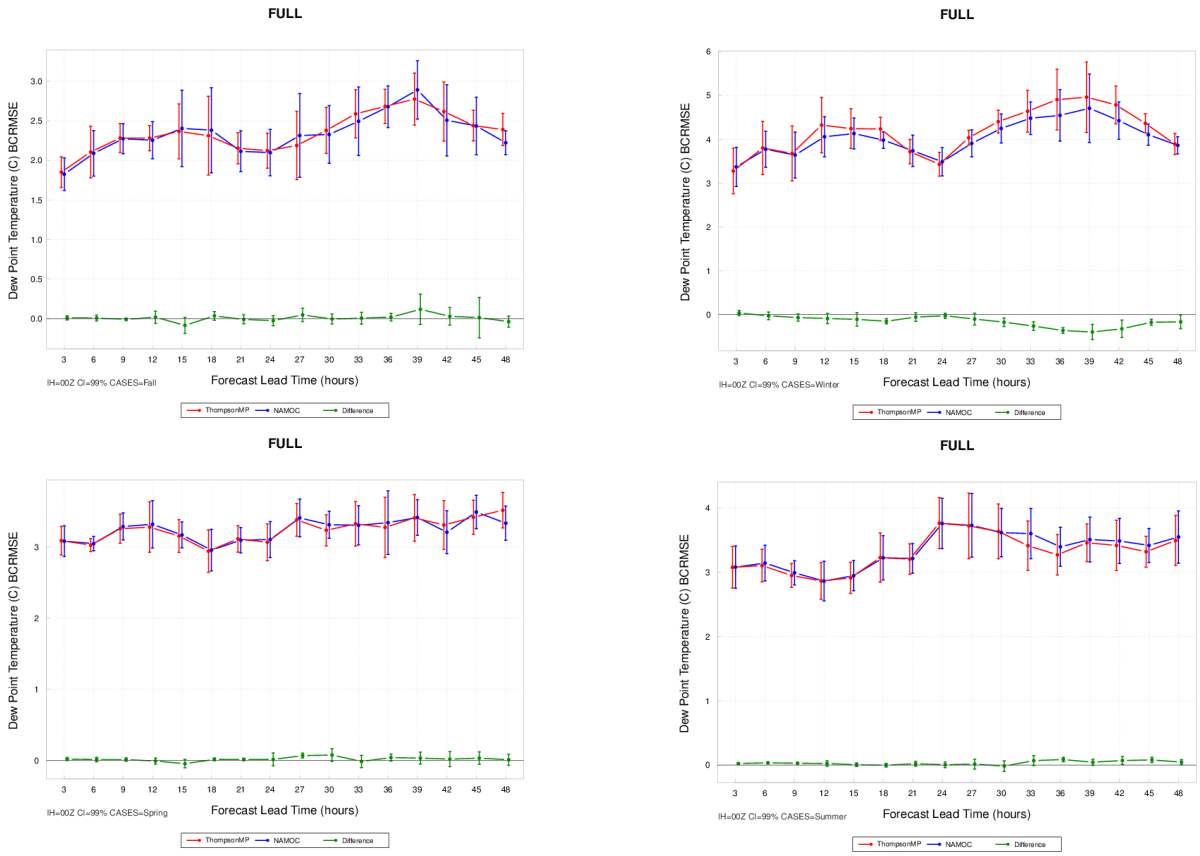

Figure 34. Time series plots of the 2 m AGL dew point temperature (°C) for median BCRMSE for all 00 UTC initializations over the full Alaska domain aggregated over the (a) fall aggregation, (b) winter aggregation, (c) spring aggregation, and (d) summer aggregation. NAMOC is in blue, ThompsonMP in red, and the differences (NAMOC-ThompsonMP) in green. The vertical bars attached to the median represent the 99% CIs.

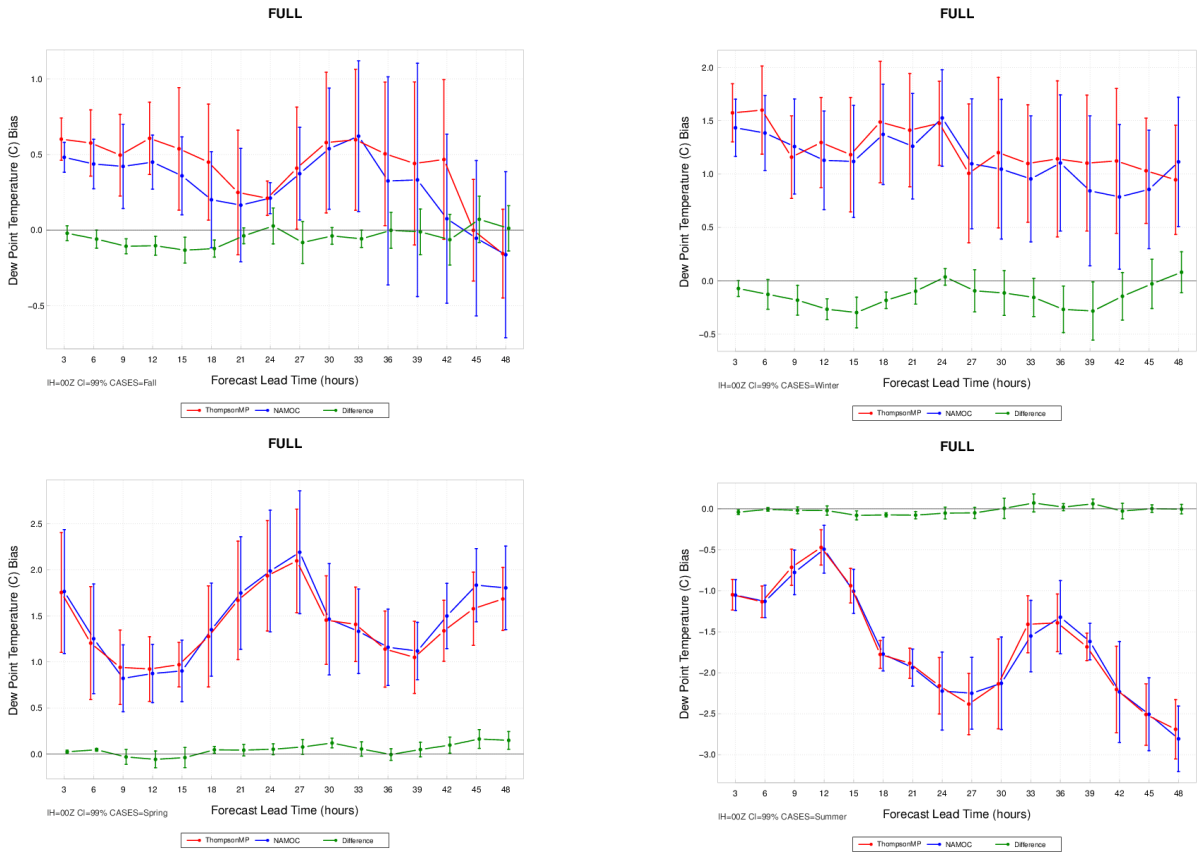

Figure 35. Time series plots of the 2 m AGL dew point temperature (°C) for median bias for all 00 UTC initializations over the full Alaska domain aggregated over the (a) fall aggregation, (b) winter aggregation, (c) spring aggregation, and (d) summer aggregation. NAMOC is in blue, ThompsonMP in red, and the differences (NAMOC-ThompsonMP) in green. The vertical bars attached to the median represent the 99% CIs.

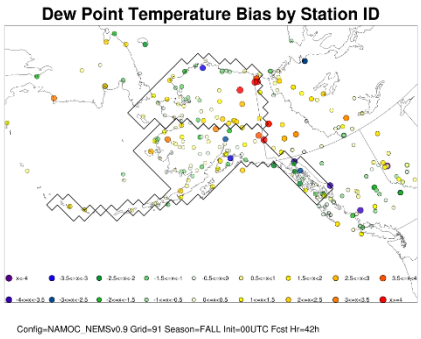

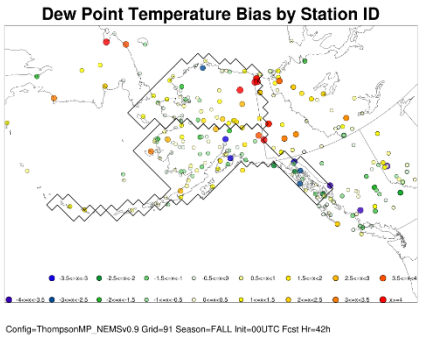

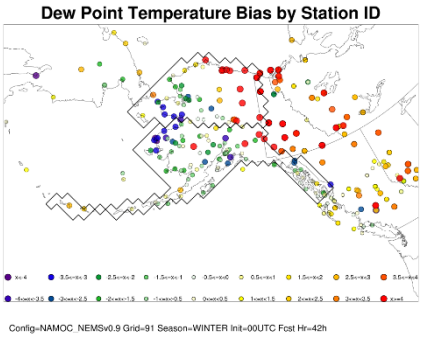

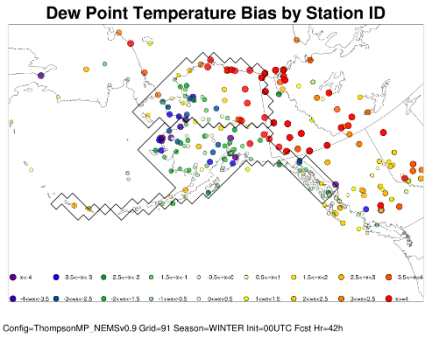

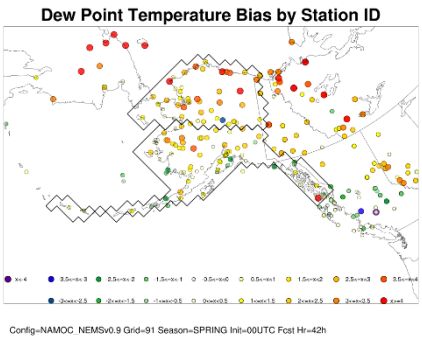

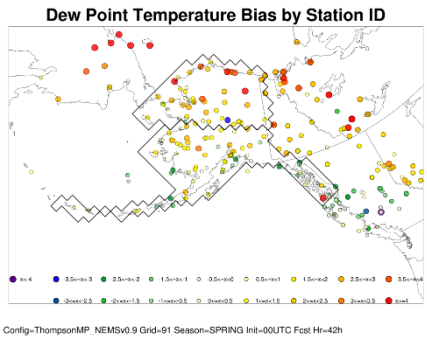

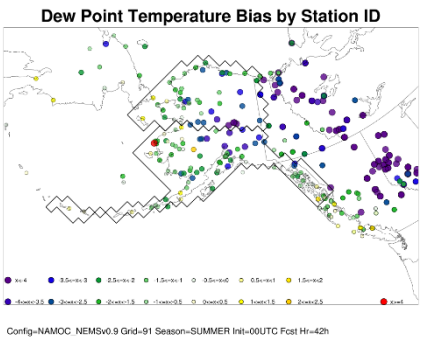

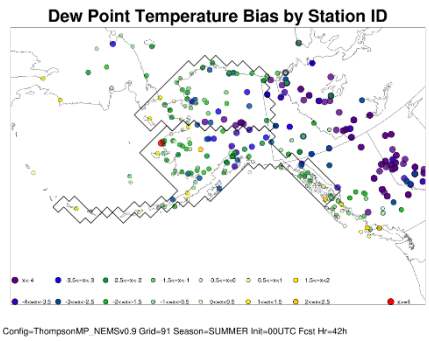

Figure 36. Spatial plots of the 2 m AGL dew point temperature (°C) for mean bias for the 42-h forecast lead time for all 00 UTC initializations over the full Alaska domain. The left column is NAMOC, and the right column is ThompsonMP. The first row is the fall aggregation, the second row is the winter aggregation, the third row is the spring aggregation, and the fourth row is the summer aggregation.

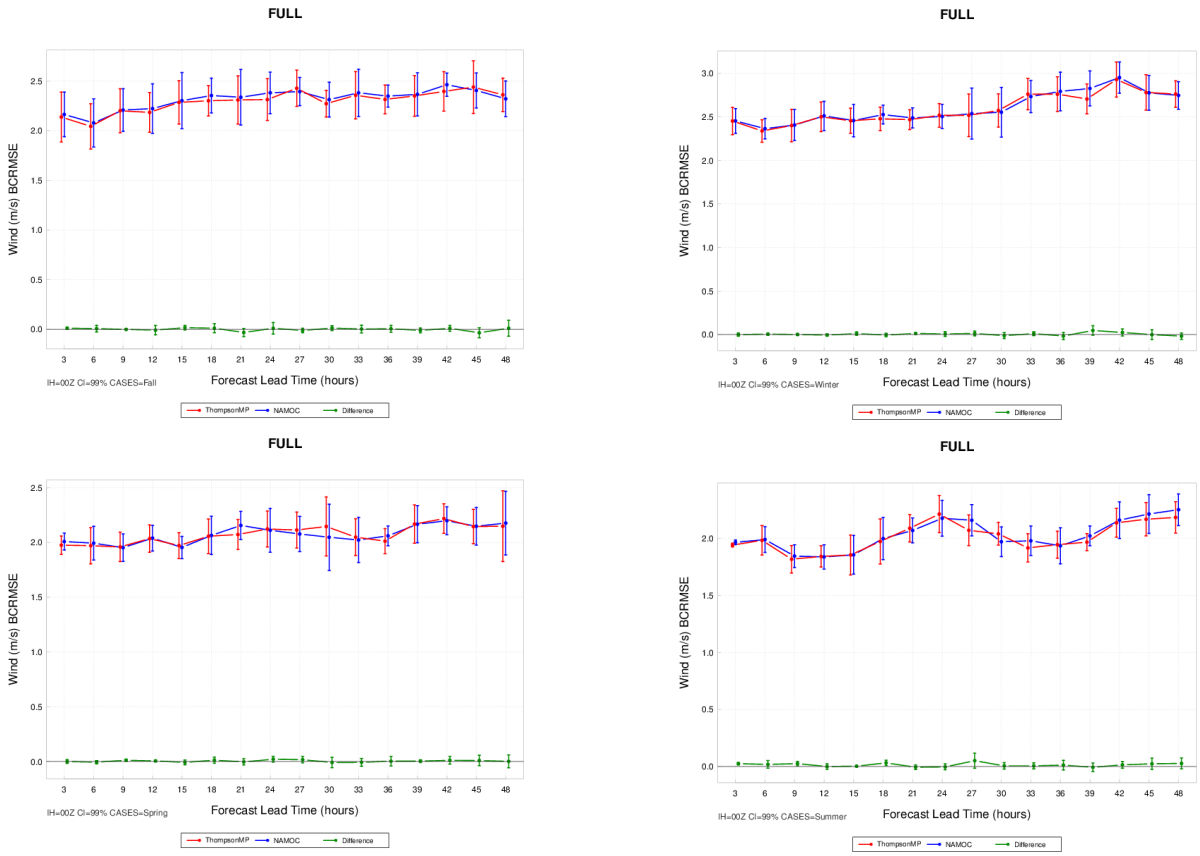

Figure 37. Time series plots of the 10 m AGL wind (m/s) for median BCRMSE for all 00 UTC initializations over the full Alaska domain aggregated over the (a) fall aggregation, (b) winter aggregation, (c) spring aggregation, and (d) summer aggregation. NAMOC is in blue, ThompsonMP in red, and the differences (NAMOC-ThompsonMP) in green. The vertical bars attached to the median represent the 99% CIs.

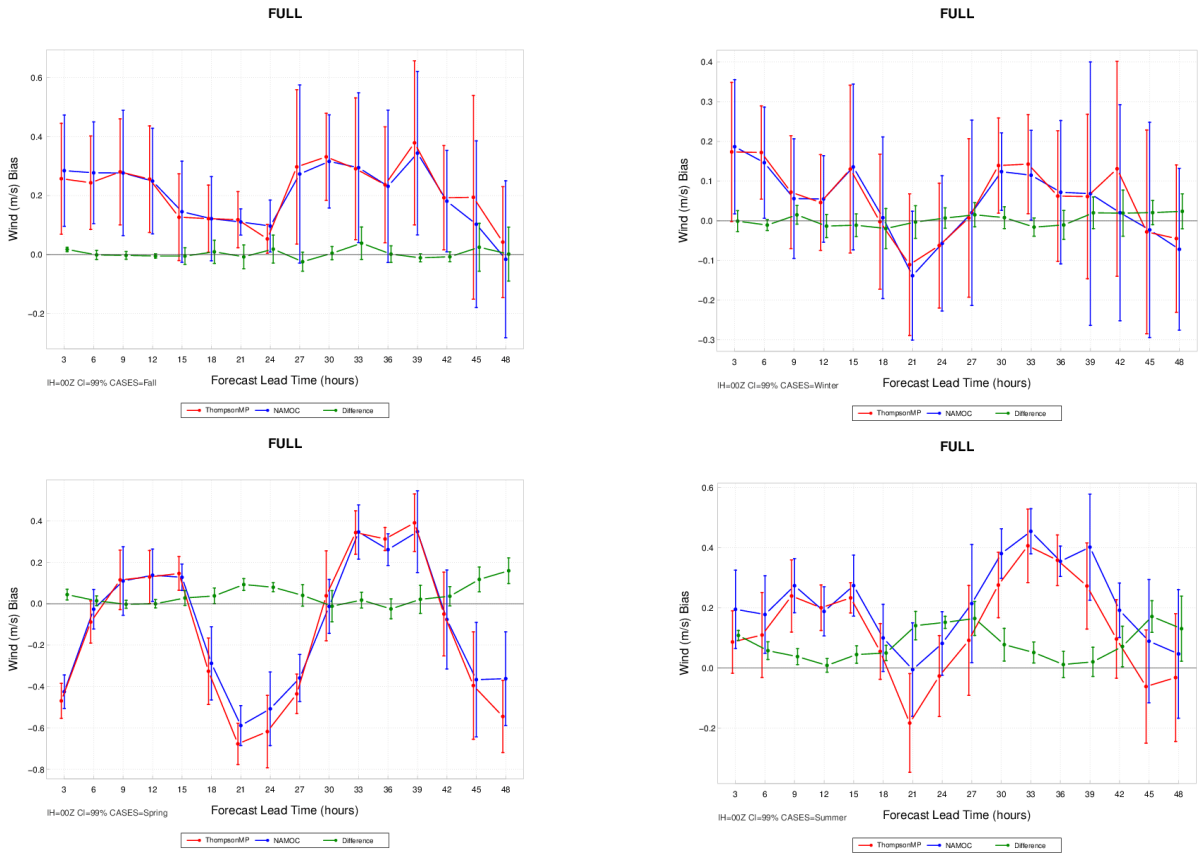

Figure 38. Time series plots of the 10 m AGL wind (m/s) for median bias for all 00 UTC initializations over the full Alaska domain aggregated over the (a) fall aggregation, (b) winter aggregation, (c) spring aggregation, and (d) summer aggregation. NAMOC is in blue, ThompsonMP in red, and the differences (NAMOC-ThompsonMP) in green. The vertical bars attached to the median represent the 99% CIs.

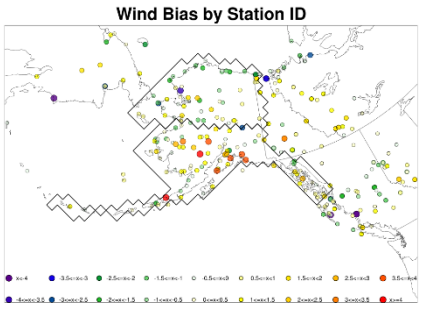

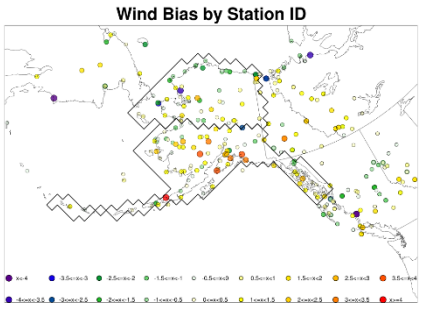

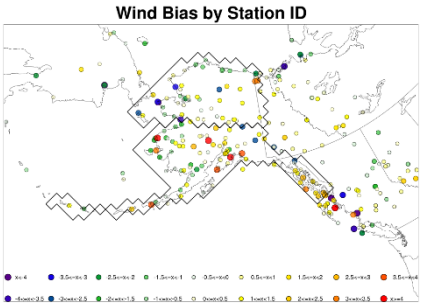

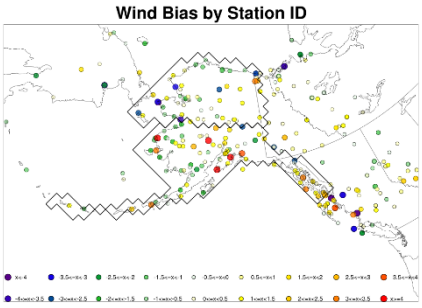

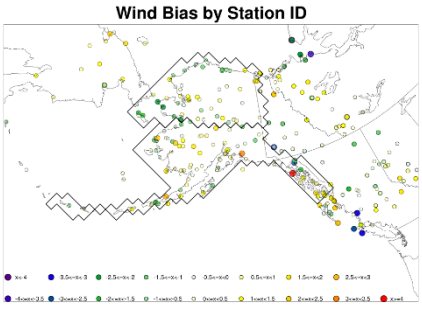

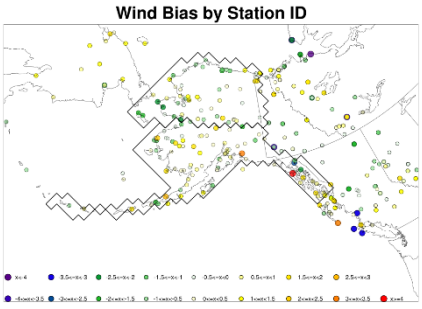

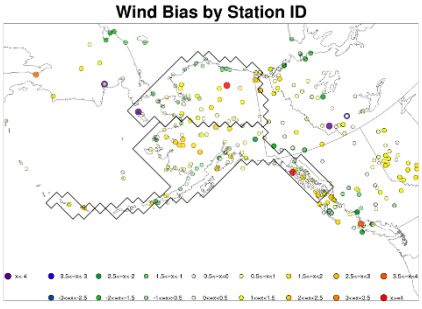

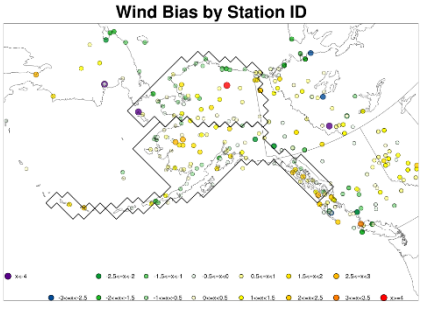

Figure 39. Spatial plots of the 10 m AGL wind (m/s) for mean bias for the 42-h forecast lead time for all 00 UTC initializations over the full Alaska domain. The left column is NAMOC, and the right column is ThompsonMP. The first row is the fall aggregation, the second row is the winter aggregation, the third row is the spring aggregation, and the fourth row is the summer aggregation.

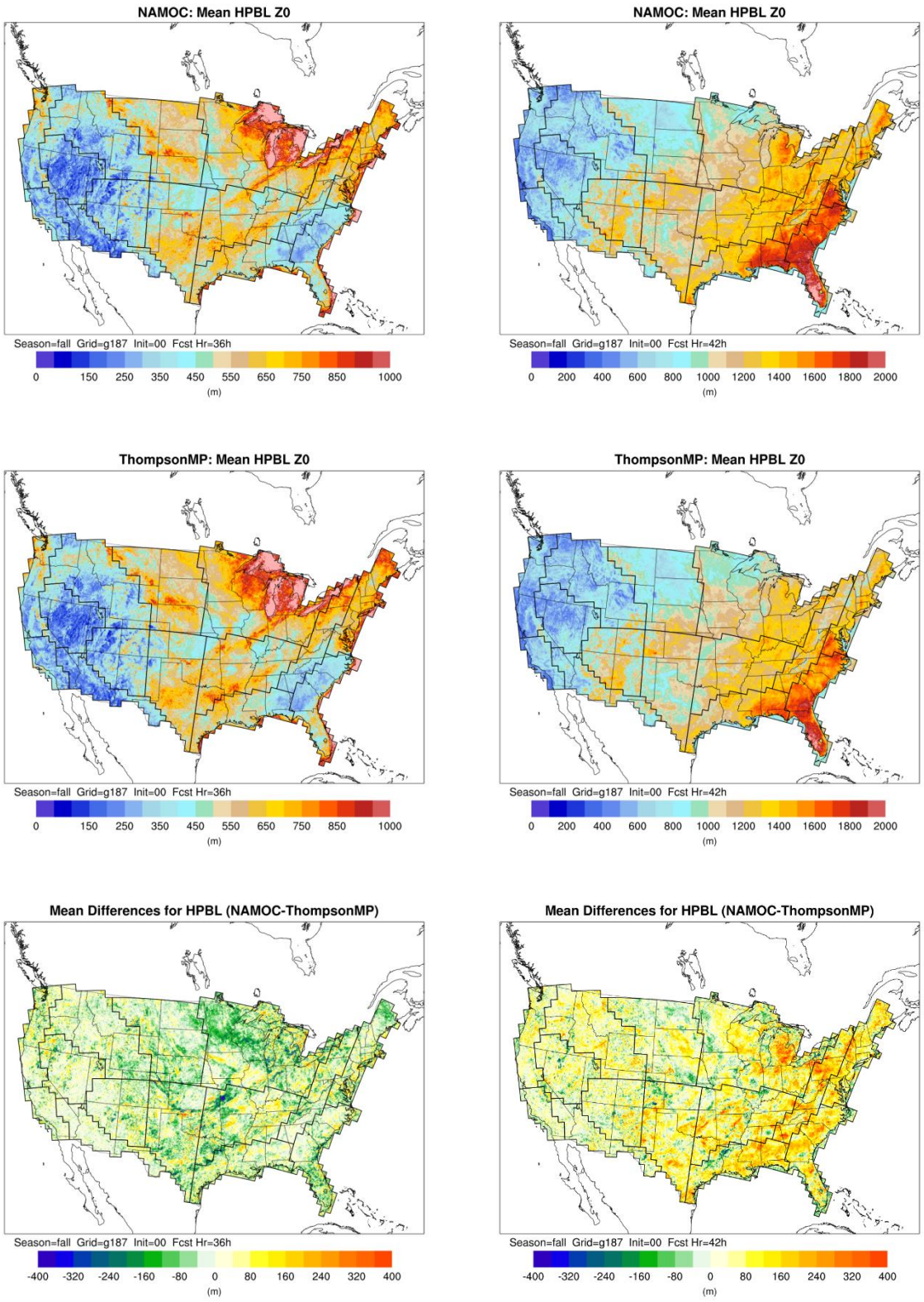

Figure 40. Mean PBL height (m) for all 00 UTC initializations during the fall aggregation for NAMOC at the (a) 36-h forecast lead time and (b) 42-h forecast lead time, for ThompsonMP at the (c) 36-h forecast lead time and (d) 42-h forecast lead time, and mean differences (NAMOC-ThompsonMP) at the (e) 36-h forecast lead time and (f) 42-h forecast lead time.

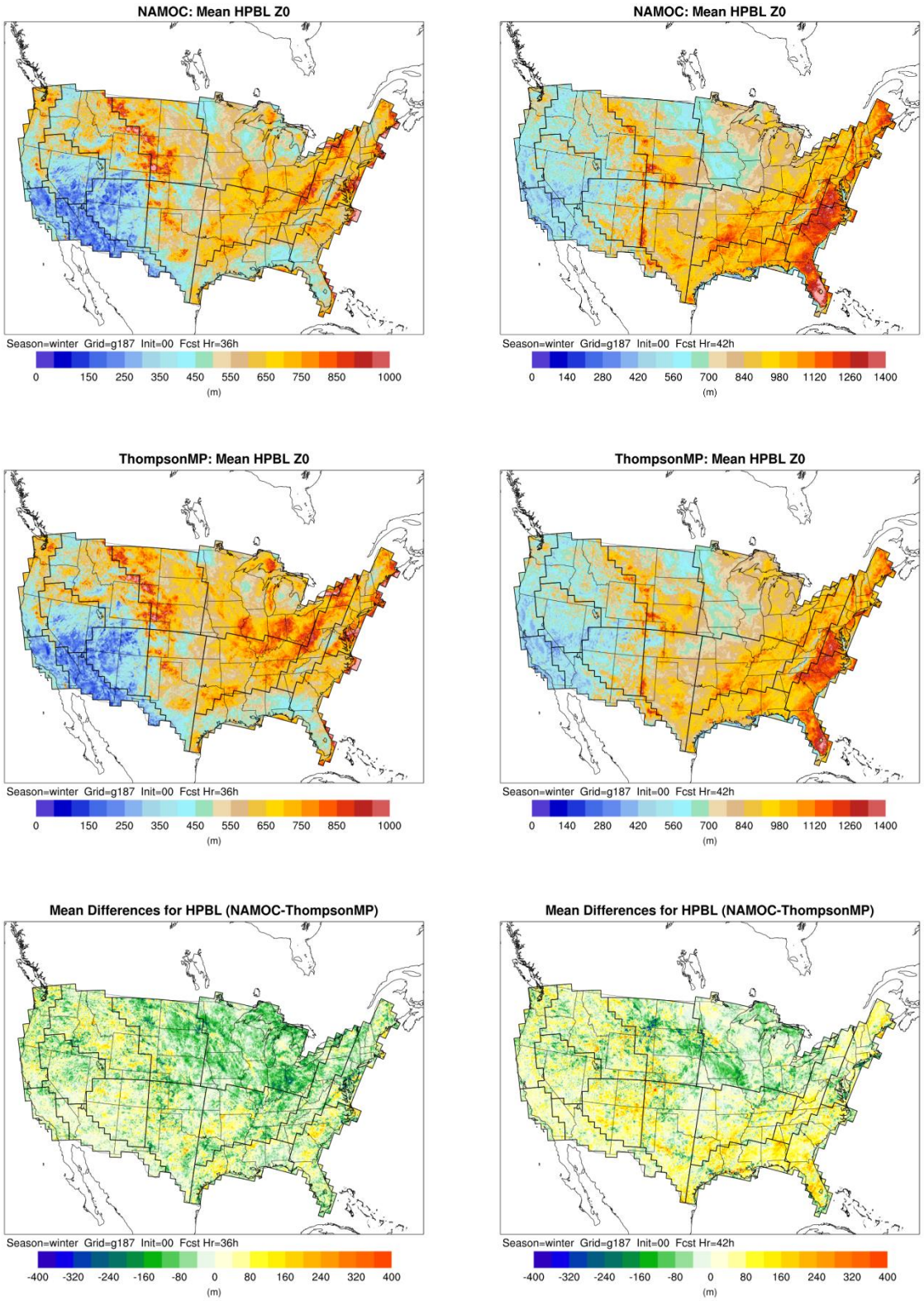

Figure 41. Mean PBL height (m) for all 00 UTC initializations during the winter aggregation for NAMOC at the (a) 36-h forecast lead time and (b) 42-h forecast lead time, for ThompsonMP at the (c) 36-h forecast lead time and (d) 42-h forecast lead time, and mean differences (NAMOC-ThompsonMP) at the (e) 36-h forecast lead time and (f) 42-h forecast lead time.

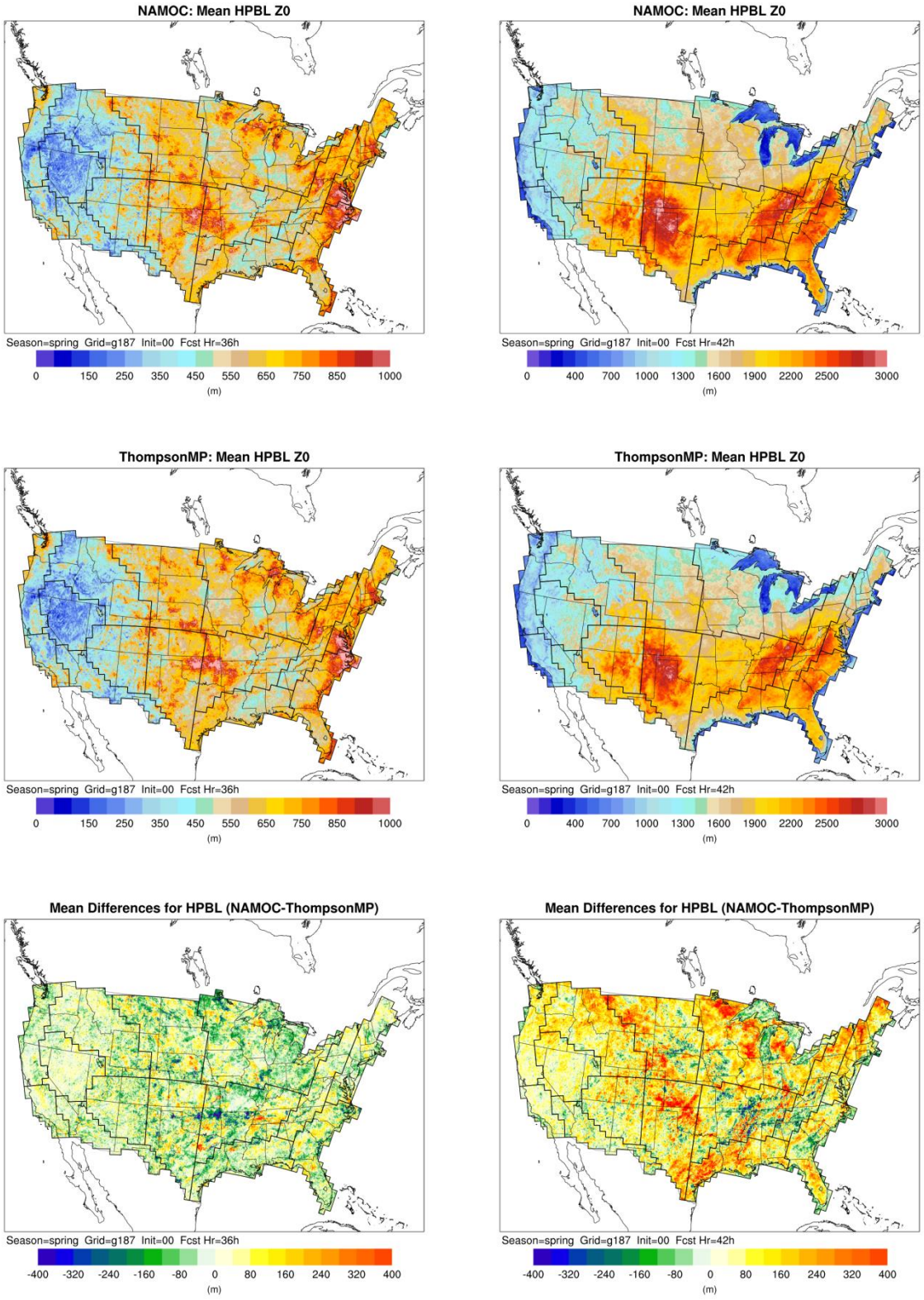

Figure 42. Mean PBL height (m) for all 00 UTC initializations during the spring aggregation for NAMOC at the (a) 36-h forecast lead time and (b) 42-h forecast lead time, for ThompsonMP at the (c) 36-h forecast lead time and (d) 42-h forecast lead time, and mean differences (NAMOC-ThompsonMP) at the (e) 36-h forecast lead time and (f) 42-h forecast lead time.

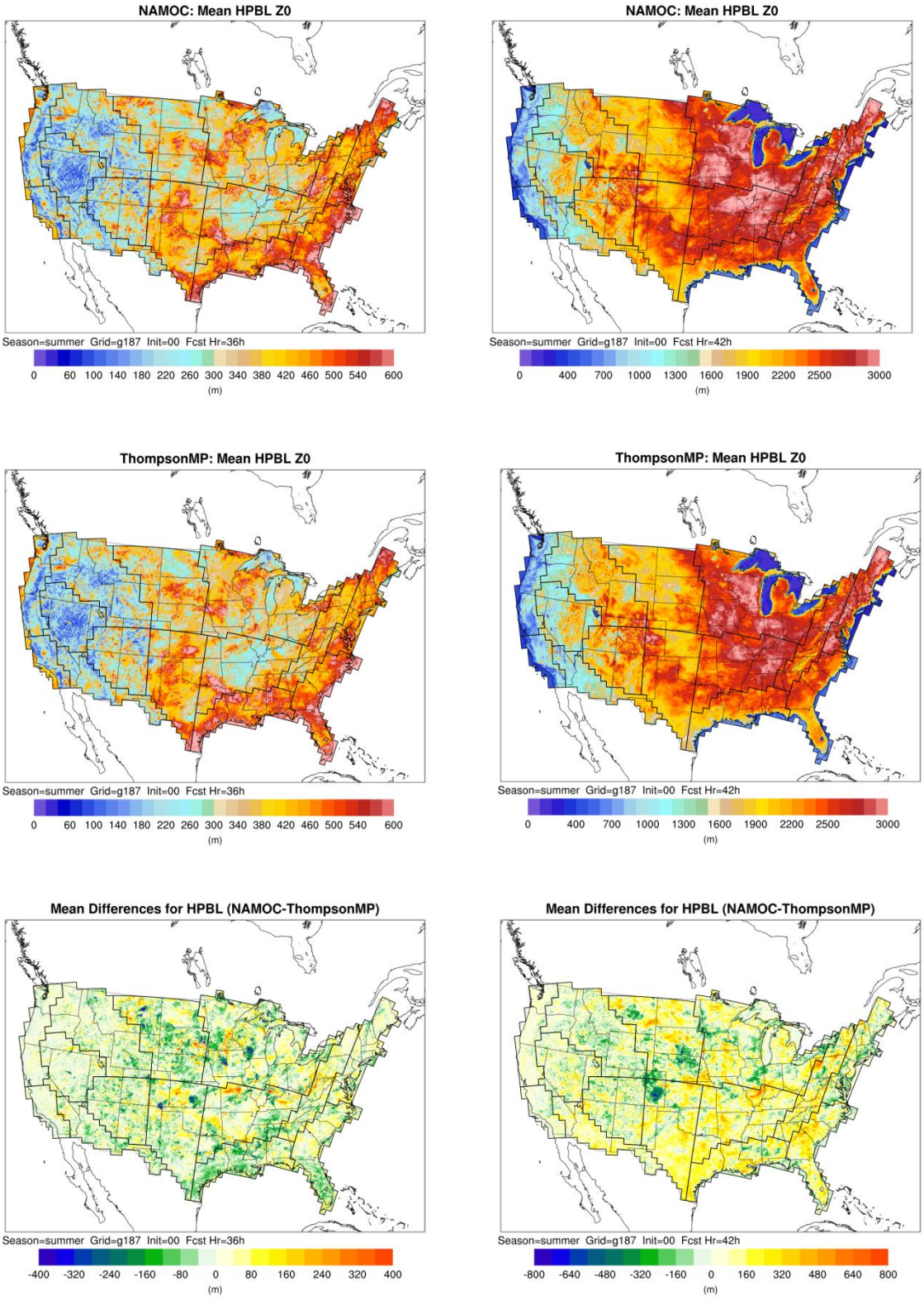

Figure 43. Mean PBL height (m) for all 00 UTC initializations during the summer aggregation for NAMOC at the (a) 36-h forecast lead time and (b) 42-h forecast lead time, for ThompsonMP at the (c) 36-h forecast lead time and (d) 42-h forecast lead time, and mean differences (NAMOC-ThompsonMP) at the (e) 36-h forecast lead time and (f) 42-h forecast lead time.

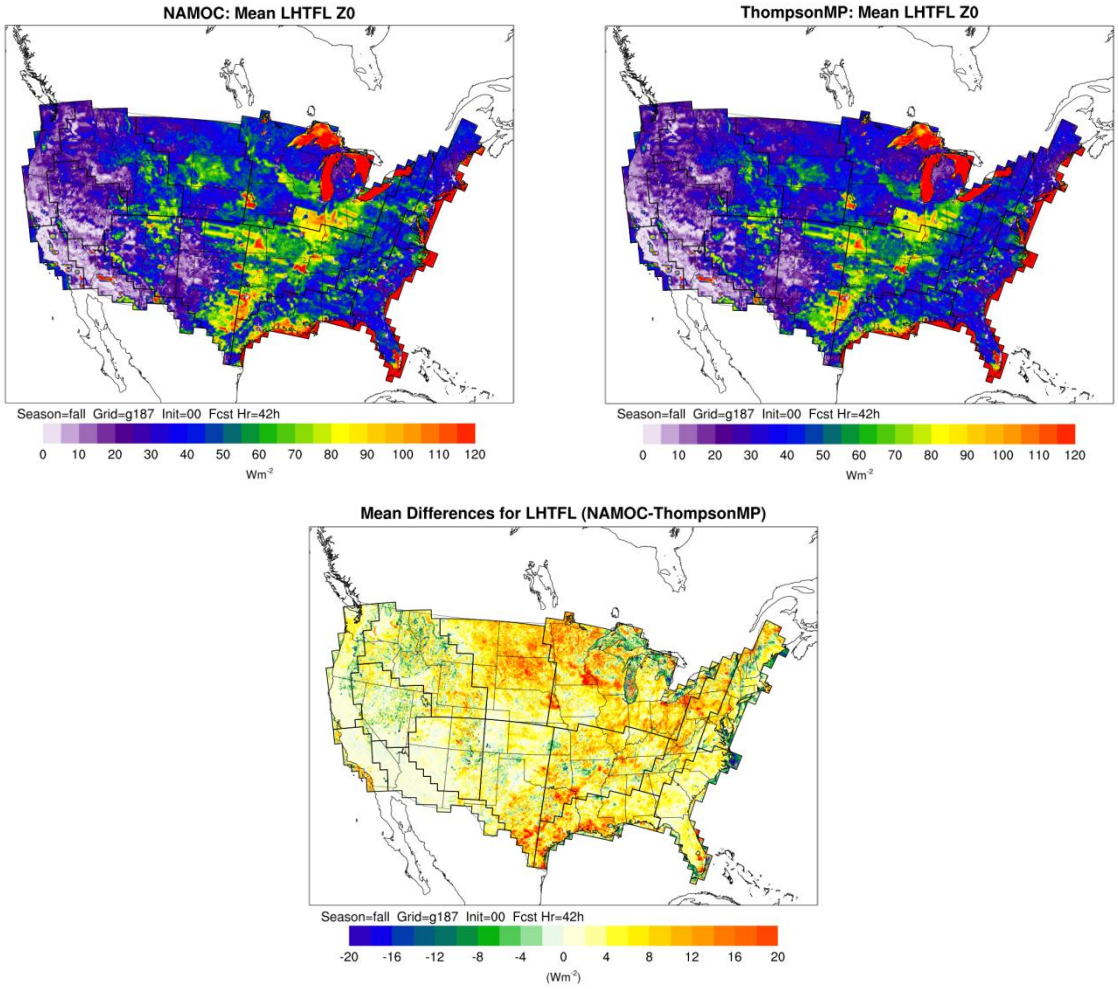

Figure 44. Mean latent heat flux (W m^{-2}) for all 00 UTC initializations during the fall aggregation at the 42-h forecast lead time for (a) NAMOC configuration, (b) ThompsonMP configuration, and (c) mean differences (NAMOC-ThompsonMP).

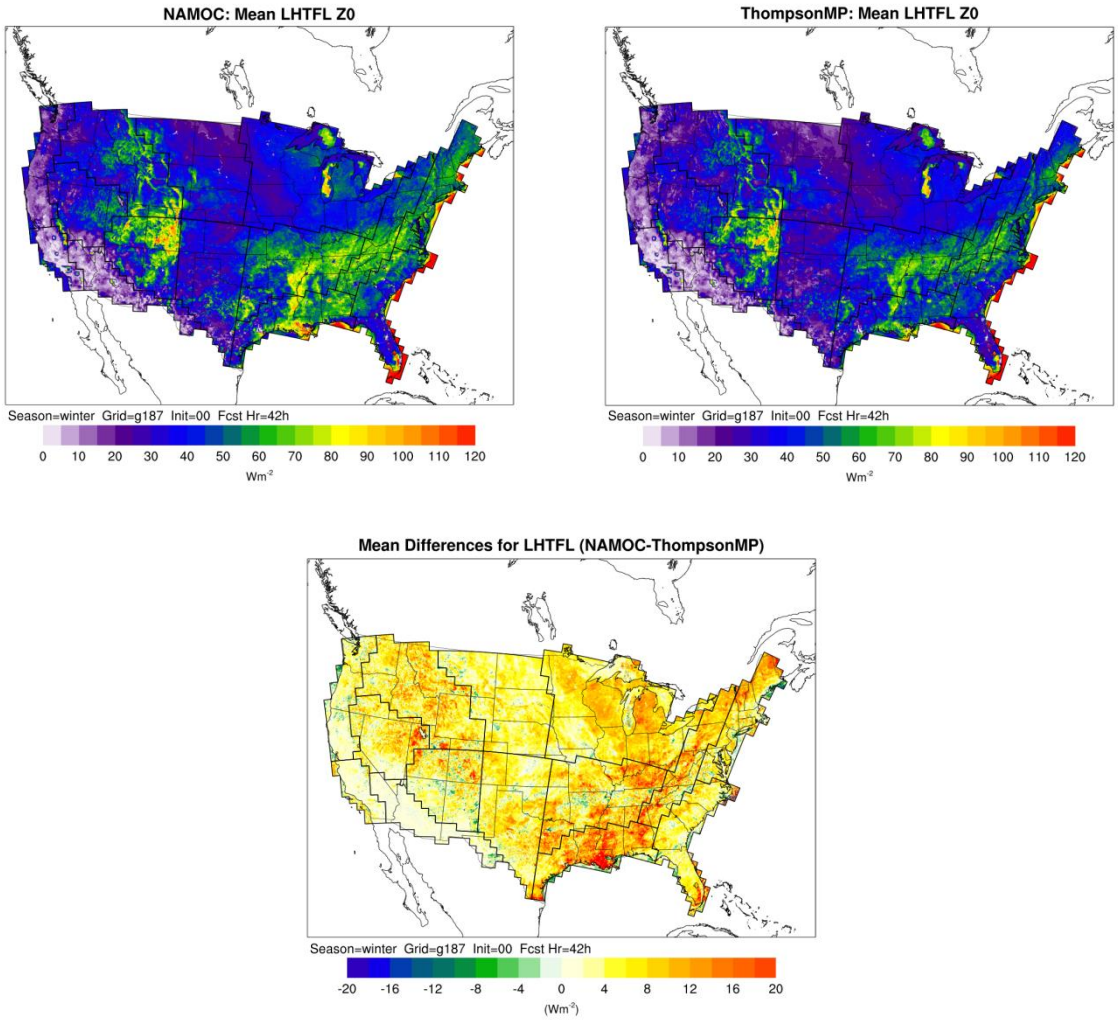

Figure 45. Mean latent heat flux (W m^{-2}) for all 00 UTC initializations during the winter aggregation at the 42-h forecast lead time for (a) NAMOC configuration, (b) ThompsonMP configuration, and (c) mean differences (NAMOC-ThompsonMP).

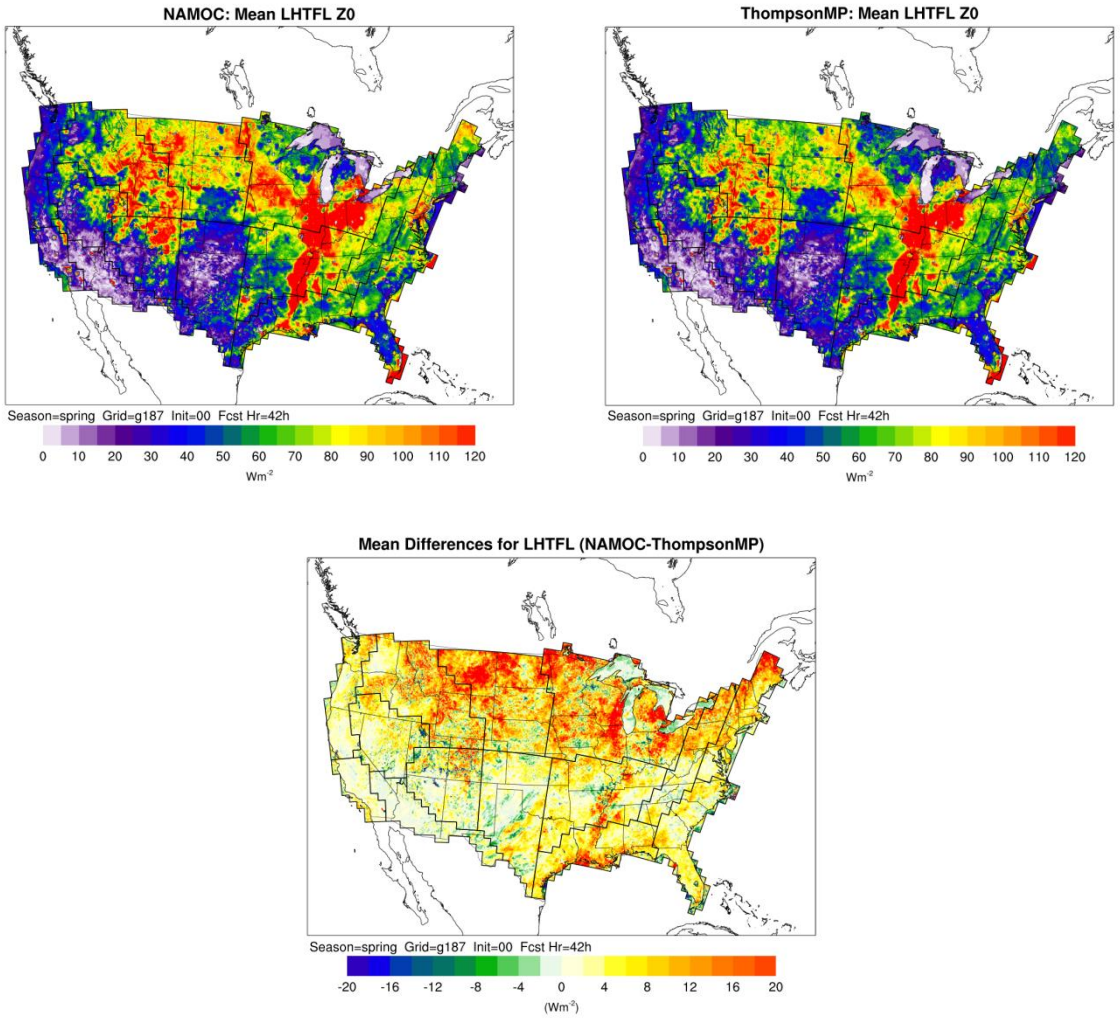

Figure 46. Mean latent heat flux (W m^{-2}) for all 00 UTC initializations during the spring aggregation at the 42-h forecast lead time for (a) NAMOC configuration, (b) ThompsonMP configuration, and (c) mean differences (NAMOC-ThompsonMP).

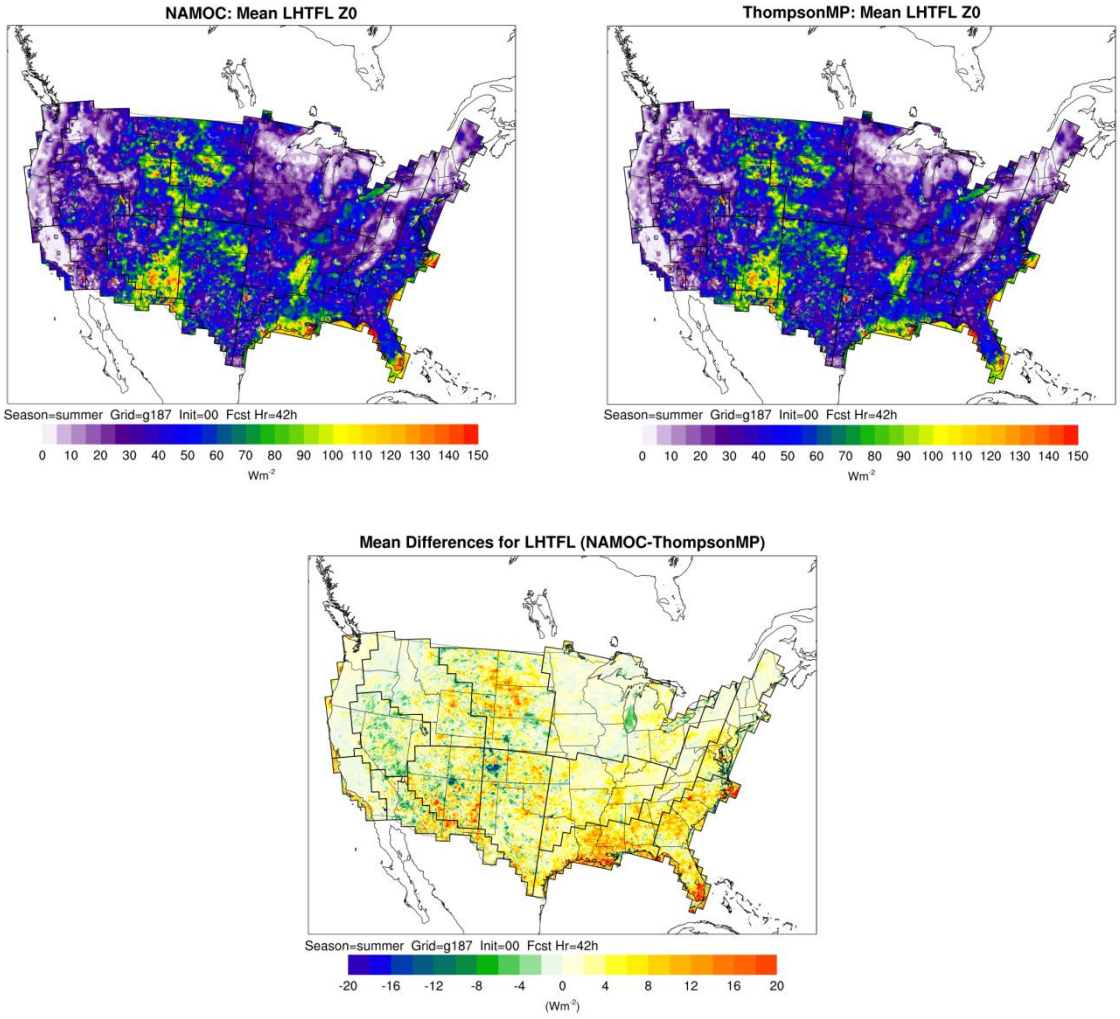

Figure 47. Mean latent heat flux (W m^{-2}) for all 00 UTC initializations during the summer aggregation at the 42-h forecast lead time for (a) NAMOC configuration, (b) ThompsonMP configuration, and (c) mean differences (NAMOC-ThompsonMP).

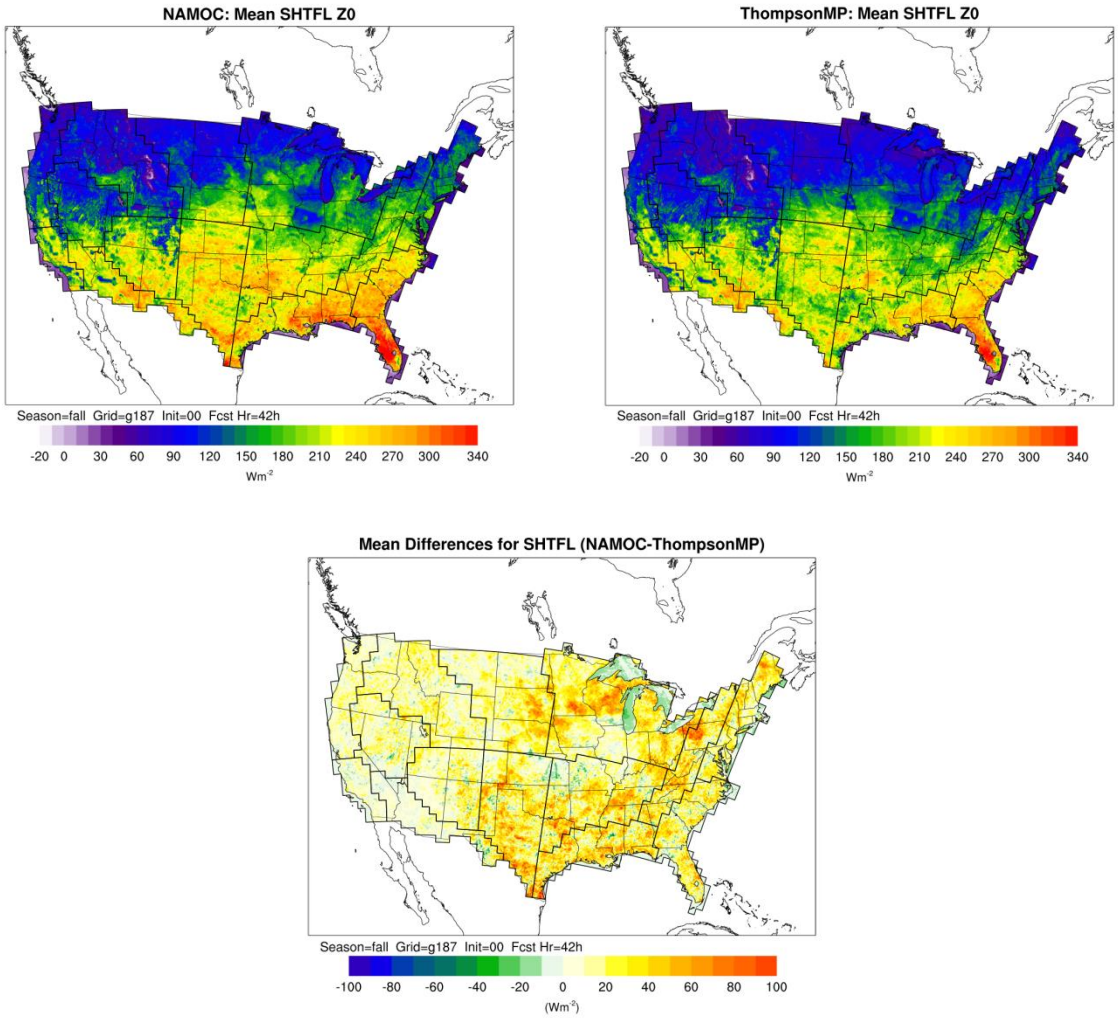

Figure 48. Mean sensible heat flux (W m^{-2}) for all 00 UTC initializations during the fall aggregation at the 42-h forecast lead time for (a) NAMOC configuration, (b) ThompsonMP configuration, and (c) mean differences (NAMOC-ThompsonMP).

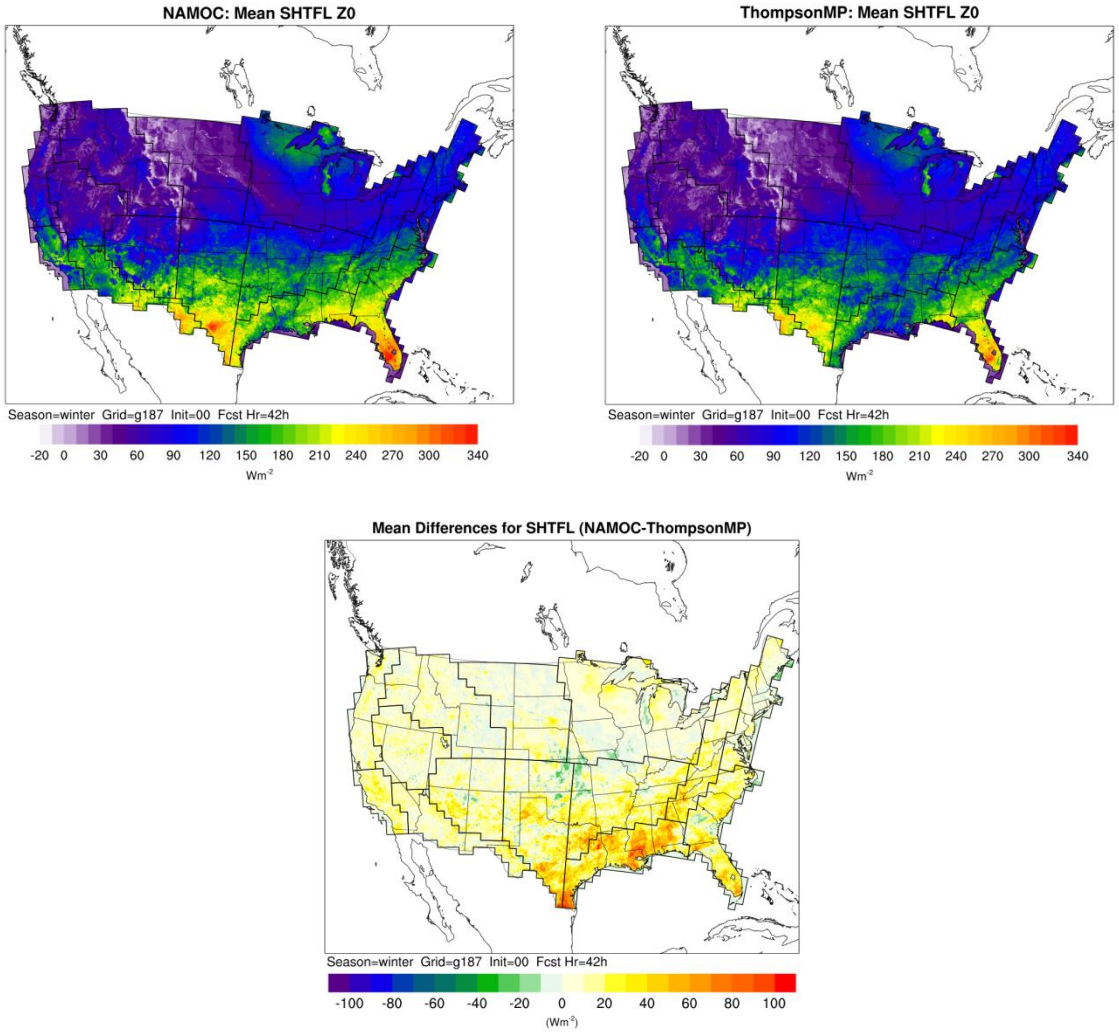

Figure 49. Mean sensible heat flux (W m^{-2}) for all 00 UTC initializations during the winter aggregation at the 42-h forecast lead time for (a) NAMOC configuration, (b) ThompsonMP configuration, and (c) mean differences (NAMOC-ThompsonMP).

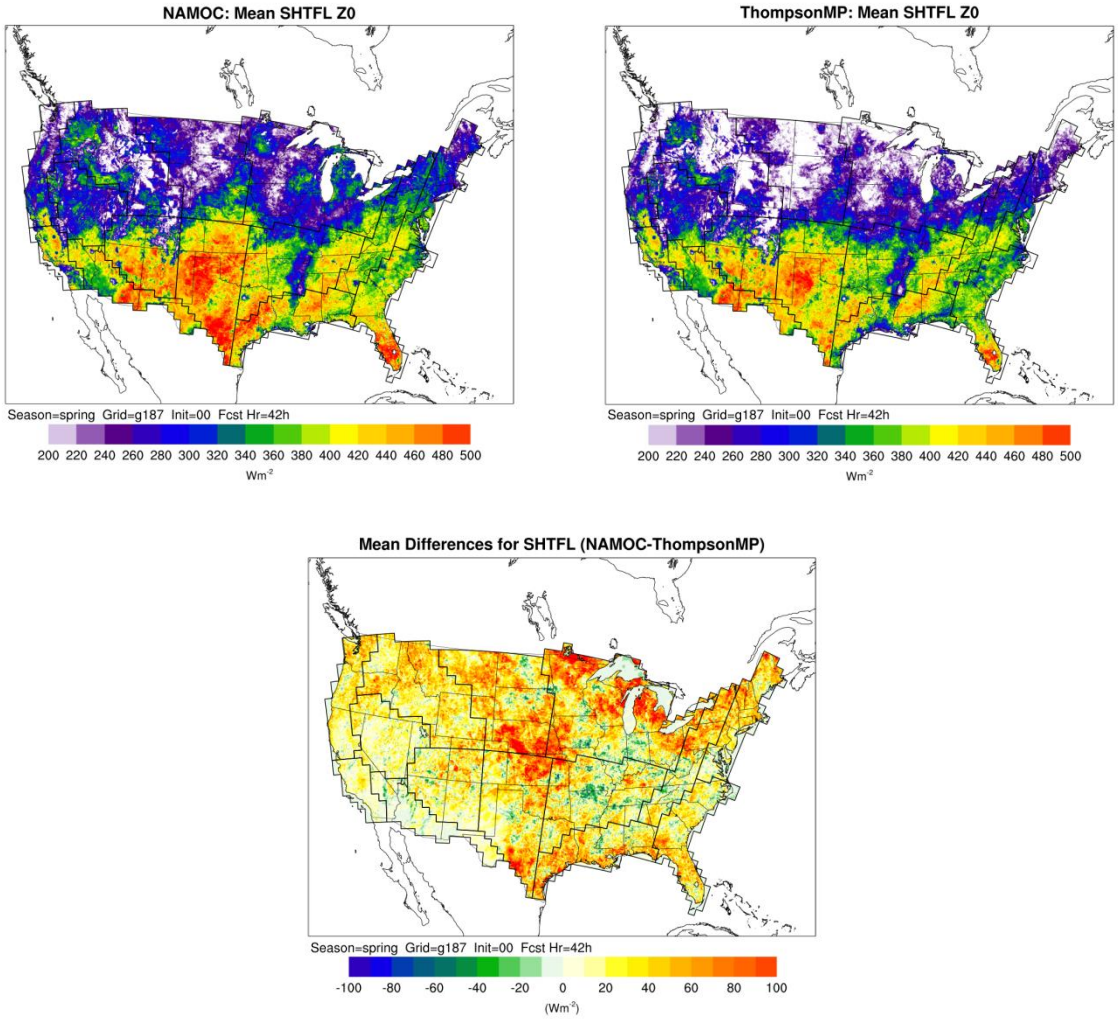

Figure 50. Mean sensible heat flux (W m^{-2}) for all 00 UTC initializations during the spring aggregation at the 42-h forecast lead time for (a) NAMOC configuration, (b) ThompsonMP configuration, and (c) mean differences (NAMOC-ThompsonMP).

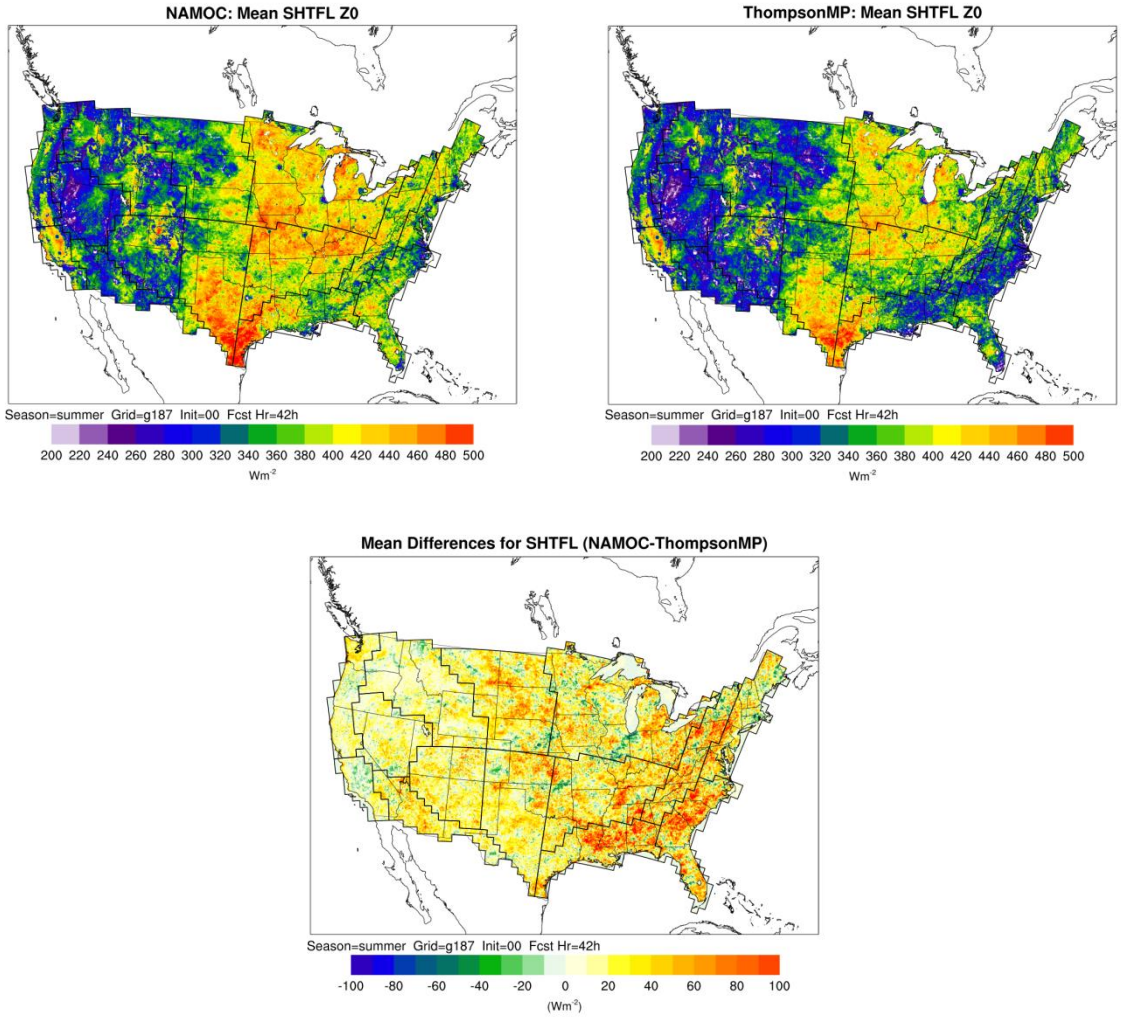

Figure 51. Mean sensible heat flux (W m^{-2}) for all 00 UTC initializations during the summer aggregation at the 42-h forecast lead time for (a) NAMOC configuration, (b) ThompsonMP configuration, and (c) mean differences (NAMOC-ThompsonMP).

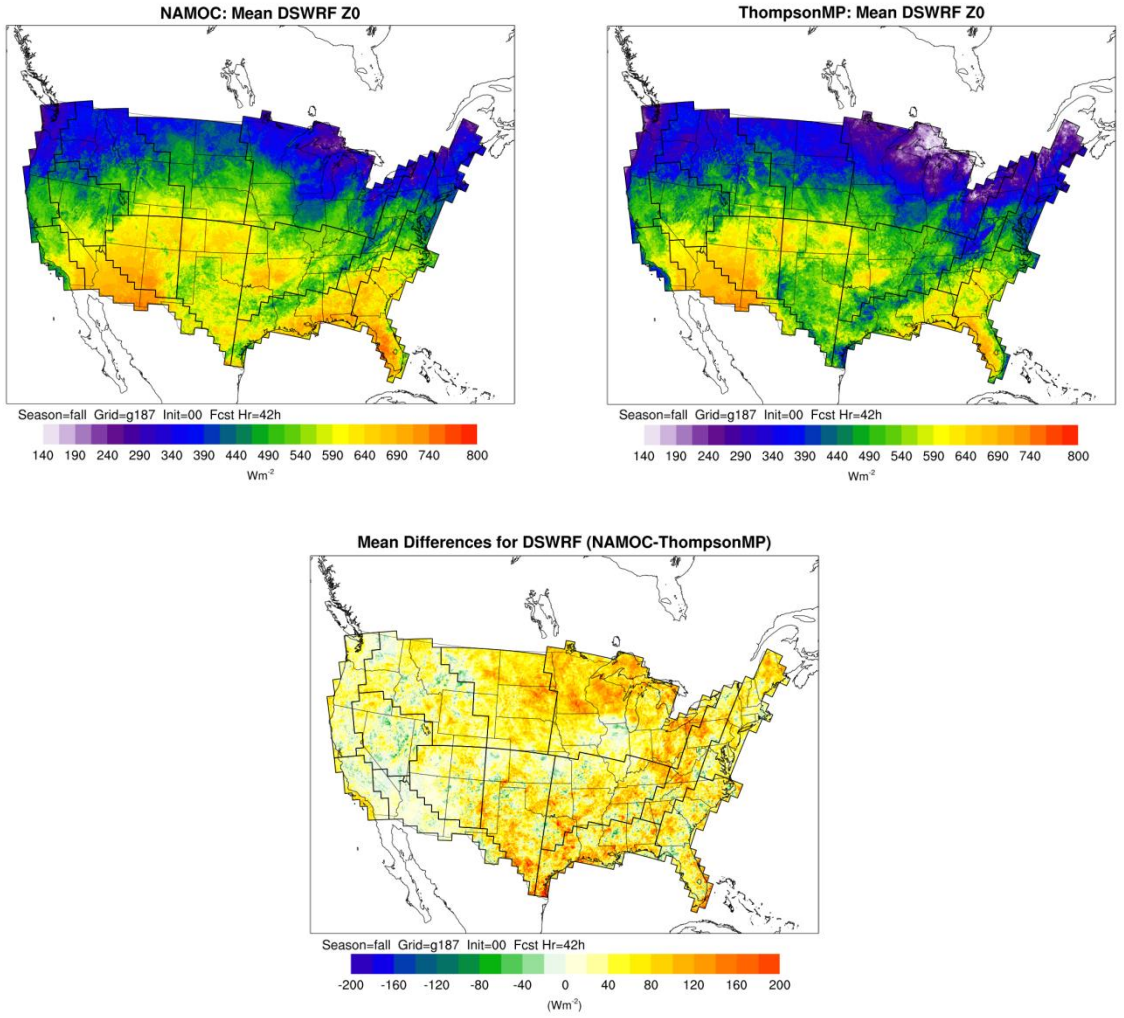

Figure 52. Mean downward short-wave radiation (W m^{-2}) for all 00 UTC initializations during the fall aggregation at the 42-h forecast lead time for (a) NAMOC configuration, (b) ThompsonMP configuration, and (c) mean differences (NAMOC-ThompsonMP).

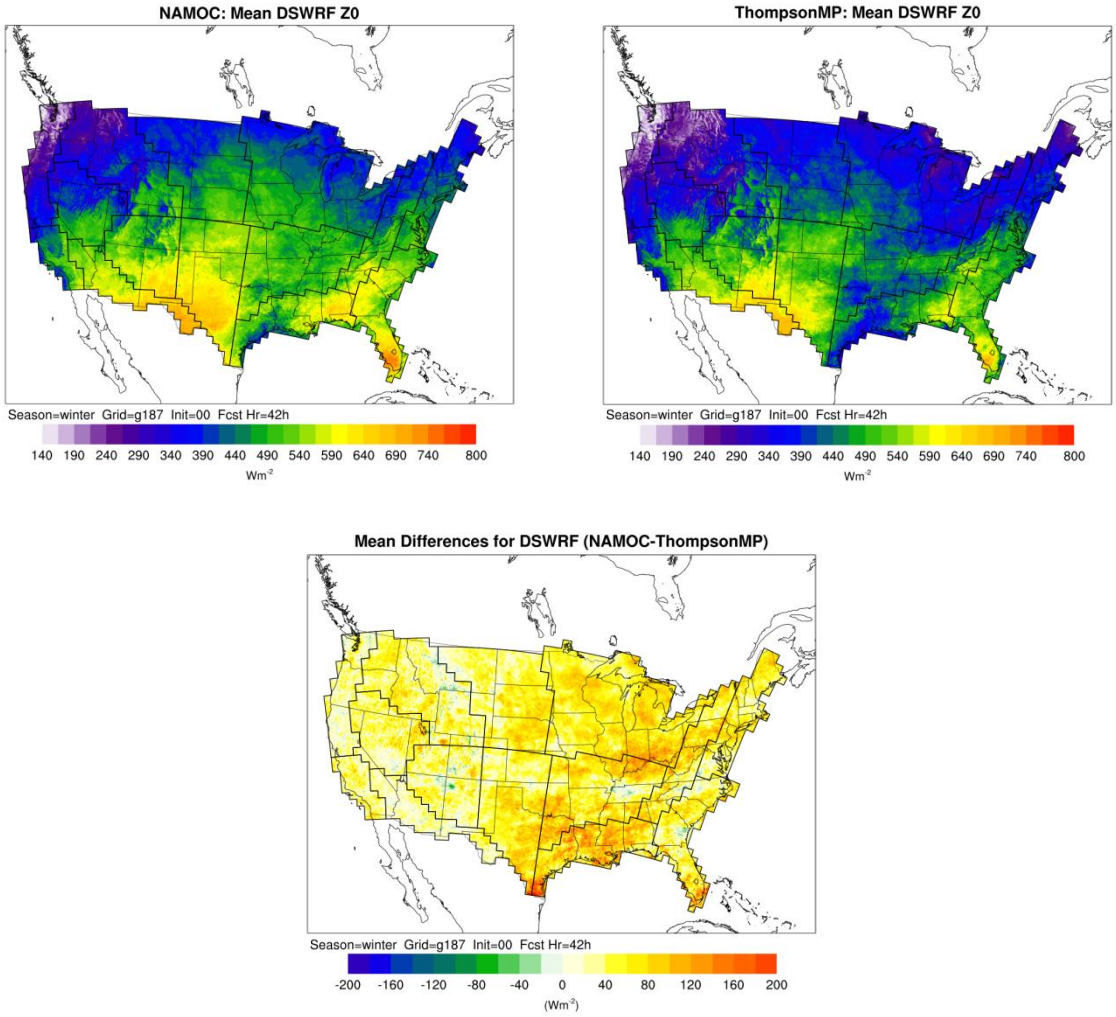

Figure 53. Mean downward short-wave radiation (W m^{-2}) for all 00 UTC initializations during the winter aggregation at the 42-h forecast lead time for (a) NAMOC configuration, (b) ThompsonMP configuration, and (c) mean differences (NAMOC-ThompsonMP).

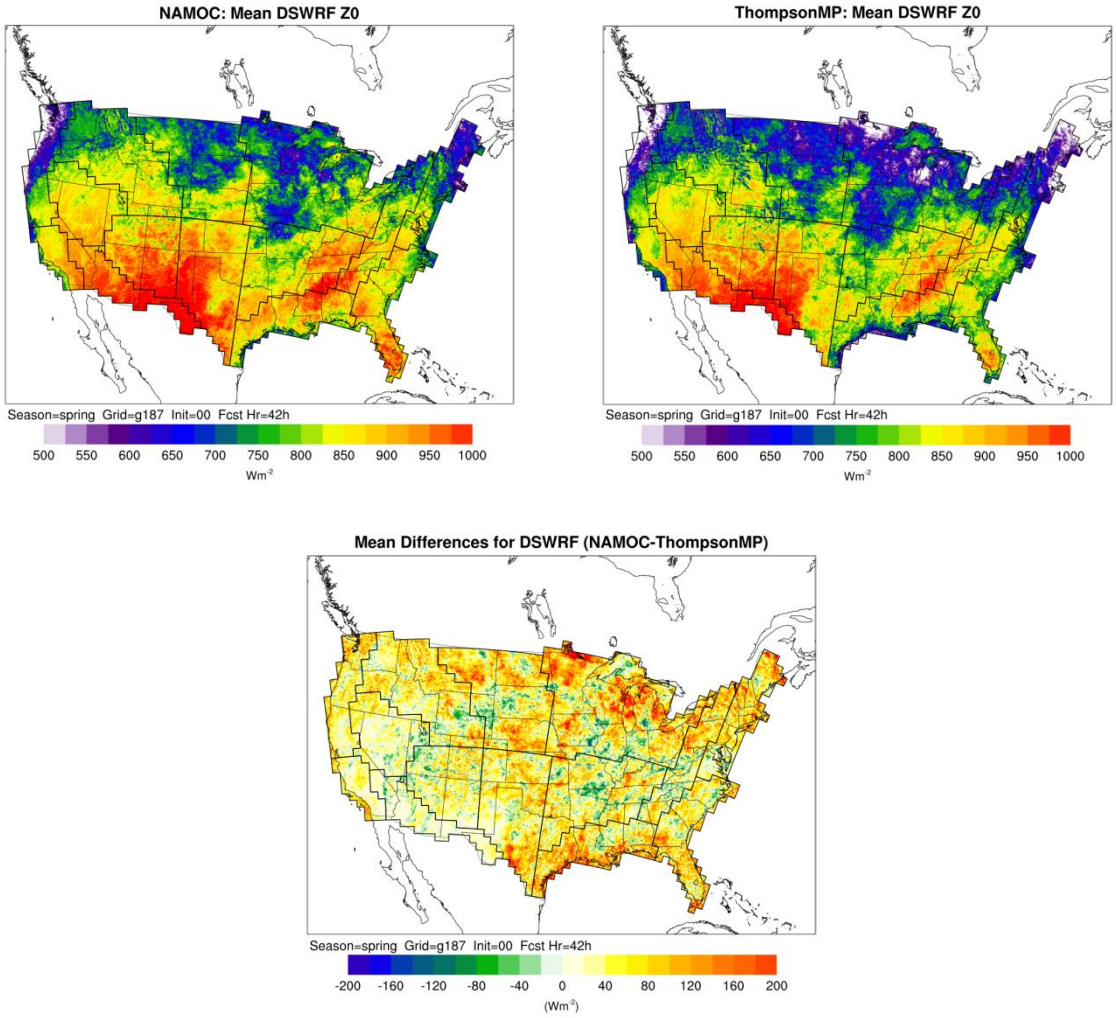

Figure 54. Mean downward short-wave radiation (W m^{-2}) for all 00 UTC initializations during the spring aggregation at the 42-h forecast lead time for (a) NAMOC configuration, (b) ThompsonMP configuration, and (c) mean differences (NAMOC-ThompsonMP).

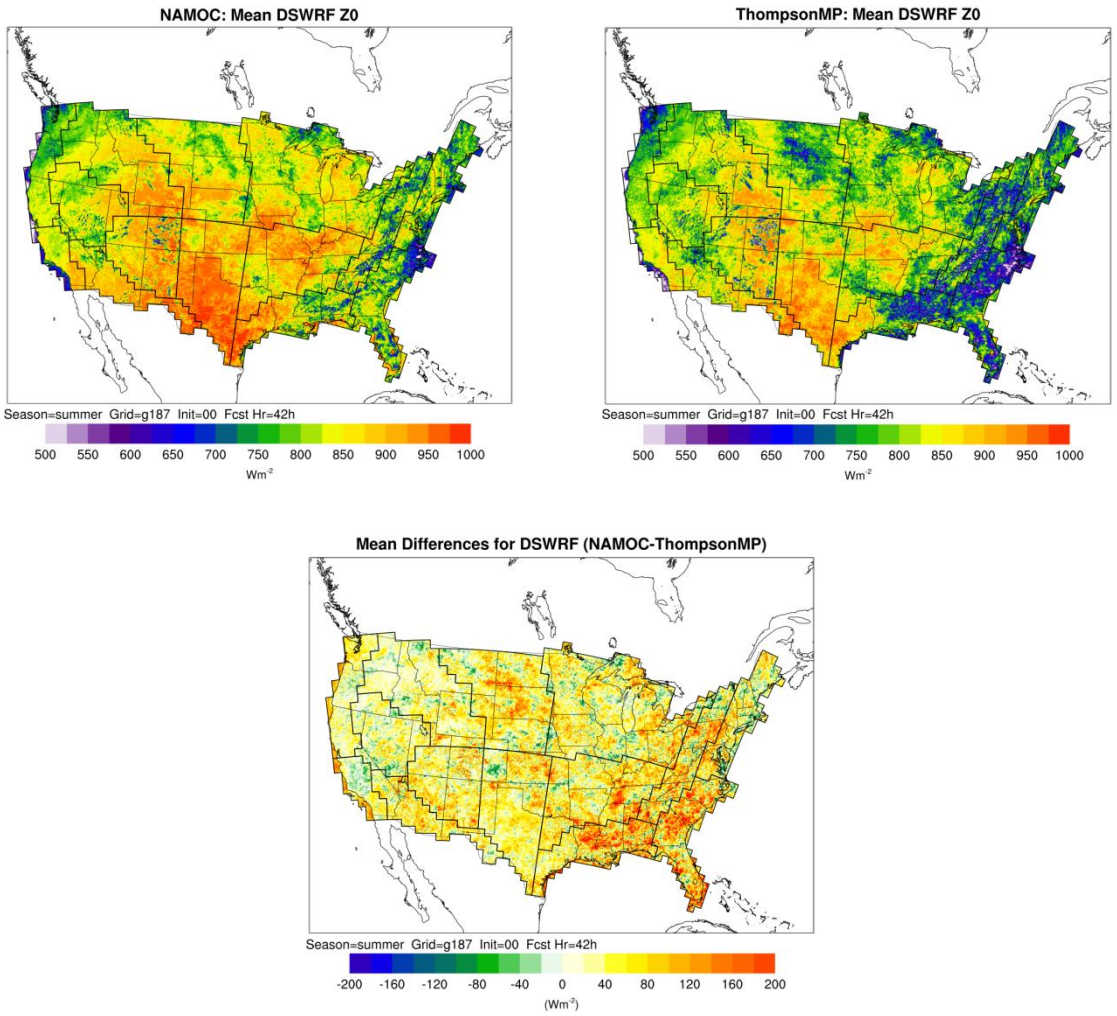

Figure 55. Mean downward short-wave radiation (W m^{-2}) for all 00 UTC initializations during the summer aggregation at the 42-h forecast lead time for (a) NAMOC configuration, (b) ThompsonMP configuration, and (c) mean differences (NAMOC-ThompsonMP).

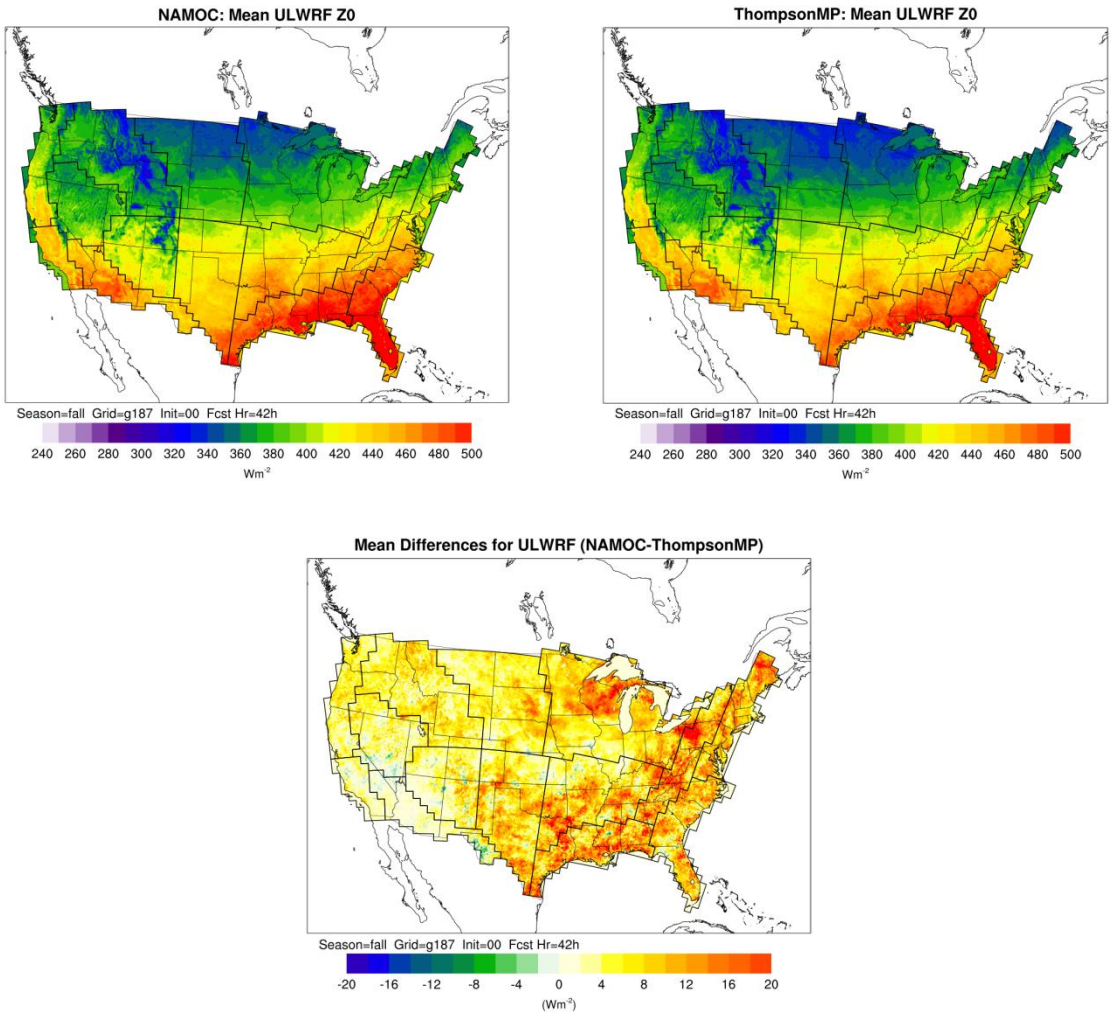

Figure 56. Mean upward long-wave radiation (W m^{-2}) for all 00 UTC initializations during the fall aggregation at the 42-h forecast lead time for (a) NAMOC configuration, (b) ThompsonMP configuration, and (c) mean differences (NAMOC-ThompsonMP).

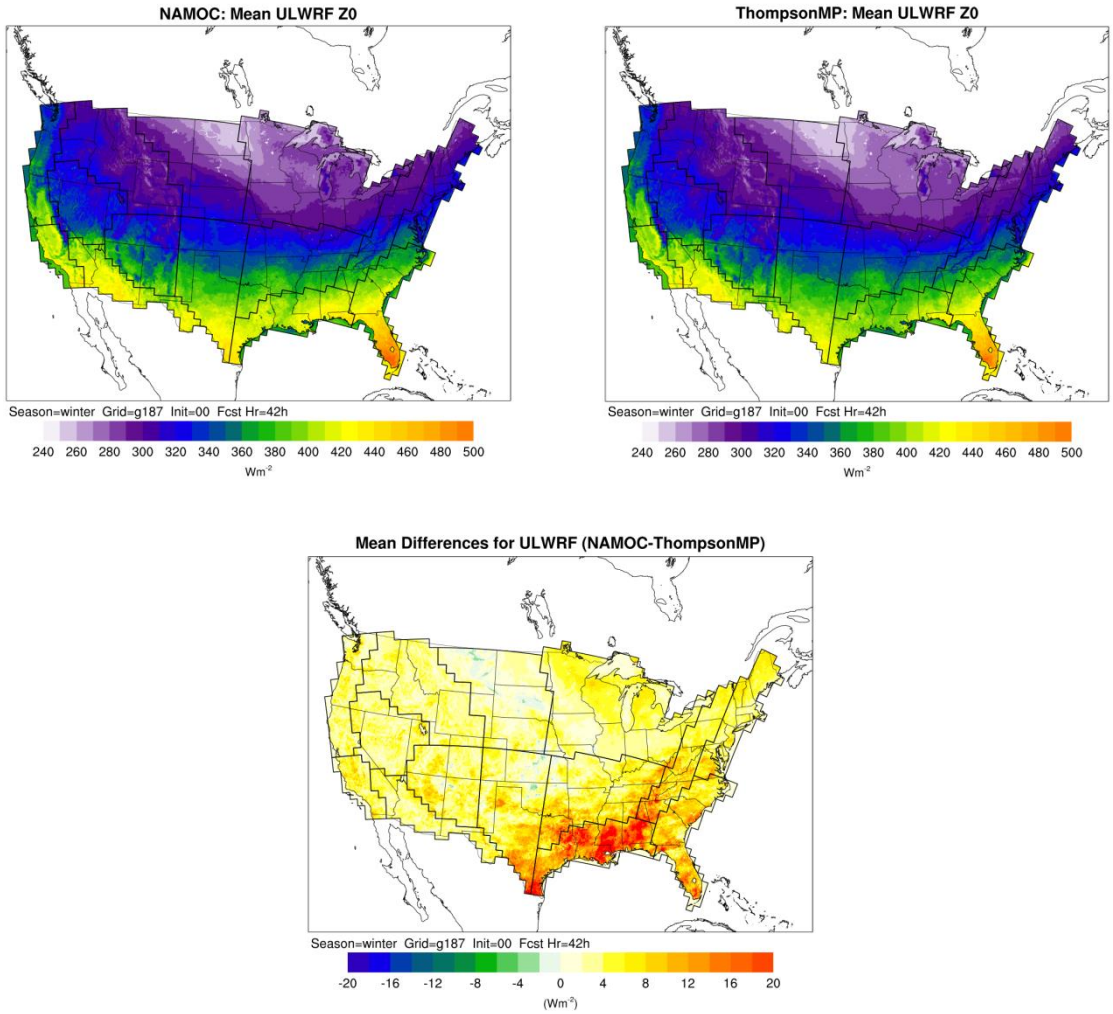

Figure 57. Mean upward long-wave radiation (W m^{-2}) for all 00 UTC initializations during the winter aggregation at the 42-h forecast lead time for (a) NAMOC configuration, (b) ThompsonMP configuration, and (c) mean differences (NAMOC-ThompsonMP).

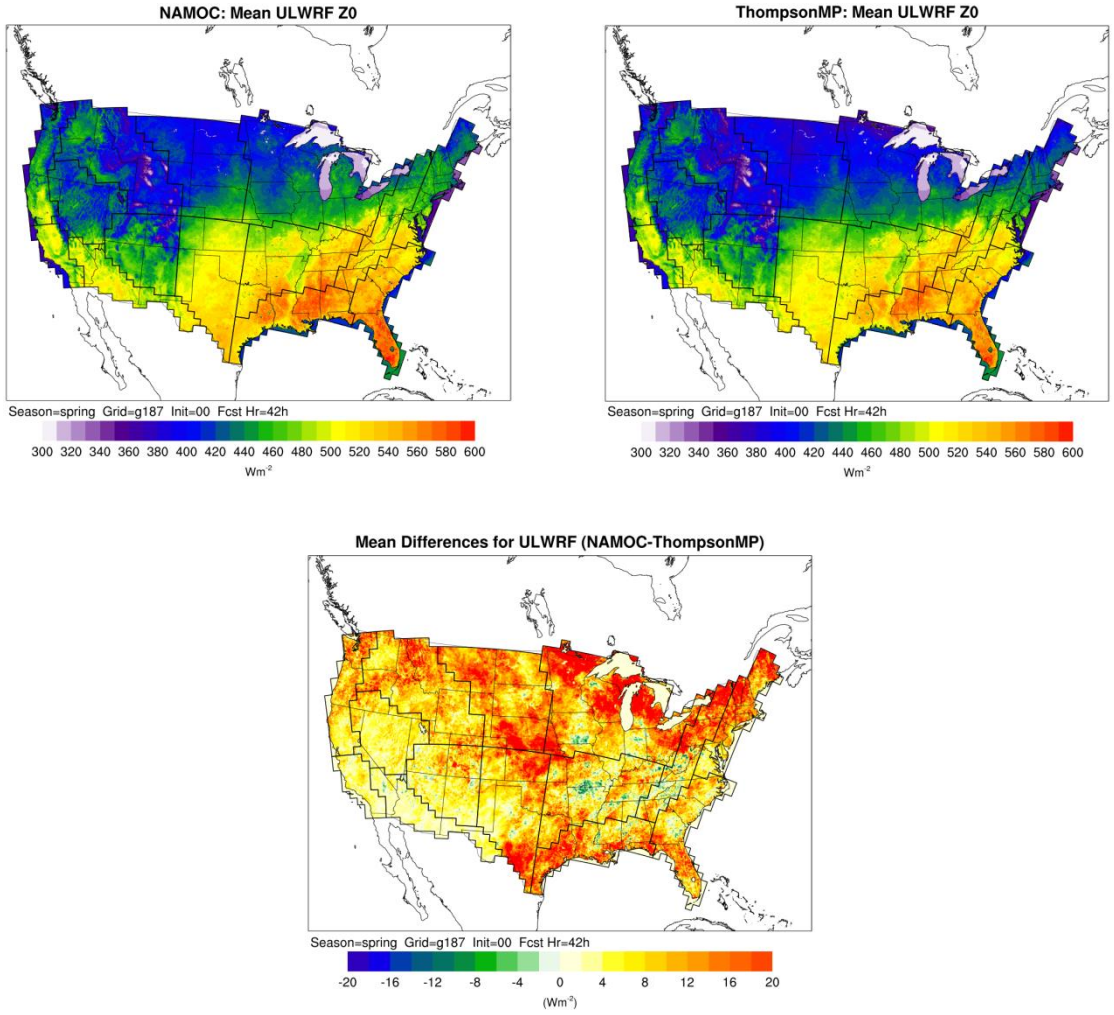

Figure 58. Mean upward long-wave radiation (W m^{-2}) for all 00 UTC initializations during the spring aggregation at the 42-h forecast lead time for (a) NAMOC configuration, (b) ThompsonMP configuration, and (c) mean differences (NAMOC-ThompsonMP).

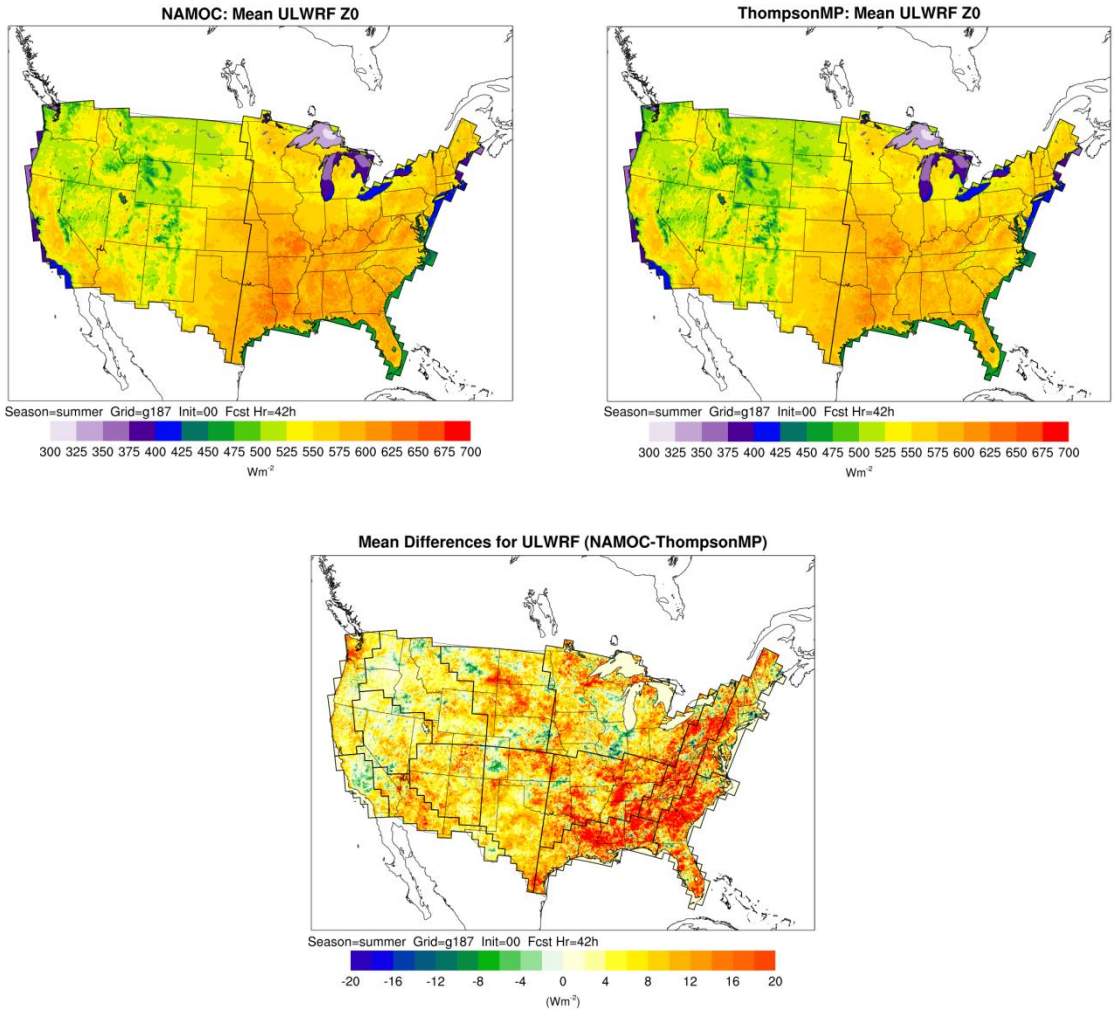

Figure 59. Mean upward long-wave radiation (W m^{-2}) for all 00 UTC initializations during the summer aggregation at the 42-h forecast lead time for (a) NAMOC configuration, (b) ThompsonMP configuration, and (c) mean differences (NAMOC-ThompsonMP).

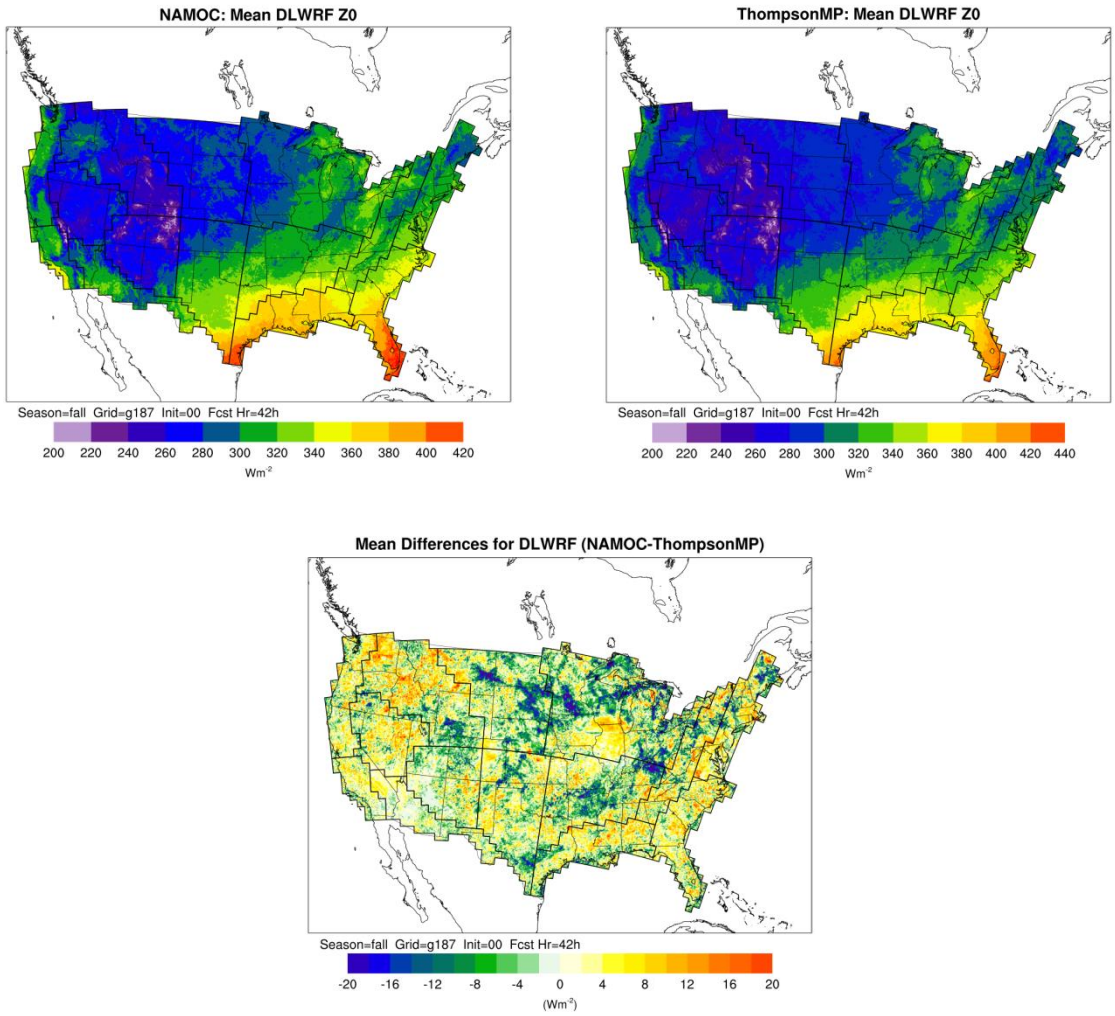

Figure 60. Mean downward long-wave radiation (W m^{-2}) for all 00 UTC initializations during the fall aggregation at the 42-h forecast lead time for (a) NAMOC configuration, (b) ThompsonMP configuration, and (c) mean differences (NAMOC-ThompsonMP).

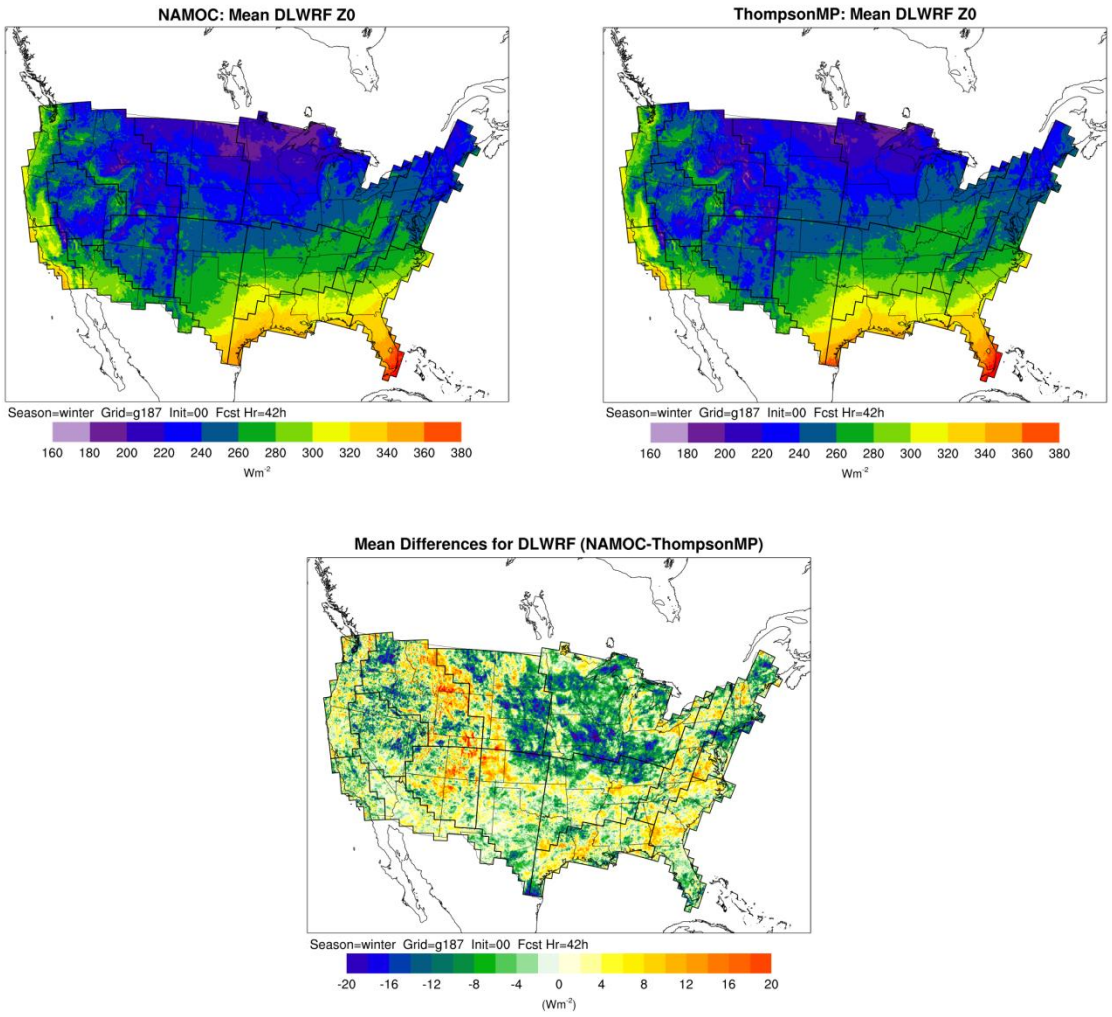

Figure 61. Mean downward long-wave radiation (W m^{-2}) for all 00 UTC initializations during the winter aggregation at the 42-h forecast lead time for (a) NAMOC configuration, (b) ThompsonMP configuration, and (c) mean differences (NAMOC-ThompsonMP).

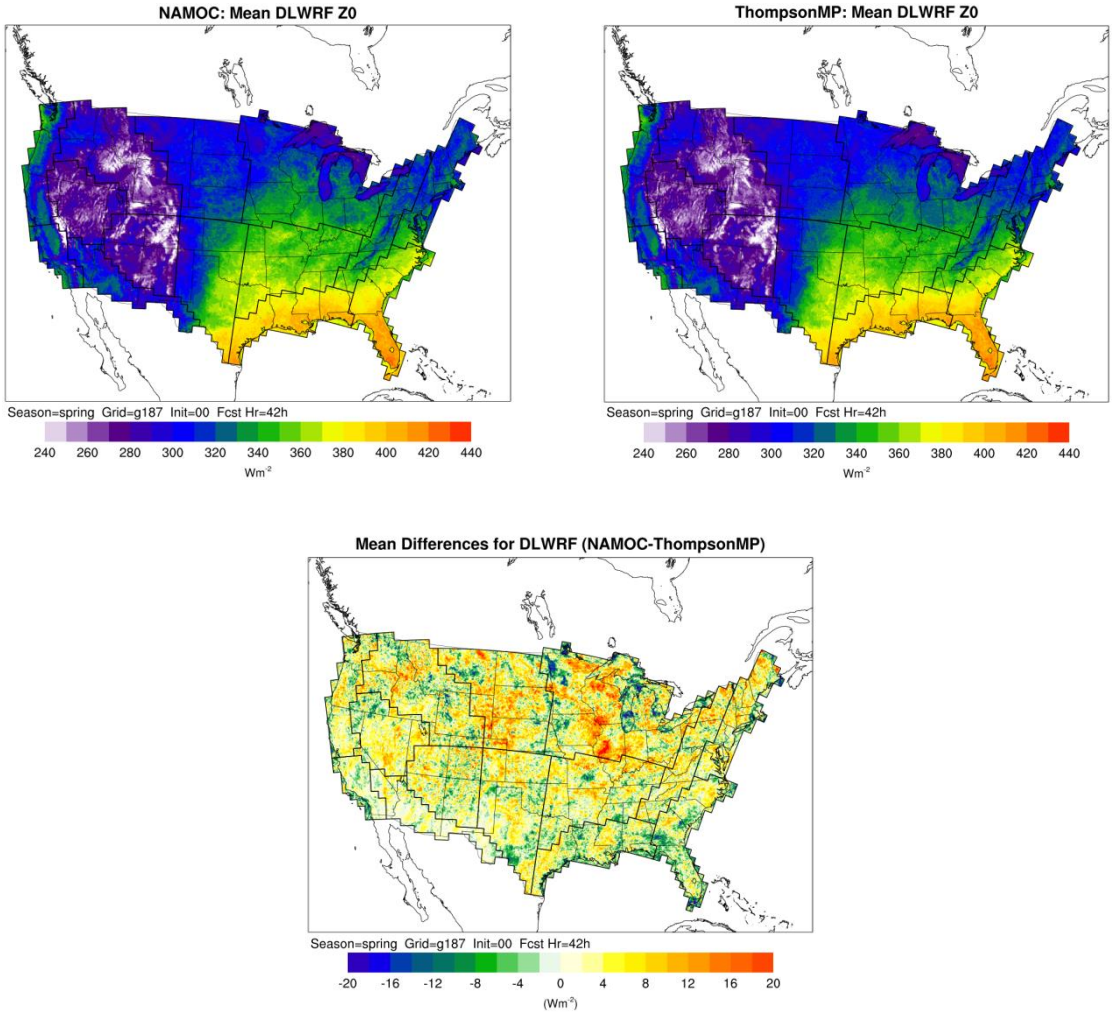

Figure 62. Mean downward long-wave radiation (W m^{-2}) for all 00 UTC initializations during the spring aggregation at the 42-h forecast lead time for (a) NAMOC configuration, (b) ThompsonMP configuration, and (c) mean differences (NAMOC-ThompsonMP).

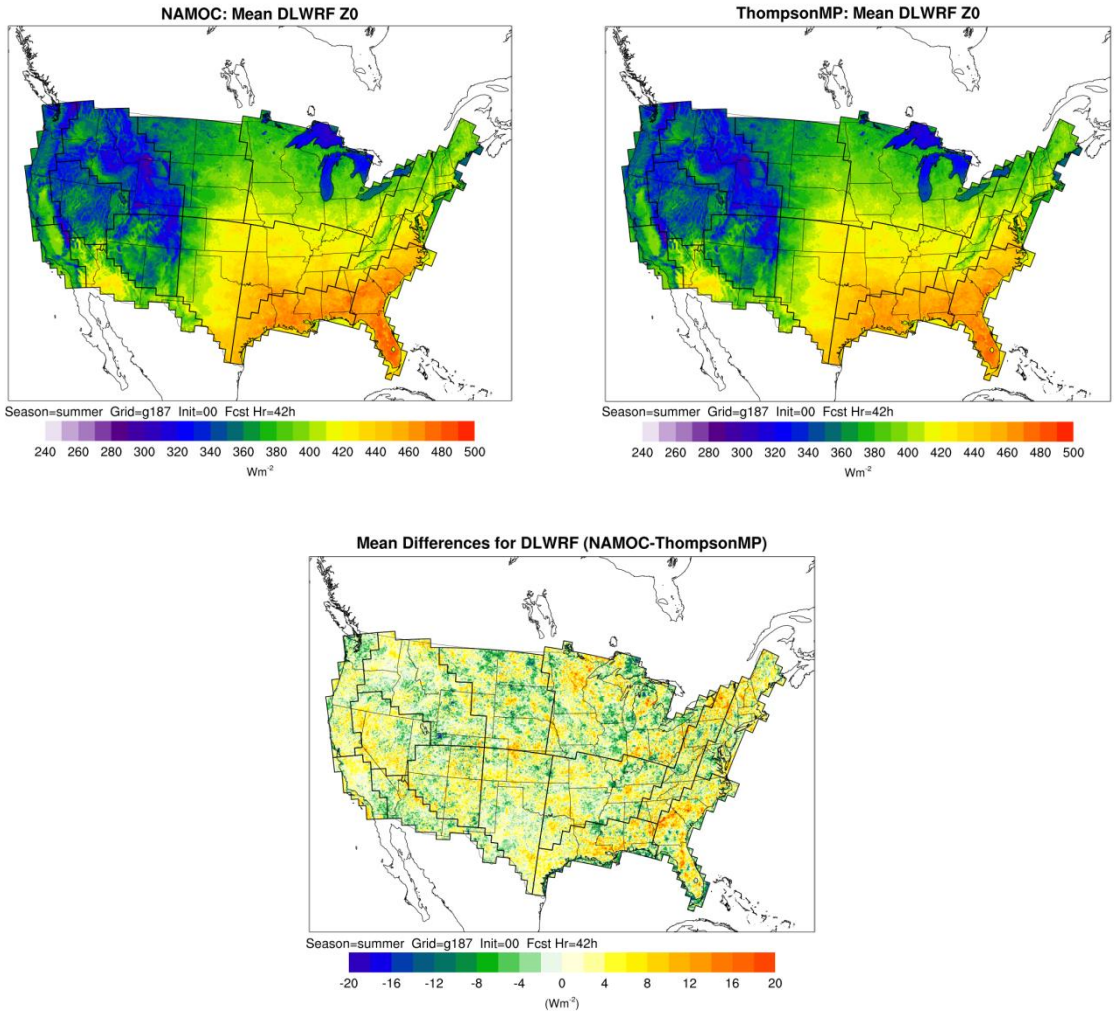

Figure 63. Mean downward long-wave radiation (W m^{-2}) for all 00 UTC initializations during the summer aggregation at the 42-h forecast lead time for (a) NAMOC configuration, (b) ThompsonMP configuration, and (c) mean differences (NAMOC-ThompsonMP).